2013-03-22

Foundational Work in Bioelectrochemical Anaerobic Reactor Design with Electron Mediators

Christopher D. Hoeger
Brigham Young University - Provo

Foundational Work in Bioelectrochemical Anaerobic Reactor Design with Electron Mediators

Christopher Hoeger

A thesis submitted to the faculty of
Brigham Young University
in partial fulfillment of the requirements for the degree of

Master of Science

Randy S. Lewis, Chair
David O. Lignell
Julianne H. Grose

Department of Chemical Engineering

Brigham Young University

March 2013

ABSTRACT

Foundational Work in Bioelectrochemical
Anaerobic Reactor Design
with Electron Mediators

Christopher Hoeger
Department of Chemical Engineering
Master of Science

Bioelectrical reactors (BER) have potential to be utilized in a wide variety of industrial applications. This work explores the kinetics involved with reduction of electron mediators (anthraquinone disulfonate and methyl viologen) in bioelectrical reactors. It also discusses on possible application of BER technology to produce ethanol from CO_2 and electricity. It is established that *Clostridium ragdahlei* is capable of sustaining life and product formation with CO_2 as the only carbon source. This means it is theoretically possible to utilize CO_2 as he source of carbon and electricity as the source of reducing equivalents for bacterial growth and product formation. A three-step mechanism composed of adsorption, surface reaction, and desorption is developed to model the reaction of dissolved electron mediators at the electrode surface of the BER. The proposed mechanism is then utilized to build a mathematical model to describe the kinetics of the BER system. This model is used to gain greater understanding of experimental kinetic data of electron mediator reduction at different voltage potentials.

It is determined that voltage potential has very small effect on the initial rate of reaction in the reactor. However, thermodynamic equilibrium is affected by the change in voltage, resulting in longer sustained initial rate at higher overpotential. Mathematically, this change affects the modeled rate constants by increasing the reverse rate constant of the rate limiting step, and also by affecting the ratio of the thermodynamic equilibrium constants of adsorption. This results in a larger amount of oxidized electron mediator adsorbed to the electrode surface at higher overpotentials, leading to the initial rate persisting further into experimental runs.

One key portion of these findings was the determination that the surface reaction step is the rate limiting step of the kinetic mechanism. This has great ramifications on future research and on future considerations for reactor design. This insight allows for better understanding of the key and fundamental workings of BER technology.

Keywords: bioelectrical reactor, kinetics, electrode surface reactions, *Clostridium ragsdahlei*

ACKNOWLEDGMENTS

I would like to express my appreciation to Dr. Lewis for his help and patience in completion of this thesis. Additional acknowledgements to Dallin Glenn and Hannah Davis for help collecting experimental data, and Chang Chen for her work in improving the experimental lab bioelectrical reactor. Finally, I would also like to say thank you to my wife, Michelle, for her support, encouragement, and patience through this project.

TABLE OF CONTENTS

LIST OF TABLES

LIST OF FIGURES

1 INTRODUCTION

1.1 Biocatalysis Using Metabolic Pathways

Biocatalysis is the process of using biological material as catalysts in chemical reactions. Biological systems are typically composed of thousands of metabolic pathways which utilize a myriad of substrates in order to create chemicals required for normal function, remove wastes, and provide energy for the organism, among other tasks that allow the organism to live. Each of these individual metabolic pathways requires a cascade of enzymes to utilize reactants and form desirable products or create energy for other processes. Complex biological systems, such as those found in mammals, perform billions of chemical reactions every second in order to allow the entire system to continue to live and accomplish daily tasks.

The field of biocatalysis, similar to that of catalysis, focuses on making use of the efficiency and speed of these processes in order to take reactants that are of lesser value and chemically synthesize desirable products. These reactions take place in cellular, enzymatic cascades, or isolated enzyme systems. Evolutionary changes have rendered these biological systems efficient, robust, and highly specific in their applications. The existence of these systems has only been known to man for the last two centuries, although their use dates back millennia. Crude utilization of biocatalysts still existed before man was aware of what exactly was causing

the changes they were seeing. More advanced integration into industrial applications began about in the 1970s, but it is still a fledgling technology.

1.2 A Comparison of Whole Cell and Enzymatic Systems

Biocatalysis has two distinctive classes, whole cell systems and enzymatic systems. Whole cell systems are, in fact, a large web of enzymatic metabolic pathways designed to support the life of an organism. But because their purpose is sustaining life, they operate very different from enzymatic systems. Enzymatic systems are more basic. A single enzyme or a cascade of enzymes takes a substrate and chemically modifies it into a more desirable product. The process is straightforward and if the enzymes are immobilized, then separation of product from solution is usually fairly simple. These systems are simple and extremely effective for processes such as hydrolysis and isomerization. They do not require vitamins or minerals in order for sustained function; all they need are the substrates and cofactors required for their individual reactions to take place. Because they are not living organisms, they must be manufactured (typically *in vivo*), purified, and immobilized for industrial use.

Whole cell systems are significantly more complex, as they are living organisms. They require vitamins, minerals, and a suitable metabolite for energy production. Fortunately, they are typically self-perpetuating and adaptable to various environments. Whole cell systems are particularly useful for applications that require cofactor regeneration such as oxidation-reduction reactions. In order for these reactions to take place, a chemical with multiple oxidation states (typically $NAD(P)^+$/NAD(P)H) must transfer electrons to or from the substrate. In order for the reaction to continue to take place indefinitely, the cofactor must be regenerated at the same rate at which it is consumed. Cellular systems already have mechanisms in place by which they can

regenerate these cofactors. Enzyme systems require at least one additional enzyme and substrate for regeneration to occur. This introduces at least two more species that need to be separated from the product species, complicating the process. Whole cells usually produce and regenerate these cofactors inside the cell, also removing the necessity of providing the cells with the required cofactor in the first place, most of which are very expensive. This same problem is described in greater detail here for dehydrogenases, an enzyme that uses the electrons from NADH or NADPH and reduces a substrate:

> Most dehydrogenases need nicotinamide adenine dinucleotide coenzymes (NADH or NADPH) for hydride transfer. Because it is impractical to use these expensive coenzymes in stoichiometric amounts, efficient coenzyme recycling transforming oxidized coenzyme back to its reduced form is essential for the productivity of bioreductions when isolated enzymes are used. Recycling is commonly achieved by another enzyme, most commonly glucose or formate dehydrogenase, or by the same enzyme using an auxiliary substrate which is typically 2-propanol. In order to avoid this inconvenience, dehydrogenases are often used as whole cell systems. However, the system may often contain many dehydrogenases catalyzing the same reaction with differing or even reversed enantioselectivities. This often makes optimization and sometimes also product isolation among metabolites and biomass complicated. [1]

It follows, therefore, that while whole cell systems or introduction of additional enzymes and species circumvent this problem, they add unwanted complexity and reduce system efficiency.

1.3 The Purpose of Bioelectrical Reactors in Biocatalysis

A bioelectrical reactor is one that makes use of biological materials and electrodes in a closed loop to allow current to run in a closed loop from one electrode to the other. This is caused by a voltage difference between the two electrodes that is either caused by the fluid surrounding the electrode or induced by applying a voltage via hardware equipment. Processes involving a bioelectrochemical reactor have been around for over thirty years [2], and the ability to create bioproducts from these processes was confirmed at least twenty years ago [3].

One important characteristic of these reactors for the future implementation is their ability to induce oxidation-reduction reactions at the electrode surface. If a suitable method can be found by which NAD(P)H can be regenerated in vitro, then oxidoreductase enzymes that require these nucleotides as a cofactor can be easily implemented as enzymatic systems without the addition of further enzymes or substrates. This removes complexity and does not require the introduction of whole cell systems which require additional vitamins, minerals, and metabolites as described above. In these applications, the reactor must be kept anaerobic at all times to prevent oxidation of the cofactor by gaseous oxygen dissolved in the aqueous solution or organic solvent.

1.4 Bioelectrochemical Reactors (BERs) in Redox Systems

While the future of the BER looks to be bright, there is one particularly large hurdle that has yet to be cleared. Most of the enzymes and whole cell systems involved in redox reactions utilize NAD(P)H as a cofactor to reduce the substrates into products. While direct electrochemical reduction of $NAD(P)^+$ to NADH is possible, it requires high overpotentials and yields of enzymatically active NAD(P)H decrease with each iteration such that after a few

regeneration cycles, no enzymatically active cofactor remains [4]. The mechanism of direct nucleotide reduction involves the transfer of one electron to its pyridinium ring, creating a radical, followed by a subsequent slow electron transfer and subsequent protenation. Unfortunately, dimerization of two NAD(P) radicals is kinetically favorable, forming the enzymatically inactive $NAD(P)_2$ instead of NAD(P)H [5]. This leads to the low yield of enzymatically active NAD(P)H mentioned above, and represents a significant problem that must be overcome before industrial utilization of BERs can be possible.

Much research has been performed to try to adjust the surface chemistry of the electrodes in order to improve NAD(P)H yield, and will be covered in greater detail in Chapter 2. One other method to bioelectrically reduce $NAD(P)^+$ is via indirect reduction. This is achieved by direct reduction of an additional electron mediator which can subsequently reduce $NAD(P)^+$. This subsequent reaction happens spontaneously in some cases, but can also be mediated via addition of another enzyme such as ferredoxin-$NAD(P)^+$ reductase [6].

1.5 Possible Applications of Bioelectrochemical Reactors (BERs) in Redox Systems

1.5.1 An Example of a Whole Cell BER System

A hypothesis has been suggested that could increase renewable energy resources. There exist a number of strains of bacteria that can create biofuels from gas substrates. A particular clostridium species, currently referred to as P11, forms ethanol and acetic acid from synthesis gas composed of CO, CO_2, and H_2. Along the current proposed microbial pathway (see Figure 1-1), gaseous carbon sources are reduced to form these products. CO_2 serves as a carbon source, H_2 as a source of electrons for reduction, and CO can be used by the bacteria either as a carbon or as an electron source. The possibility exists for CO_2 to be the only required gas substrate if a

suitable nongaseous electron source is available. Since the bacteria reside in media composed mostly of water, electrolysis of water could provide this electron source. It is therefore feasible that bioproducts such as the ethanol and acetic acid produced by P11 can be formed from CO_2 and electricity by use of a bioelectrochemical anaerobic reactor. However, an economic analysis is critical towards identifying the feasibility of such processes. A rigorous analysis would need to include engineering constraints (kinetics, thermodynamics, transport, etc.) that can potentially limit the process.

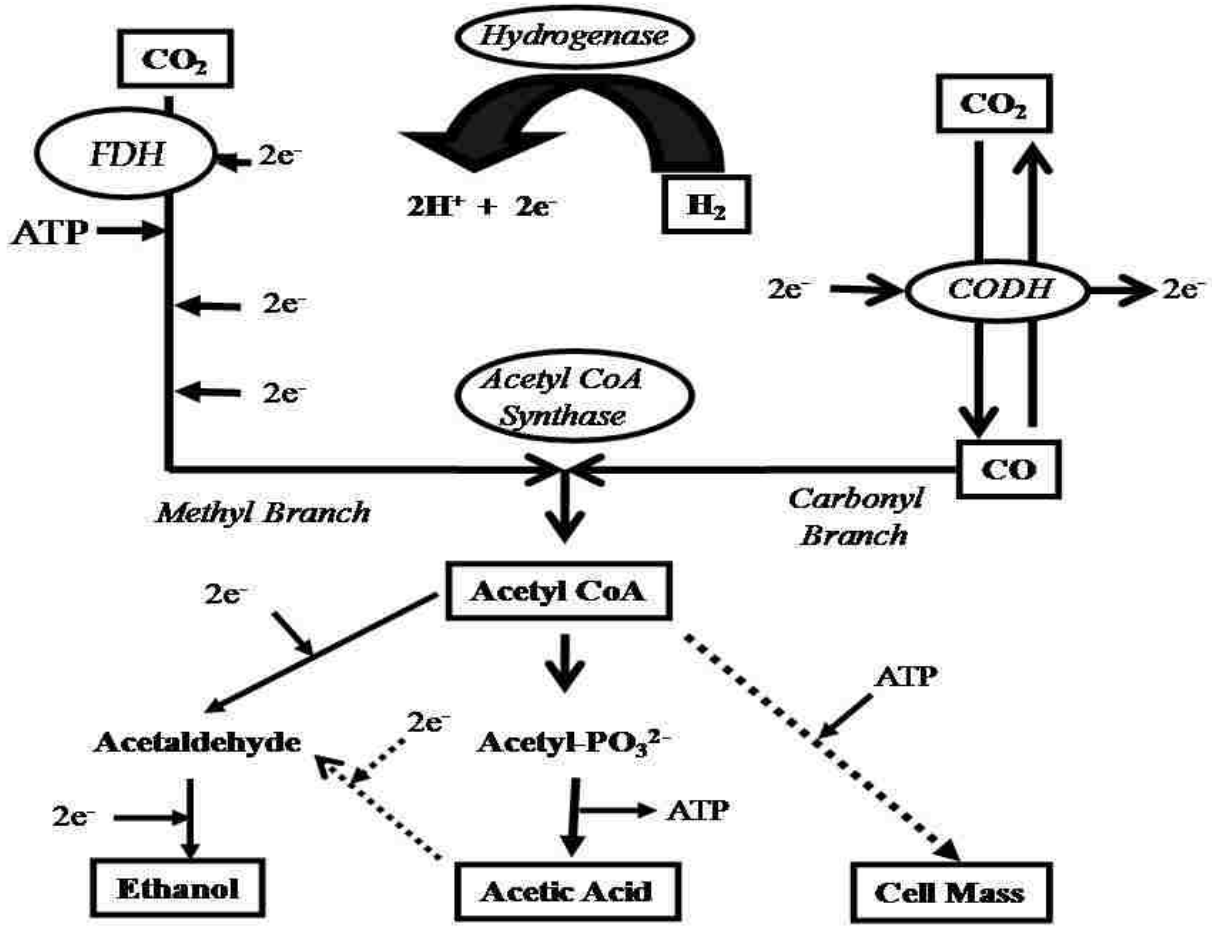

Figure 1-1 - Simplified acetyl-COA pathway[7]

The process would involve the use of an external electricity source to create a voltage potential in a BER containing two chambers that are separated by a cation exchange membrane

(see Figure 1-2). The voltage potential drives the electrolysis of water, which allows electrons to flow from the anode to the cathode, where they are picked up by an electron acceptor or used to form H_2. These electrons are then further shuttled through a microbial pathway to form bioproducts. In the case of the electron acceptor, an electron transport chain is the mechanism by which the electrons enter the microbe and are used to reduce CO_2 into the final products. In the case of H_2, a hydrogenase enzyme within the cell is the mechanism by which the electrons enter the microbe and reduce CO_2 into products. If the external electricity comes from renewable sources, carbon-neutral fuel production or carbon-negative product synthesis is possible.

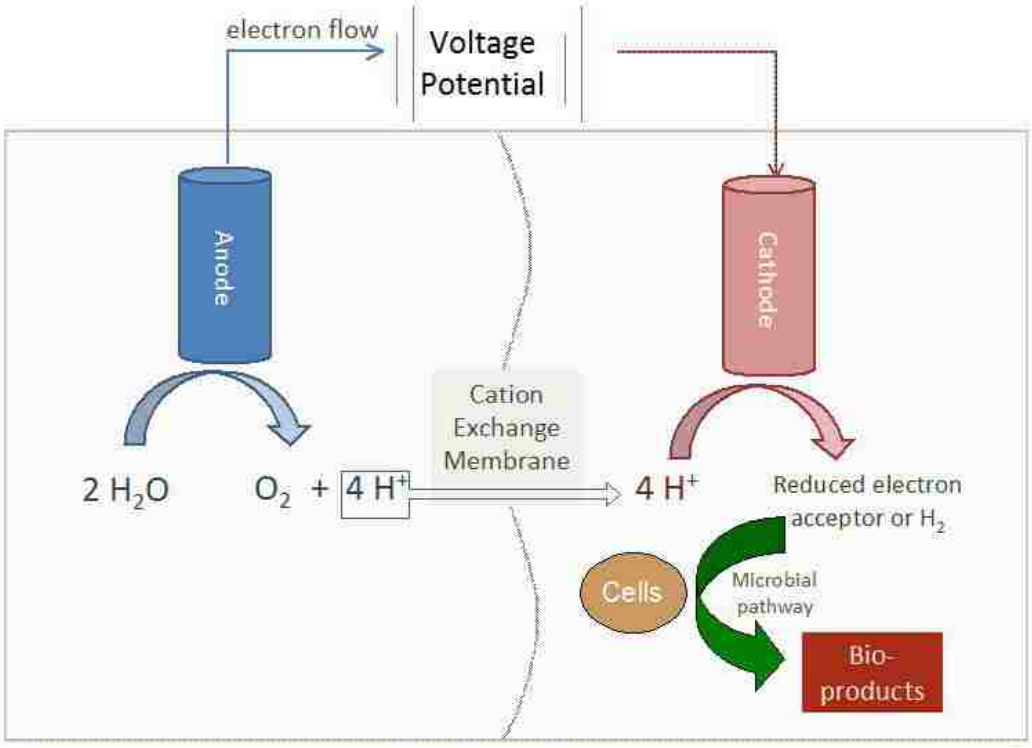

Figure 1-2 - Schematic of bioelectrical anaerobic reactor whole cell system

There are various microbes and various electron acceptors that could accomplish this process. Drawing from previous research performed at Brigham Young University, P11 will act as the example microbe for this system. For purposes of the example reactions below, methyl

viologen (MV) acts as the electron mediator for indirect reduction of $NAD(P)^+$. The following sequence of chemical reactions is provided to illustrate the chemistry involved in using the proposed reactor with this strain of bacteria and electron shuttle molecule to produce ethanol:

- Anodic reaction (generate electrons)

$$6H_2O \Leftrightarrow 12H^+ + 3O_2 + 12e^- \quad (1\text{-}1)$$

- Cathodic reaction (parallel reactions to consume electrons and reduce the electron acceptor)

$$6MV^{2+} + 12\ e^- \Leftrightarrow 6MV^0 \quad (1\text{-}2)$$

$$12e^- + 12H^+ \Leftrightarrow 6H_2 \quad (1\text{-}3)$$

- Further reactions at the cell

$$6MV^0 + 6NAD^+ + 6H^+ \Leftrightarrow 6\mathrm{MV}^{2+} + 6NADH \quad (1\text{-}4)$$

$$2CO_2 + 6NADH + 6H^+ \Leftrightarrow C_2H_5OH + 3H_2O + 6NAD^+ \quad (1\text{-}5)$$

- Total net stoichiometric reaction (with no H_2 formation at the cathode)

$$2CO_2 + 3H_2O \Leftrightarrow C_2H_5OH + 3O_2 \quad (1\text{-}6)$$

The reaction cascade displays the cyclical and regenerative nature of BER chemistry. The electron shuttle molecule (in this case MV), and enzyme cofactor (NADH), are reduced and oxidized with each full cycle, resulting in them neither being consumed nor produced as the reaction takes place. This allows the reaction to theoretically continue indefinitely, although in actual physical systems, some decomposition or inactivation does occur. In addition, the side reaction of forming H_2 at the cathode (Equation 1-3) can reduce the efficiency of the process.

1.5.2 **Examples of Enzymatic Systems**

As previously mentioned, BERs can also work with single enzyme systems or enzyme cascade systems. This removes complexity, allows for better optimization and product isolation,

and is able to provide enantiomeric selectivity, creating a more pure and higher yielding product. The set up would be the same as displayed in Figure 1-2 except that the substrate would have to be added to the cathodic chamber for reduction to form products. The sequence of reactions would be similar as to those listed in Equations 1-1 through 1-6, but the end products could be any bioproduct, not necessarily ethanol. An alternative could also be utilization of a coupled enzymatic oxidative reaction in the anodic chamber, such as glucose dehydrogenase mentioned above in order to provide the necessary electrons for substrate reduction. This improved stereospecificity is even more important for the production of specialty chemicals that would be available in these systems

One example of specialty chemicals that are in high demand and could be created in such a system is statins, which are used to treat dyslipidemias and high cholesterol and other coronary conditions. Atorvastatin (a.k.a. Lipitor) is the top-selling branded pharmaceutical in the world according the Pfizer annual report. One important step in statin synthesis requires attaching the so-called statin side-chain, and the products need to be enantiomerically pure. This can be achieved via classical metal catalysis or via dehydrogenases, with dehydrogenases having added advantages in both selectivity and enantiomeric purity [1, 8].

This enzymatic system relies on electron-shuttling cofactors to accomplish these redox reactions. This example represents only one of the oxidoreductases that could have large significance in the pharmaceutical and fine chemical industries. Therefore, as the BER technology increases, it could mean a significant change in the way these chemicals are produced. The ability to produce these chemicals more efficiently and less expensively could lead to improved treatment and improve quality of life.

1.6 **Research Objectives**

The goal of this research has been to build a prototype reactor for bioelectrical experiments and to obtain the foundational data and preliminary proof-of-concept experiments required in order to fully understand the scope of research that can be done. Two objectives were identified in order to fully achieve this goal, and they are summarized here.

1.6.1 **Objective 1 – Reactor Design**

The reactor design for the scope of this work has to fulfill the two main objectives below. Developing a reactor with sufficient flexibility to be able to run whole cell P11 experiments and kinetic rate experiments with varying electron mediators is the first important task requiring completion before research is able to continue. The reactor has to be sterilizable, have the ability to become fully anaerobic, and requires a number of different gases to which it could be attached. Additionally, for kinetic rate experiments, the reactor has to be attached to a flow-through spectrophotometric system that is also fully anaerobic. Finally, the design has to incorporate temperature control so that temperature could be eliminated as an independent variable in rate data and so that standard cell conditions could be used, the ability for variable stir-rates to occur to check mass transfer assumptions, and the ability to control potential and/or current between each of the cells.

1.6.2 **Objective 2 – Kinetic Modeling of Electron Mediators**

As discussed above in section 1.4, there exist a number of significant problems that make it difficult to directly reduce $NAD(P)^+$ to NAD(P)H. It is therefore of value to get a feel for what options may prove to be the best for indirect nucleotide reduction. Two organic chemicals that

can be used as electron shuttles have been identified and were tested to see which are kinetically favorable. The two selected chemicals were: anthraquinone-2,6-disulfonate (AQDS) and methyl viologen (MV). Two additional chemicals that have been identified for future study but were not analyzed in this work are benzyl viologen (BV), and neutral red [9]. Each of these chemicals has multiple oxidation states and it has been proven that each can play a role in the metabolism of clostridium species [10, 11].

These four chemicals noted above were identified for a number of reasons. First, each of these chemicals has been used in bioelectrochemical experiments in the past, and can easily be found throughout the literature. Also, with the exception of methyl viologen and benzyl viologen, each species has a different functional group that becomes oxidized or reduced (see Figure 1-3). The viologens have two pyridine rings, NR has an amine, and AQDS is a quinone. The selection of both MV and BV was made in order to attempt to quantify any steric affects that would result from the larger benzene rings possibly blocking the active sights. As stated above, BV and NR kinetics are not included in this work.

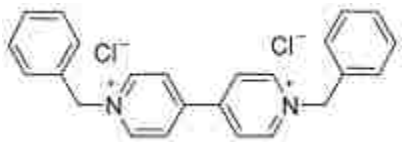

Benzyl Viologen

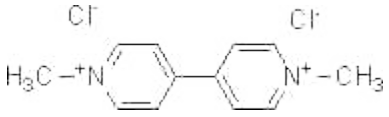

Methyl Viologen

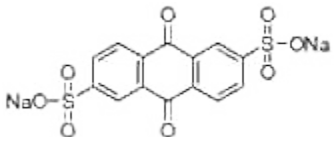

Anthraquinone-2,6-Disulfonate

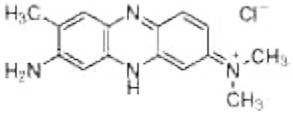

Neutral Red

Figure 1-3 - Structures of selected electron mediators

One additional aspect of the kinetics needs to be explored is the dependence of the rate on the voltage differential between the anode and cathode. A larger voltage potential induces a higher current and greater driving force for reduction at the cathode, which is assumed cause an increase in the observed rate. Increased voltage potential comes at the cost of higher energy costs, so kinetic data will allow for future optimization of what voltage level is required for industrial applications.

One more consideration for kinetic rate data is that the system must not be mass transfer limited if the rate is to be the true rate based on electrode-substrate interaction. The concentration in the bulk must match the concentration at the electrode in order for the model of a continuous stirred-tank reactor to be valid. Different stir rates were tested in order to be certain that this assumption was valid.

2 LITERATURE REVIEW

2.1 Introduction

Processes involving a bioelectrochemical reactor have been around for over thirty years [2], and the ability to create bioproducts from these processes was confirmed at least twenty years ago [3]. The application of this technology is varied, but most recent speculation about their uses has centered around waste treatment [12] [13] and fuel cells [14]. Most studies center around conversion of wastes or inexpensive compounds (e.g. glycerol and glucose) into more useful materials such as hydrogen, ethanol, and electric current. Some kinetic studies have been run on these reactors [15], but much research could still be performed in order to characterize the reactions and mechanisms that take place in these reactors [11].

2.2 Bioelectrical Reactor Design

One of the main focuses of current research in bioelectrical reactors is their actual design. As discussed earlier, the main components of such a reactor are the electrodes and a source, either chemical or electrical, that induces chemical reaction within the reactive medium.

2.2.1 **Electrode Design**

Virtually any conductive material can be used as an electrode. Examples of materials that have been used are carbon [16], titanium [17], platinum [18], stainless steel [19], copper [5], gold [5] and lead [20]. In addition to the wide variety of materials used, they are also found in different configurations and electrode types. Examples of platinum electrodes include wire [18], foil [21], mesh [22], and plate [23]. Titanium electrodes have also been utilized as wires [17] or plates [24]. Iron rods [21] lead plates [20], and stainless steel plates [20], rods [25], and mesh [26] have also been used. Carbon has been utilized in the form of amorphous carbon [16], activated carbon [27], glassy carbon [28], and many forms of graphite, including graphite blocks [29], graphite powder [11], and graphite felt [30].

One of the more interesting and biologically applicable examples of graphite design was performed in an attempt to increase NAD^+/NADH regeneration efficiency. Damian et. al. sputtered gold, copper, and platinum-modified gold onto glass slides [5]. Their work found that the dimerization of NAD^+ was mitigated by the platinum-modified electrode. Dimerization occurs when two NAD radicals combine to form NAD_2, which occurs fairly regularly on both the copper and gold electrodes. Platinum, however, has a very high affinity for hydrogen. It is hypothesized that this increase in adsorbed hydrogen allows for them to be more readily available when an NAD radical is formed. This allows for increased regeneration efficiency from 29.7% on the gold electrode to 63% on the platinum-modified surface.

2.2.2 **Chamber Configuration**

In addition to electrode configuration and materials, the configuration of the reaction vessel is also a subject of research. The main standard for microbial fuel cells and bioelectrical

reactors is a two chambered system with the chambers separated by a membrane [11]. However, there have been other systems developed utilizing a single chamber. These single chamber fuel cells do not require a proton exchange membrane, and are attractive due to their simplicity, low operational cost, and high power density, but have lower coulombic efficiency [31]. Fan's work attempts to overcome this efficiency problem by reducing the internal resistance of the system. There have also been reactor designs that utilize a reaction chamber that is devoid of both membranes and electron mediators [32]. Such systems require direct interaction of the cells with the electrode surface, which has been scientifically proven as feasible in at least one bacteria culture [33].

2.3 **Electron Mediators in Biological Systems**

There have been a large number of studies performed that utilize the electron mediators previously discussed in biological systems. These electron mediators can change the cellular systems where they are found in systems connected to a BER and also in systems that are not providing external electrical stimulation. In either case, they alter the metabolism of the species present. Applications of methyl viologen, neutral red, and anthraquinone disulfonate will be discussed separately.

2.3.1 **Methyl Viologen in Biological Systems**

Methyl viologen has been used in applications involving biological processes to modify or stimulate metabolic function of the cells. Methyl viologen was used in a waste water treatment application in a BER for reduction of toxic trichloroethene to harmless products such as ethene and ethane [28]. Their application used a methyl viologen modified electrode that allowed for the

bacteria to accept the reducing equivalents directly from the electrode surface. This allows for the methyl viologen to be immobilized on the electrode surface, and keeps it from possibly contaminating the waste water. In a product formation application, this approach would keep the product in a purer state.

Methyl viologen has also been used in BER applications in order to enhance and change the yields of the bacteria in the reactors. While not used as the main source of reducing equivalents, it has been shown in *Clostridium acetobutylicum* that fermentation with methyl viologen increased the yield of butanol by 26% while lowering the acetone yield by 25% [34] . In a similar series of studies utilizing the same bacteria, it was shown that methyl viologen addition raised yields of butanol up to 467% at low pH [6]. Additionally, a linear relationship was found between the broth redox potential and the rate of $NAD(P)^+$ reduction by ferredoxin $NAD(P)^+$ reductase [17].

2.3.2 **Neutral Red in Biological Systems**

Neutral red was also used with *C. acetobutylicum* in order to alter the typical metabolic pathway [35]. This study establishes that neutral red can replace ferredoxin in the redox reactions within the cells. While neutral red was introduced into the species, it was not utilized in a BER setup. Similar to the findings with methyl viologen, introduction of neutral red shifted the products from acids to alcohols. It is proposed that the addition of neutral red alters electron flow from hydrogen production to NAD(P)H production, which triggers the change in product distribution.

Extensive work with neutral red in biological systems was performed by Doo Hyun Park. Initial tests utilizing neutral red showed that it can act as an electron channel in *Actinobacillus succinogenese* [36]. The study proves that electrically reduced NR was able to chemically reduce

$NAD(P)^+$. The same group also developed a modified electrode surface with immobilized carboxymethylcellulose that contained covalent bonds to NAD^+, neutral red, and fumarate reductase [37]. Neutral red acted as an electron mediator to reduce NAD^+ and subsequently synthesize fumarate via succinate reduction.

Perhaps the most pertinent study that was performed relative to this work was utilizing neutral red as the sole electron donor for growth and metabolite production in *A. succinogenese* [36]. Neutral red was used in a BER as the sole electron source for bacterial growth and production of methane from CO_2. A voltage potential of -1.5 V was used in these studies. This established that BER technology could be utilized in a setup similar to the one described in chapter 1.

2.3.3 **Anthraquinone-2,6-disulfonate in Biological Systems**

Antrhraquinone-2,6-disulfonate has also been utilized as both an electron mediator and an electron acceptor in biological systems. Its presence has been shown to change the metabolic pathway of anaerobic consortia away from methanogenisis and give a competitive advantage to quinone reducing bacteria [38]. In a separate study, denitrification in two anaerobic consortia was shown to occur in the presence of AQDS as the terminal electron acceptor [39].

AQDS has also been utilized in waste water treatment systems. Its utilization as an electron mediator allowed for perchlorate reduction in a BER system [11]. The reducing equivalents generated from splitting water allowed for reduction of AQDS to AH_2DS, which donated its electrons to the microbial species for perchlorate reduction. The study also described a novel bacteria that was isolated and able to reduce perchlorate in a BER without an electron mediator. It is hypothesized that this may be due to utilization of hydrogen generated at the cathode surface.

2.4 **Possible BER Product Formation Applications**

It has been well established that product formation is possible in BER systems, but it is important to point out how many various reactions actually could utilize such a system and to what effect they could be utilized. Oxidoreductases – enzymes that are involved in either oxidation or reduction reactions – perform many reactions that are of great importance to the medical and specialty chemical industries, as well as the energy and environmental industries. This section will describe reactions which could benefit from utilization of BER technology.

Chemical syntheses include xylitol production from xylose [9]. Xylose reductase is able to take the sugar xylose, which can be isolated from wood, and reduce it to xylitol, a specialty chemical that is used as a sweetener. This is an example of a specific product that could be formed inside a BER. There are also a wide number of intermediates within the chemical industry that would benefit from this technology. BER technology could be easily utilized to create optically pure keto alcohols [40]. These compounds are important building blocks in the fine chemical and pharmaceutical industry [41] [42]. What is unique about these active compounds is that when they are prepared by enzymatic systems, the stereochemistry of the product can be controlled, with extremely high yields achievable.

Another very important potential product that could benefit from BER technology is the production of statins, a class of drugs that are utilized to lower cholesterol. Biocatalysis can be used to create the statin side chain [1] (Asako, Shimizu et al. 2009). The statin side chain creation is one of the key steps in the formation of statin drugs, and also must be enantiomerically controlled, which it can be through biocatalysis. Many other possible applications exist, including the reduction of alpha-halo ketones [43] as well as enentioselective keto-reductions, racemizations, stereoinverstions, and imine reductions [44]. A host of other

compounds that could be synthesized in electroenzymatic systems can be found in Kohlmann's review [4]

2.5 **Other BER Applications**

There are many other uses for BER technology besides product formation. The flexibility of the BER lends itself to many different applications. Two that have been the subject of much research are waste water treatment and microbial fuel cells. Waste water has a host of toxic chemicals that can be either reduced or oxidized to remove their toxicity. Microbial fuel cells and microbial electrolysis cells may also become a future outlet for energy storage and advanced biological batteries. Some work on these applications is described here.

2.5.1 **Waste Water Treatment**

Waste water contains contaminants which can be dealt with by application of BER technology. AQDS, as mentioned above, was instrumental in a study involving perchlorate reduction [11]. There are many similar applications of reduction to waste water that remove harmful contaminants. Some of these applications involve electron mediators, such as Thrash's work, while others did not involve electron mediators. Denitrification is a common application. The concept of denitrification has been studied in depth. It was found that, as would be expected, higher current led to greater denitrification [27]. This same work also established that denitrification rates were affected by the oxygen and hydrogen supplied through electrolysis. Long term studies have also been performed to verify the industrial applicability of waste water denitrification by electrochemical means, some studies even going as long as a full year [16] [24].

On the opposite side of the reaction, oxidation reactions can also prove meaningful in waste water treatment. Where reduction reactions require energy input in order to remove the contaminants, oxidation reactions supply energy that can be harvested in another form. One such example is the conversion of glycerol waste from biodiesel productions into hydrogen and ethanol by means of bioelectrochemical cells utilizing thionine as an electron mediator [12]. Such applications take contaminants and unwanted products and convert them into useful end products. This form of waste water treatment, while exciting in its nature, still has a number of key challenges that remain before industrial implantation [45].

2.5.2 **Microbial Fuel Cells and Microbial Electrolysis Cells**

The topic of microbial fuel cells is broad, and its applications are immense. Microbial fuel cells are able to generate current from decomposition of organic molecules. Microbial Electrolysis Cells utilize the same technology, but produce methane or hydrogen from the organics. The above reference of ethanol and hydrogen production from glycerol is an example of a microbial electrolysis cell. There is much excitement over this technology as its commercialization could mean another energy source, and one that could be predominantly supplied by renewable resources.

The principle organic substance used in most early electricity-generating experiments was sugars. Sugars have very high energy density and can be utilized by most microbes. Many small-scale fuel cells have been built that allow bacteria to feed off the glucose, sending the reducing equivalents through a BER and harnessing the current. Although research has been going on in these areas for long periods of time [3] [46], there is still a great deal of research that needs to be performed before large-scale commercialization. Improved efficiency and lower-cost reactors are constantly being studied, some even able to achieve sustained power generation in

passive and quiescent conditions [14]. Most recent work, like the study cited above, are into the field of waste water treatment, industrial sludge, or biodegradable wastes, since these sources are extremely low cost and have environmental remediation benefits in addition to the value of the products produced [47].

2.6 **Chapter Summary**

This chapter began by analyzing work on the physical design of BER technology. This included a look into the materials utilized in the electrodes as well as differences in the design of one and two chamber designs. It also included a description of systems devoid of a membrane, and their strengths and weaknesses. This was included to provide a framework for the design of the reactor used in these experiments, and to provide a wider view for possible future reactor design.

Next, the utilization of electron mediators in biological systems was covered. This included examples of their use in BER systems and their use in non-BER systems. These descriptions provide context for the future kinetic experiments described later in Chapters 4 and 5. Additionally, they establish the role of these mediators in future biological experimentation, including possible future work with P11 or other bacteria.

Finally, applications of BER technology were covered. This included a description of important products that could be formed by application of BER systems with oxidoreductases. Furthermore, its application into waste water treatment and microbial fuel and electrolysis cells was described. These provide important context as well as suggest areas to which the research that is described in this work could be applied.

The research presented in this thesis will address the lack of engineering analysis regarding the use of electron mediators. While many studies have been performed which analyze the effects of electron mediators on biological systems, many of these studies report observations without any critical thinking or analysis of the kinetics and thermodynamics of the observed phenomena. The work contained in this thesis will provide depth to the understanding of the mechanisms of electrode kinetics and give background and understanding for future application of BER technology to microbial and enzymatic systems.

3 FOUNDATIONAL WORK WITH P11

3.1 Thermodynamic Calculations

One aspect of microbiology that is rarely covered in academic papers is thermodynamics. Thermodynamics allows some insights that help to explain the phenomena that are seen as data is reported and collected. As this project moved forward, it became important for us to assess the feasibility of future industrial utilization of BER technology. Specifically, what yields are possible in a system that employs only small concentrations of slightly soluble electron mediators in place of gaseous electron donors.

Oxidation-reduction reactions are unique in that they are based on the sum of two individual half-reactions. The convention for all half reactions is to write the oxidized species and electrons on the reactant side of the chemical equation, with the reduced species on the product side of the equation as follows, where Ox represents the oxidized species, Rd represents the reduced species, and n is the number of electrons consumed for the reduction.

$$Ox + ne^- \Leftrightarrow Rd \tag{3-1}$$

Each half-reaction is assigned a standard potential (E_{red}^0) based off of the standard Gibb's energy (ΔG^0) according to Equation 3-1:

$$\Delta G^0 = nFE^0 \tag{3-2}$$

where F in Equation 3-1 is the Faraday constant, which is equal to 96,485 coulombs/mole, and n is the number of electrons generated in the case of reduction, or consumed in the case of oxidation. Standard potentials are only true at pH 7 and 25 °C and for standard concentrations (typically 1 mol/liter for aqueous species and 1 bar for gaseous species, although different standards do exist). Although the convention is to write the reactions proceeding from the oxidized state to the reduced state, if two half reactions are coupled, one of them is, in actuality, proceeding from the reduced state to the oxidized state. In this case, when the reaction is written backward, the sign of the reduced standard potential (E_{red}^0) is switched to become the oxidized standard potential (E_{ox}^0). Mathematically, this equality is stated here in Equation 3-3.

$$E_{ox}^0 = -E_{red}^0 \tag{3-3}$$

The standard potential for the full reaction (E^0) is then defined as the sum of the reduced and oxidized standard potentials, as seen here.

$$E^0 = E_{red}^0 + E_{ox}^0 \tag{3-4}$$

This standard potential can then be adjusted to the actual potential (E) of the given system by utilization of the Nernst Equation (Equation 3-5).

$$E = E^o - \frac{RT}{nF} \ln\left(\frac{\prod a_p^{\nu}}{\prod a_r^{\nu}}\right) \tag{3-5}$$

In Equation 3-5, R is the ideal gas constant, T is the system temperature, n is number of electrons generated or consumed, F is the Faraday constant, a_p is the activity of the product species, a_r is the activity of the reacting species, and ν is the chemical coefficient obtained from the balanced chemical reaction. It should be noted that the activity of water is unity, the reference state for H^+ is pH 7, the reference state for a gas is 1 bar, and the reference state for other species is 1 M. Any two half-reactions can be coupled, and the reaction will proceed until equilibrium is

achieved. This occurs mathematically when the actual potential (E) according to the Nernst Equation equals zero. This is achieved by varying the concentrations of the unknown products or reactants accordingly to achieve equilibrium.

As shown in Appendix I, equilibrium concentrations were predicted for ethanol formation using various electron mediators to assess equilibrium constraints for an electron mediator process. In the P11 system, the overall products are ethanol and acetic acid. For illustrative purposes, only calculations for ethanol are shown. If CO_2 is the only carbon source, the half-reaction leading to ethanol formation is:

$$2CO_2 + 12H^+ + 12e^- \Leftrightarrow C_2H_5OH + 3H_2O \quad (3\text{-}6)$$

This reaction has a calculated standard potential of E^0_{red} = -323 mV (see Appendix I). The standard potential (E^0_{red}) for $MV^{2+} \rightarrow MV^+$ is -446 mV, $BV^{2+} \rightarrow BV^+$ is -360 mV, AQDS is -184 mV, and NAD^+ is -320 mV [48, 49]. Since the electron mediators donate the electrons, $E^0_{ox} = -E^0_{red}$ is used for the mediator. Thus, if one wants the equilibrium ethanol concentration in a pH 7 (reference state for H^+) aqueous solution to be 1 mol/liter, the ratio of reduced electron mediator to oxidized electron mediator has to be adjusted in Equation 3-5 until the potential (E) equals zero.

Table 3-1 shows a summary of the ratio of reduced electron mediator/oxidized electron mediator required for each of the electron mediators that were just mentioned to achieve 1 mol/liter ethanol at pH 7 and a CO_2 partial pressure of 1 bar. A quick glance at these values makes it immediately apparent that thermodynamics play a large role in determining how feasible these electron donors are. With MV, only one of every 130 molecules needs to be reduced in order to be in equilibrium with 1 mol/liter of ethanol, whereas with AQDS, 2,470,000,000 of every 2,470,000,001molecules need to be in its reduced state to achieve the

same equilibrium conversion. Thus, MV is more thermodynamically favorable for coupling with CO_2 to form ethanol. AQDS is the least thermodynamically favorable of the species in Table 3-1.

Table 3-1 - Thermodynamic calculated ratio

Electron Mediator	**Required Ratio**
Methyl Viologen	7.68E-03
Benzyl Viologen	0.24
NADH	1.254
AQDS	2.47E+09

3.2 H_2 CO_2 Study

3.2.1 Introduction

In order to establish the capability of P11 for utilization in a BER, it needed to be established that CO was not a necessary component for bacterial growth and product formation. This was a key step in determining the feasibility of possible production of carbon-neutral fuels via a fermentation process. Additionally, if growth is not viable without CO, it may be possible to grow cells with syngas then switch to product formation with a BER with the mature cells. This experiment was designed to answer both of these questions.

3.2.2 Materials and Methods

The recipe for cell broth media is contained in Table 3-2 through 3-7. The media for cell growth is prepared by mixing together all the ingredients listed in Table 3-2, with the exception of cysteine sulfide solution. The pH of this mixed solution is then adjusted to 6.0 using 5N

potassium hydroxide solution. The media is then distributed into 250 mL bottles (Wheaton) for passaging and for experimentation. Three passage bottles are prepared with approximately 30 mL of media solution, while the experiment bottles have approximately 50 mL per bottle. In order to provide the anoxic environment required for cell growth, the bottles are brought to a boil and allowed to boil for 5 minutes while the liquid is continuously purged with N_2 gas. #1 Rubber stoppers and metal caps (Wheaton) are immediately placed to seal the bottles in their anoxic state. Purging the liquid with N_2 at high heat ensures that all dissolved O_2 in the media is purged from the system. The headspace above the liquid is then cyclically vacuumed and subsequently filled with ~20 psig N_2 through a 22-guage needle inserted through the rubber stopper. This cycle is repeated three times to remove any oxygen that may have been introduced during the sealing and capping process. At this point the cysteine sulfide (1 mL for every 100 mL of media present) is injected by a syringe through the rubber stopper and acts as a final O_2 scavenger. The bottles are then placed in an autoclave for 15 minutes at 121 °C. Bottles are allowed to cool to room temperature of their own accord, removed from the autoclave, and refrigerated until inoculation.

Inoculation of P11 (*Clostridium ragsdalei*) occurs from source bottles originally obtained from Dr. Ralph Tanner of the University of Oklahoma. Passaging bottles are purged with syngas (30% H_2, 30 % CO_2, and 40% CO) up to ~20 psig, heated to 37 °C in a shaking incubator and inoculated with 10% volume of P11 inoculum (e.g. 3 mL of 0.6 optical density solution in 30 mL passage bottle). The first passage is inoculated and allowed to grow until it has reached the exponential growth phase, at which point it is used as the inoculum for the second passage bottle. This process repeats for the third passage bottle, which is used as the inoculum for the experiment bottles.

Table 3-2 - Media composition per liter

Component	Amount
Mineral Solution (Table 3-3)	25 mL
Calcium Solution (Table 3-4)	10 mL
Metals Solution (Table 3-5)	10 mL
Vitamin Solution (Table 3-6)	10 mL
Cysteine Sulfide Solution (Table 3-7)	10 mL
MES Buffer	10 gm
Resazurin	10 drops
Yeast Extract	0.5 gm

Table 3-3 - Mineral solution

Component	Product #	Company	gm/L
Magnesium Sulfate Heptahydrate	M-1880	Sigma	20
Potassium Chloride	P-5405	Sigma	10
Potassium Phosphate Monobasic	P-5655	Sigma	10

Table 3-4 - Calcium solution

Component	Product #	Company	gm/L
Calcium Chloride Dihydrate	C-3881	Sigma	10

Table 3-5 - Metals solution

Component	Product #	Company	gm/L
Nitrilotriacetic Acid	N-9877	Sigma	2
Manganese (II) Sulfate Monohydrate	221287	Sigma	1
Cobalt (II) Chloride Hexahydrate	202185	Sigma	0.2
Nickel (II) Chloride Hexahydrate	223387	Sigma	0.2
Sodium Selanate, Anhydrous	S-8295	Sigma	0.1
Ammonium Iron (II) Sulfate Hexahydrate	F-3754	Sigma	0.8
Zinc Sulfate Heptahydrate	221376	Sigma	1
Sodium Molybdate Dihydrate	331058	Sigma	0.02
Sodium Tungstate Dihydrate	223336	Sigma	0.2

Table 3-6 - Vitamin solution

Component	Product #	Company	gm/L
p-(4)-Aminobenzoic Acid	A-9878	Sigma	0.005
d-Biotin	B-4639	Sigma	0.002
D-Pantothenic Acid Hemicalcium Salt	P-5155	Sigma	0.005
Folic Acid	F-8758	Sigma	0.002
MESNA (Sodium 2-Mercaptoethanesulfonate)	M-1511	Sigma	0.01
Nicotinic Acid	N-0761	Sigma	0.005

Table 3-6 - Vitamin solution

Pyridoxine Hydrochloride	P-9755	Sigma	0.01
Riboflavin	R-9881	Sigma	0.005
Thiamine Hydrochloride	T-4625	Sigma	0.005
Thioctic Acid (Lipoic Acid)	T-1395	Sigma	0.005
Vitamin B-12	V-2876	Sigma	0.005

Table 3-7 - Cysteine sulfide solution

Component	**Product #**	**Company**	**gm/L**
Sodium Sulfide Nonahydrate	S2006	Sigma	40
L-cysteine	C7352	Sigma	40

Experiment bottles were prepared in three groups which differed only with regards to the gas composition in the headspace as described here:

Group 1: Control – This group was purged with syngas

Group 2: Syngas switching to H_2 and CO_2 balance N_2 – This group was purged with syngas during the growth phase, and a mixture of 30% H_2, 30% CO_2, and 40% N_2 after the growth phase was completed

Group 3: H_2 and CO_2 balance N_2 – This group was purged with a mixture of 30% H_2, 30% CO_2, and 40% N_2

Each group was run in triplicate and gas purging occurred approximately every two days. Before gas purging, total gauge pressure of the headspace above the cell broth, a gas sample, and

a liquid sample were taken. Optical Density was taken at 660 nm using a Shimadzu PharmaSpec UV-1700 to measure cell growth. The pH of the liquid sample was then measured using an Oakton pH meter. The liquid samples were then spun in a Labnet Spectrafuge for 14 min at 13,000 rpm. The supernatant was removed and frozen for subsequent analysis in a flame ionization detector Shimadzu gas chromatograph. Gas samples were analyzed immediately in a thermal conductivity detector Shimadzu gas chromatograph. The gas composition analysis combined with the total pressure readings allowed us to calculate gas utilization by the cells. Additionally, group 2 was switched from syngas to the H_2, CO_2, N_2 mixture at day 7.8, the fifth data point in each graph.

3.2.3 **Results**

Experimental data can be found in Figures 3-1 through 3-5. Figure 3-1 shows the optical density readings (proportional to cell concentration) at 660 nm, indicating rate of cell growth. As can be seen, both group 1 and group 2 experienced an exponential growth phase as expected followed by a stagnation phase. Growth in group 3 growth, however, was significantly slower than growth in the other groups and showed no exponential behavior, but rather almost steady-state growth across the entire course of the experiment.

Figures 3-2 and 3-3 show total formation and per cell formation of ethanol and acetic acid over the course of the experiment. The data show that total ethanol formation was greatest in group 1, while group 3 actually produced the most acetic acid by the end of the experiment (although the rate was slower). Interestingly, almost no ethanol production occurred in group 2 once it was switched onto the gas mixture that contained no CO, although acetic acid formation seems to have continued. Figures 3-4 and 3-5 indicate that on a per cell basis, group 3 outperforms both group 1 and group 2.

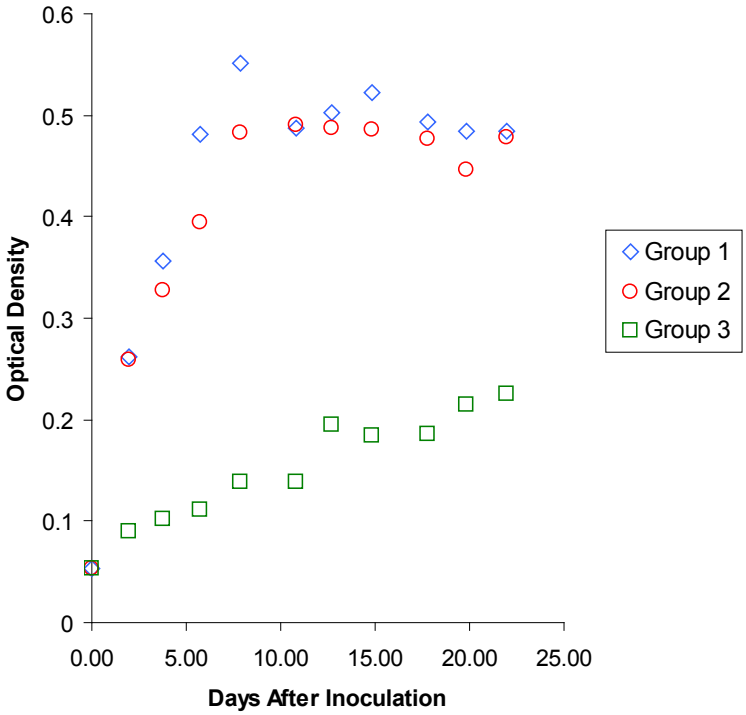

Figure 3-1 - Optical density of cells

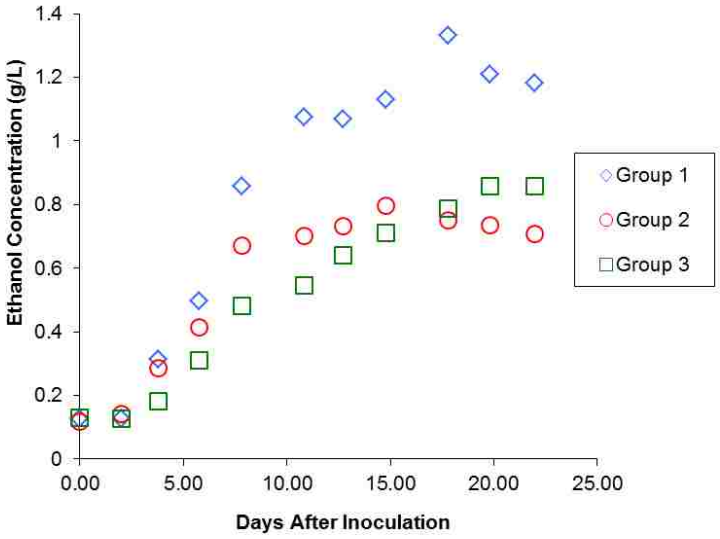

Figure 3-2 - Total ethanol concentration

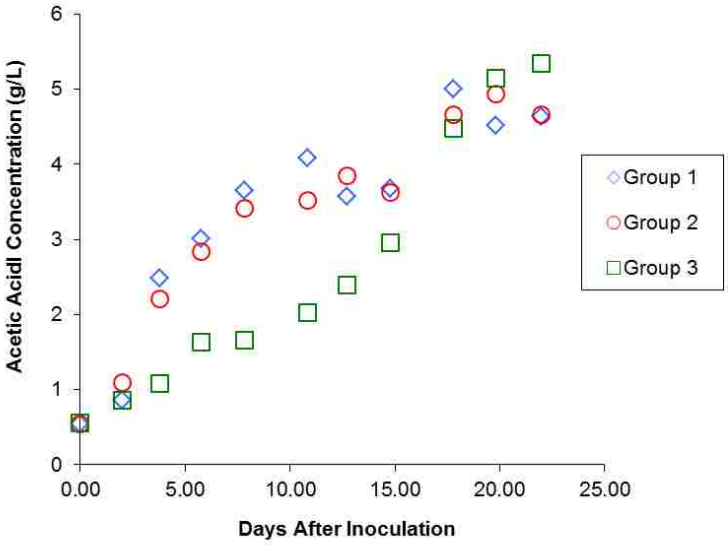

Figure 3-3 - Total acetic acid concentration

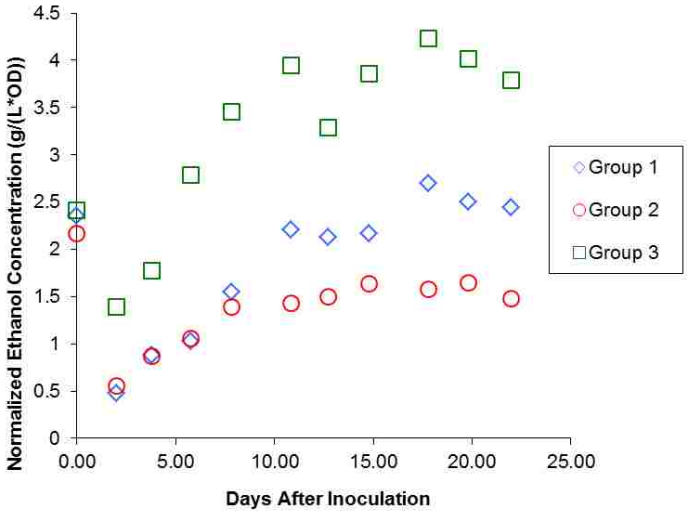

Figure 3-4 - Ethanol concentration normalized by optical density

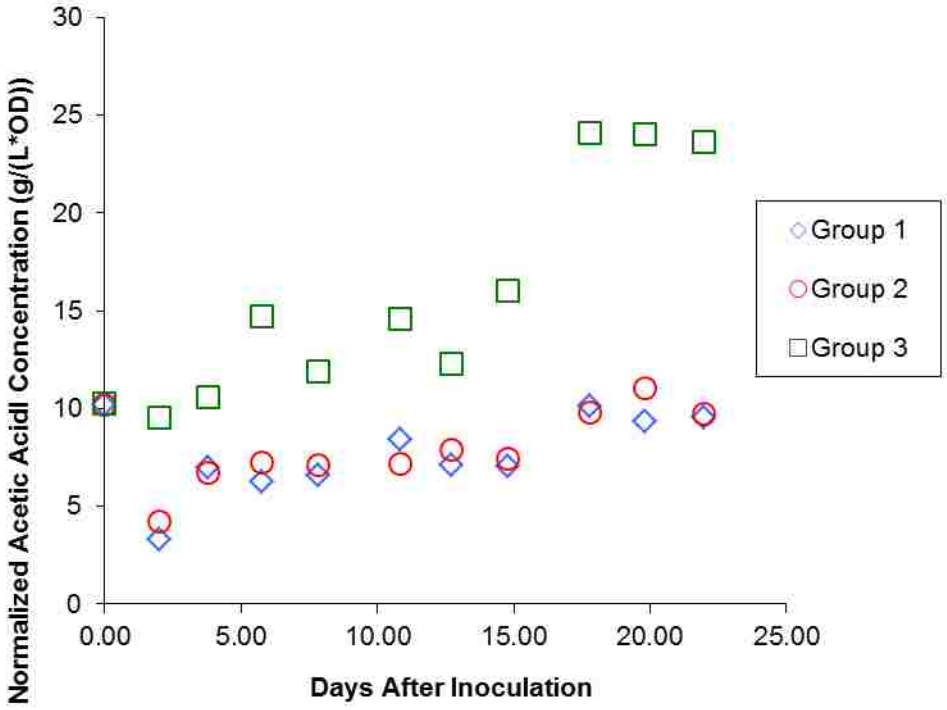

Figure 3-5 - Acetic acid concentration normalized by optical density

3.2.4 **Discussion**

The first and most important observation is that growth can indeed occur even without the presence of CO in the headspace gas. This result further fuels the feasibility of BER application to P11. Growth was significantly slower than in the reactors with syngas. Groups 1 and 2 showed very similar growth data, which should be expected since they were both fed the same gas through the growth phase.

Upon further investigation of the full acetyl-COA pathway shown in Figure 1-1, it can be seen that the first step of the methyl branch requires the reduction of CO_2 to formate. This is a very energetically unfavorable step, having a standard potential of -579 mV. If we analyze the thermodynamics, we find that if this reaction is coupled with the oxidation of CO to CO_2, and partial pressures are assumed to be equal to their value directly after regassing (13.6 psia for CO

and 10.2 psia for CO_2), the equilibrium concentration of formate is 2.3×10^3 g/L (see Appendix I for all thermodynamic calculations). Since gas is consumed over the course of the experiment, the same calculation was also performed with the partial pressures measured just before regassing. At these lower gas partial pressure conditions, an equilibrium formate concentration of 6.04×10^2 g/L was calculated. Coupling the CO_2 to formate reaction with the oxidation of H_2 to $2H^+$ at regassing conditions results in an equilibrium formate concentration of 9.2×10^{-5} g/L at any pH. At the partial pressures measured just before regassing, the equilibrium formate concentration is 2.6×10^{-5} g/L. Thus, the formate concentration in equilibrium (which is hypothetical since formate will be used in the metabolic pathway) with the CO to CO_2 half-reaction is 10^7 times greater than the formate concentration in equilibrium with the H_2 to H^+ half-reaction. This magnitude was essentially independent of whether the partial pressure at regassing was used or the partial pressure before regassing was used. If there is no CO in the headspace, then the carbonyl branch requires reduction of CO_2 to CO before formation of acetyl-COA can occur. The equilibrium partial pressure of CO that is coupled with the oxidation of H_2 to $2H^+$ is only 3.7×10^{-8} atm at regassing conditions and 1.0×10^{-8} atm at conditions prior to regassing. Thus, very little CO is available for product formation if H_2 is the sole source of reducing equivalents. The above analyses show that the absence of CO would lead to slower growth.

It is valuable at this juncture to point out that these concentrations are the absolute highest concentrations achievable at equilibrium, and that actual concentrations should be less. This probably explains the slow growth experienced by Group 3. It seems logical that the rate limiting step in this system is either reduction of CO_2 to formate or CO_2 to CO, since both are so energetically unfavorable. The concentrations of both formate and CO would be so low that it

seems once they are made they are immediately used. This could also provide an explanation for the almost steady-state growth increase seen in Group 3 of Figure 3-1. In a typical bacterial batch system such as Groups 1 and 2, where reactants are readily available, kinetics allow for exponential growth followed by a transition to a stationary phase [50]. The bacteria in Group 3 seem to be limited by available reactants rather than by metabolic pathway kinetics. If the availability of reactants is low and almost constant, then the rate-limiting step causes all other reactions to proceed at steady-state, causing consistent, but slow and non-exponential growth.

Product formation of Group 3 is very promising. On a per cell basis, Group 3 almost doubles the ethanol production of Group 1 and almost triples the acetic acid production of the other two groups. Group 2 product formation lagged that of Group 1, suggesting that a switch from syngas to CO-free gas did not result in additional product formation. This was also confirmed by gas samples which showed virtually no gas utilization in Group 1 or Group 2 after the switch was made (see Figure 3-6). The increase in product formation in Group 3 may be due to the lack of CO, which has been shown to be an inhibitor of hydrogenase [51]. A correlation has been shown to exist in P11 between hydrogenase activity and ethanol production [7], so removing a known hydrogenase inhibitor, and thereby increasing hydrogenase activity, could lead to additional product formation.

3.2.5 **Conclusions**

This study included very important findings for the work of this thesis. First, it established that bacterial growth of P11 is not completely dependent on the presence of CO. Group 3 was able to show sustained growth, albeit at a lower rate, with CO_2 as the only sustained source of carbon for cellular growth. Second, it also established that growth is possible with an electron donor that is not CO. Since CO can act both as a carbon source and an electron source, it

was important to establish that neither of these roles was absolutely vital to growth and product formation. If either growth or product formation was dependent on the presence of CO, there would be no possible way for a BER to create products utilizing P11 with an induced voltage potential as the source of electrons and CO_2 as the only carbon source, as was postulated in Chapter 1.

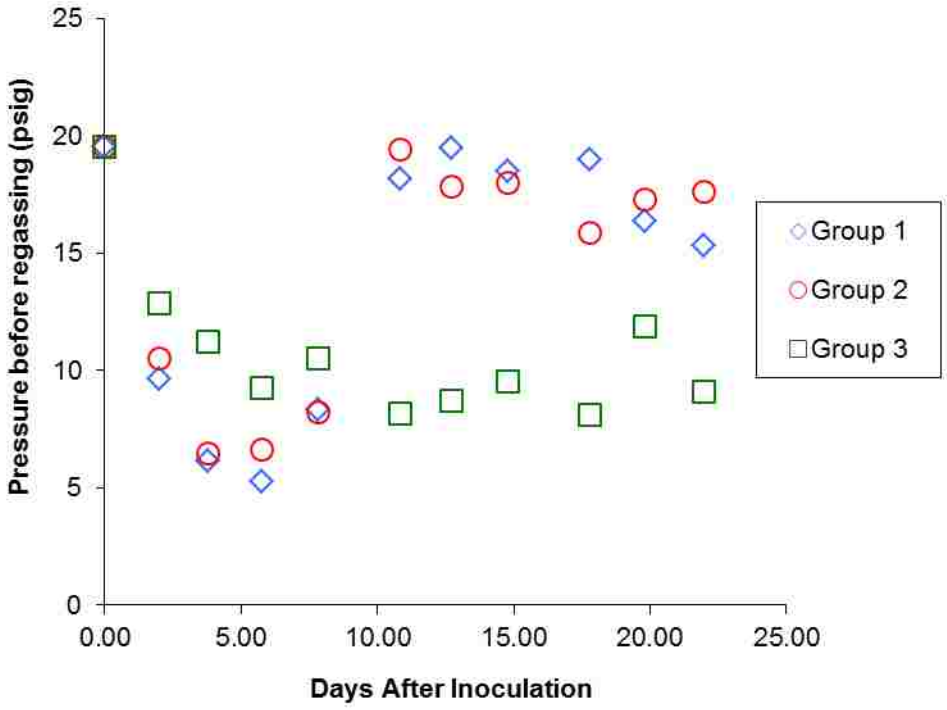

Figure 3-6 - Gauge pressure in bottles before purging and regassing to 20 psig

One other interesting piece of data was the increased product formation in the slowly growing Group 3. On a per cell basis, it widely outperformed both Group 1 and Group 2. This means that there exist possible opportunities for greater product formation than has been seen in standard bottle reactors. One explanation could be the previously mentioned link between ethanol production and hydrogenase activity. Future research could shed more light on additional reasons for this observed phenomenon.

4 KINETIC MODELING OF ELECTRON MEDIATOR REDUCTION

4.1 Introduction

One of the most important aspects of proving out the concept of the BER reactor is to quantify the rate at which reduction of the electron mediator occurs. In the pathway necessary to reduce suitable electron acceptors into more desirable products, there are two main reactions which occur. The first is the reduction of the electron mediator at the electrode. The second is the reduction of the reactant to product. As most enzymes are highly efficient in substrate reduction, and this reaction occurs at very fast rates, it becomes important to characterize the rate of reduction at the electrode surface because in many instances this could become the rate-limiting step.

Developing a model to characterize the mechanism and rate at which this reduction occurs becomes a central and imperative portion of this research. Once the rate law is defined and understood, optimization of the reactor design becomes possible. Key factors that affect the rate can be characterized and understood, allowing for more efficient reactor design and utilization of all available resources for further development of BER applications.

4.2 Kinetic Model Development

4.2.1 Three Step Mechanism

There are three main steps along the path to reduction of the electron mediator once the individual molecules are dissolved in the bulk solution of the chamber. In order for reduction to occur, the dissolved molecules must adsorb to the surface of the electrode to facilitate electron transfer. Once adsorption to the surface occurs, the surface reaction must take place, during which the oxidized electron mediator is reduced via electron transfer from the anode surface. The final step of reduction is for the now reduced species to desorb from the electrode surface back into the bulk solution.

In summary, in the three step process, a generic electron mediator, A, undergoes adsorption onto the electrode surface. This adsorbed mediator will be referred to as A*. The accompanying reaction of this first step is written in this work as follows:

$$A \leftrightarrow A^* \tag{4-1}$$

The second step in the mechanism is direct reduction of the adsorbed oxidized species A* to its reduced form, which is referred to as B*. The accompanying reaction of the second step is written in this work as follows:

$$A^* \leftrightarrow B^* \tag{4-2}$$

The third and final step is desorption of the adsorbed reduced species B* back to the bulk in its final dissolved state, B. The accompanying reaction of the third step is written in this work as follows:

$$B^* \leftrightarrow B \tag{4-3}$$

This three step mechanism and the corresponding reactions are visually represented below in Figure 4-1.

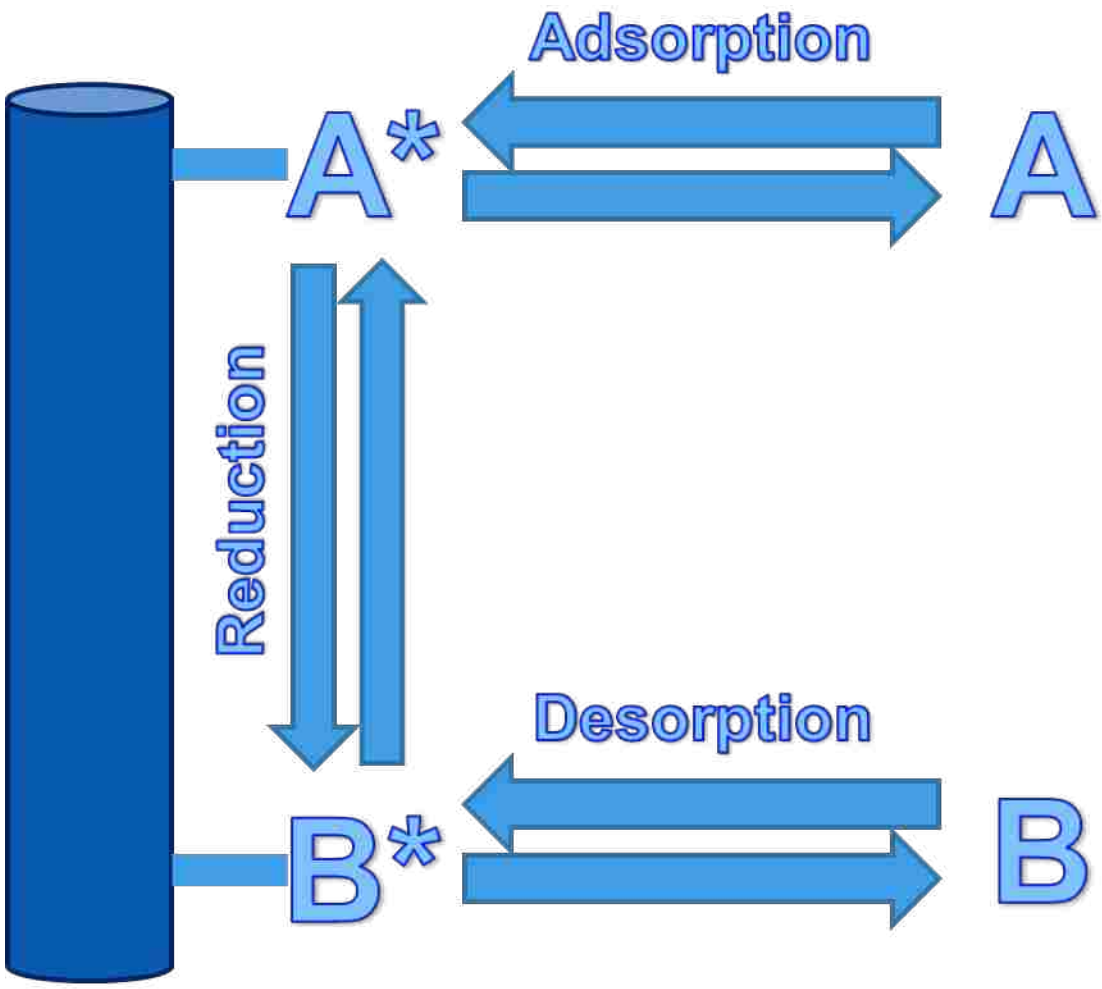

Figure 4-1 - Visual representation of the three step mechanism

4.2.2 Kinetic Definition of the Three Step Mechanism

Each of these reaction steps can be described using a kinetic rate law. The rates in each of these fundamental 3 steps can each be described by a separate rate law. The rate of adsorption can be characterized as follows:

$$r_a = k_{A,a}(C_A \cdot C^*) - k_{A,d}(C_{A^*}) = k_{A,a}(C_A \cdot C^* - \frac{C_{A^*}}{K_a}) \quad (4\text{-}4)$$

where r_a is the rate of adsorption, $k_{A,a}$ is rate constant of the rate of adsorption of A, $k_{A,d}$ is the rate constant of the reverse rate of adsorption of A, otherwise known as the rate of desorption of A, K_a is the adsorption equilibrium constant for A ($k_{A,a}/k_{A,d}$), C_A is the moles of species A per unit reactor volume, C^* is the moles of free surface sites per unit reactor volume, and C_{A*} is the moles of adsorbed A on the surface of the electrode per unit reactor volume.

The rate law corresponding to the surface reaction, during which the reduction of A* to B* occurs on the surface of the electrode, is written as follows:

$$r_{sr} = k_{A,sr,f}(C_{A^*}) - k_{B,sr,r}(C_{A^*}) = k_{A,sr,f}(C_{A^*} - \frac{C_{B^*}}{K_{sr}}) \quad (4\text{-}5)$$

where r_{sr} is the rate of the surface reaction, $k_{A,sr,f}$ is the rate constant of the forward rate of reaction for A*, which can also be described as the rate of reduction, $k_{B,sr,r}$ is the rate constant of the reverse rate of reaction, which can also be described as the rate of oxidation, K_{sr} is the surface reaction equilibrium constant ($k_{A,sr,f}/k_{B,sr,r}$), and C_{B*} is the moles of adsorbed B on the electrode surface per unit reactor volume.

The rate of desorption is described as follows:

$$r_d = k_{B,d}(C_{B^*}) - k_{B,a}(C_B \cdot C^*) = k_{B,d}(C_{B^*} - K_r C_B \cdot C^*) \quad (4\text{-}6)$$

where r_d is the rate of desorption, $k_{B,d}$ is the rate constant of desorption, $k_{B,a}$ is the rate constant of the reverse rate of desorption, otherwise known as the rate of adsorption, K_r is the adsorption equilibrium constant for B ($k_{B,a}/k_{B,d}$) and is equal to $1/K_d$ where K_d is the desorption equilibrium constant, and C_B is the moles of species B per unit reactor volume. The adsorption equilibrium constant is used instead of the desorption equilibrium constant by convention.

4.3 Combined Rate Law

4.3.1 Diffusion Assumption

There is one assumption that is already included into the three-step mechanism above. One might notice the negligence of any bulk diffusion to the electrode surface and away from the electrode surface. This is manifest in the rate laws by using the bulk concentration of the reactant and product as the concentration present at the electrode surface. Exclusion of diffusion from the rate law can be justified due when sufficient continuous stirring occurs within the reaction chambers. It can therefore be assumed that the concentration at the surface of the electrode is the same as the bulk concentration. This assumption was experimentally tested and verified by modifying the stirring rate in the reactor and measuring the kinetics.

4.3.2 Derivation of a Combined Rate Law

Characterization of the entire kinetic process is therefore a combination of each of the three consecutive rate steps. In order to arrive at such an expression, the rates of change of each individual species for a well-mixed batch system are defined using the rate laws set forth in Equations 4-4, 4-5, and 4-6.

$$\frac{dC_A}{dt} = -r_a \tag{4-7}$$

$$\frac{dC_{A^*}}{dt} = r_a - r_{sr} \tag{4-8}$$

$$\frac{dC_{B^*}}{dt} = r_{sr} - r_d \tag{4-9}$$

$$\frac{dC_B}{dt} = r_d \tag{4-10}$$

At this point, a steady-state approximation for the intermediate adsorbed species is utilized. It seems reasonable to assume that this would hold true no matter which step is rate limiting. If adsorption is the rate limiting step, then the surface reaction would occur immediately upon absorption, thus keeping the rate of change of absorbed A and absorbed B constant. If surface reaction is the rate-limiting step, a majority of the surface would be covered with A waiting to undergo reaction to B, and again, the rate of change of either species would be negligible. Similarly, if desorption is the rate-limiting step, a surplus of B would build up on the surface until desorption of B occurred, which would also justify the assumption that the rate of change of the intermediate absorbed species is negligible. Utilization of the steady-state approximation in this case indicates that the three rates will be equal:

$$r_a = r_{sr} = r_d \tag{4-11}$$

One final definition is required in order for the derivation to continue. Since there is a predefined surface area upon which absorption can occur, it is assumed that some total number of moles of surface sites exists, which is designated as S_{tot}. This allows us to relate the number of vacant and absorbed spots since they will always sum to S_{tot} as follows:

$$S_{tot} = S^* + N_{A^*} + N_{B^*} \quad or \quad C_{tot} = C^* + C_{A^*} + C_{B^*} \tag{4-12}$$

where N_{A*} is the number of moles of adsorbed A on the electrode surface, N_{B*} is the number of moles of adsorbed B on the electrode surface, and S^* is the number of moles of vacant surface sites. The variable C_{tot} is defined in Equation 4-12 as the total moles of surface sites per unit volume of reactor, and is equal to the sum of the concentrations of vacant surface sites (C^*), absorbed A (C_{A*}), and absorbed B (C_{B*}).

Thus, there are three equations (Equation 4-11 constitutes two equations and Equation 4-12 the other) and three unknowns to solve for the unmeasurable species (C^*, C_{A*} and C_{B*}) in

terms of the measureable species A and B (C_A, C_B) and rate constants. Also, to simplify these equations, only three kinetic rate constants are used. k_a, k_{sr}, and k_d in these equations are equivalent to $k_{A,a}$, $k_{A,sr,f}$, and $k_{B,d}$ in the equations above. Upon substitution and simplification, r_a becomes:

$$r_a = \frac{C_{tot}[C_A - C_B/K]}{\left[\left(\frac{1}{K_a \cdot k_{sr}} + \frac{1}{k_a} + \frac{1}{K \cdot k_d}\right) + \left(\frac{1}{K_a \cdot k_{sr}} + \frac{1 + K_{sr}}{K_a \cdot k_d}\right) K_a \cdot C_A + \left(\frac{1}{K_a \cdot k_{sr}} + \frac{1 + K_{sr}}{K_{sr} \cdot k_a}\right) K_r \cdot C_B\right]} \quad (4\text{-}13)$$

Since $r_a = r_d$ (Equation 4-11), $-dC_A/dt = dC_B/dt = r_a$ and these two equations can be used to predict C_A and C_B with time. Seven parameters (k_a, k_{sr}, k_d, K_a, K_{sr}, K_r, C_{tot}) have been previously defined although C_{tot} can be embedded in these parameters to reduce the number of parameters to six. The overall thermodynamic equilibrium constant K is a product of the other equilibrium constants and is defined as:

$$K = \frac{K_a \cdot K_{sr}}{K_r} \quad (4\text{-}14)$$

This overall combined rate equation has also been verified in literature [52]. It allows insight into the key parameters which dictate the rates at which the kinetic reduction in the anode chamber proceeds. More importantly, however, it allows insight into the rate-limiting step of the proposed three-step mechanism when comparing with experimental data. The rate law takes on a different form if the reaction is adsorption controlled, surface reaction controlled, or desorption controlled. Experimental verification of the rate-limiting step is possible. This knowledge is a key to future reactor design to optimize the reactor setup and promote conversion of reactants to their respective products as described in the introduction to this chapter.

4.3.3 **Assumption of Irreversibility**

One additional assumption that can be added to the combined rate law is that each of the three individual steps is irreversible. Because of the induced voltage potential in the reactor, no oxidation ought to be occurring in the cathode chamber. The final combined rate equation with this assumption included is as follows:

$$r_a = \frac{C_{tot} \cdot C_A}{\left[\left(\frac{1}{K_a \cdot k_{sr}} + \frac{1}{k_a} + \frac{1}{K \cdot k_d}\right) + \left(\frac{1}{K_a \cdot k_{sr}} + \frac{1 + K_{sr}}{K \cdot k_d}\right) K_a \cdot C_A + \left(\frac{1}{K_a \cdot k_{sr}} + \frac{1 + K_{sr}}{K_{sr} \cdot k_a}\right) K_r \cdot C_B\right]} \quad (4\text{-}15)$$

4.4 **Rate Laws of Rate-limited Reactions**

As discussed above, each step in the three-step mechanism could potentially become the rate-limiting step, and understanding which truly is the rate-limiting step is important for future BER design purposes. It becomes very important, therefore, to predict what the experimental outcomes would be under each of these proposed scenarios. Experimental data can then be used to confirm which of the three steps dictates the overall speed of the overall reaction.

4.4.1 **Adsorption Controlled Rate Law**

If the rate-limiting step is the adsorption step in the process, the rate constant for this step is much smaller than the surface reaction rate constant and the desorption rate constant. Mathematically, this statement results in the following inequality:

$$k_{sr}, k_d \gg k_a \quad (4\text{-}16)$$

If true, this modifies the overall combined rate equation as follows:

In most cases, all quotients that do not contain the inverse rate constant of adsorption will be small relative to those that do. This eliminates a significant amount of constants and completely eliminates the bulk concentration of the oxidized electron mediator, A, from the denominator. The resulting equation defines the rate law if adsorption is the rate controlling step:

$$r_a = \frac{C_{tot}[C_A - C_B/K]}{\left(\frac{1}{k_a}\right)+\left(\frac{1+K_{sr}}{K_{sr}\cdot k_a}\right)K_r\cdot C_B} = \frac{k_a\cdot C_{tot}[C_A - C_B/K]}{1+\left(1+\frac{1}{K_{sr}}\right)K_r\cdot C_B} = \frac{k_a\cdot C_{tot}[C_A - C_B/K]}{1+\frac{K_a}{K}\cdot C_B + K_r\cdot C_B} \quad (4\text{-}17)$$

The last equality is achieved by utilizing Equation 4-14. Equation 4-17 indicates that if the overall reaction is limited by adsorption, then the initial rate of formation of B ($dC_B = r_a$ with C_B negligible) becomes first order in terms of C_A.

4.4.2 **Surface Reaction Controlled Rate Law**

If the rate-limiting step is the surface reaction step, the rate constant for this step is much smaller adsorption rate constant or surface reaction rate constant. Mathematically, this statement results in the following inequality:

$$k_a, k_d \gg k_{sr} \quad (4\text{-}18)$$

If true, this modifies the overall combined rate equation as follows:

Again, all quotients not involving the inverse surface reaction rate constant step can be considered negligible and be removed from the equation. In this case, no entire terms are eliminated from the denominator, but the dependence becomes much clearer due to the

elimination of so many additive terms. The resulting equation gives us rate law in the event that the rate-limiting step is the surface reaction.

$$r_a = \frac{C_{tot}[C_A - C_B/K]}{\frac{1}{K_a \cdot k_{sr}} + \frac{1}{K_a \cdot k_{sr}} K_a \cdot C_A + \frac{1}{K_a \cdot k_{sr}} K_r \cdot C_B} = \frac{k_{sr} \cdot C_{tot}[C_A - C_B/K]}{\frac{1}{K_a} + C_A + C_B} \quad (4\text{-}19)$$

The form of this equation leads to an initial rate of formation of B ($dC_B = r_a$ with C_B negligible) that is independent of C_A (as long as $K_a >> 1$).

4.4.3 **Desorption Controlled Rate Law**

If the rate-limiting step is the desorption step, the rate constant for this step is much smaller than the other steps. Mathematically, this statement results in the following inequality:

$$k_a, k_{sr} \gg k_d \quad (4\text{-}20)$$

If true, this modifies the overall combined rate equation as follows:

In this case, all quotients that do not contain the inverse rate constant of desorption will be small relative to those that do. This eliminates a significant amount of constants and completely eliminates the bulk concentration of the reduced electron mediator, B, from the denominator. Once these terms are eliminated, the defining equation for the rate law if desorption is the rate-controlling step is:

$$r_a = \frac{C_{tot}[C_A - C_B/K]}{\left[\frac{1}{K \cdot k_d} + \left(\frac{1 + K_{sr}}{K \cdot k_d}\right) K_a \cdot C_A\right]} = \frac{K \cdot k_d \cdot C_{tot}[C_A - C_B/K]}{[1 + (1 + K_{sr}) K_a \cdot C_A]} = \frac{k_d \cdot C_{tot}[C_A - C_B/K]}{\left[\frac{1}{K} + \frac{K_r}{K_{sr}} \cdot C_A + K_r \cdot C_A\right]} \quad (4\text{-}21)$$

The form of this equation leads to an initial rate of formation of B ($dC_B = r_a$ with C_B negligible) that is also independent of C_A. Thus, C_B as a function of time would be a linear curve until most

of the conversion of A has occurred, and then an asymptotic approach to equilibrium as A becomes fully converted to B.

4.4.4 **Development of Parallel Ordinary Differential Equation Model**

While the above models for adsorption, surface reaction, and desorption controlled rates for the three-step process in Figure 4-1 provided an understanding of what is to be expected for B as a function of time in terms of the initial shape of the curves (zeroth or first order), they are not as accurate for modeling of the experimental data. Rather than attempting to fit experimental data with the models described in sections 4.4.1 through 4.4.3, a system of ordinary differential equations (Equations 4-37 through 4-42) were derived for the mechanism in Figure 4-1. An additional mechanism of B* → C* → C for the MV studies was also included in developing the differential equations to model the experiments in which MV^{2+} was reduced to MV^{0}. For instance, B* in Figure 4-1 can convert to C* on the surface and then C* can desorb to form product C. For the experimental work reported in Chapter 5, it should be noted that A is represented by MV^{2+} or AQDS, B, the experimentally measured species, is represented by MV^{+} or AH_2DS, and when applicable, C is represented by MV^{0}. The pseudo steady-state assumption of the absorbed species (C_{A*}, C_{B*}, and C_{C*}) is not a required assumption for the model shown below and, as shown below, this assumption is not always completely accurate. Removal of this assumption results in the ability to give a more accurate model and corresponding interpretation of the results.

In the derivations, C_A, C_B, and C_C, are converted to fractional values of A, B, and C – denoted as F_A, F_B, and F_C – by dividing by the total starting concentration C_A^0. The absorbed concentrations, C_{A*},C_{B*}, and C_{C*}, are converted to their fractional coverage – denoted as θ_A,

θ_B, and θ_C – by factoring out C_{tot}. The described steps are shown here in a line-by-line fashion to show the derivation of Equations 4-37 and 4-38. Derivations for Equation 4-39 and 4-42 are not shown, but follow the same steps.

The first derivation is for the rate of change of the fraction of A, F_A. For a well-mixed batch reactor with a constant volume, the material balance for species A is:

$$\frac{dC_A}{dt} = -k_{A,a} \cdot C_A \cdot C^* + k_{A,d} \cdot C_{A^*} \tag{4-22}$$

C* is then replaced with $C^* = C_{tot} - C_{A^*} - C_{B^*} - C_{C^*}$:

$$\frac{dC_A}{dt} = -k_{A,a} \cdot C_A \cdot (C_{tot} - C_{A^*} - C_{B^*} - C_{C^*}) + k_{A,d} \cdot C_{A^*} \tag{4-23}$$

C_{tot} is also factored out of all terms on the right hand side of the equation where $\theta_A = C_{A^*}/C_{tot}$, $\theta_B = C_{B^*}/C_{tot}$, and $\theta_C = C_{C^*}/C_{tot}$:

$$\frac{dC_A}{dt} = -k_{A,a} \cdot C_{tot} \cdot C_A \cdot (1 - \theta_A - \theta_B - \theta_C) + k_{A,d} \cdot C_{tot} \cdot \theta_A \tag{4-24}$$

Both sides are then divided by C_A^0 to get the differential equation in terms of F_A, which is equal to C_A/C_{A0}:

$$\frac{dF_A}{dt} = -k_{A,a} \cdot C_{tot} \cdot F_A \cdot (1 - \theta_A - \theta_B - \theta_C) + k_{A,d} \cdot \frac{C_{tot}}{C_A^0} \cdot \theta_A \tag{4-26}$$

Finally, new a new rate constants $k_{A,a}$' is obtained by combining several constants:

$$\frac{dF_A}{dt} = -k_{A,a}' \cdot F_A \cdot (1 - \theta_A - \theta_B - \theta_C) + k_{A,d} \cdot \frac{C_{tot}}{C_A^0} \cdot \theta_A \tag{4-27}$$

At this point, one might ask why the ratio of total concentration of surface sites to starting concentration has not been absorbed into the constants. The reason for this becomes clear as the differential equation for θ_A is derived. The material balance for C_{A^*} is:

$$\frac{dC_{A^*}}{dt} = k_{A,a} \cdot C_A \cdot C^* - k_{A,d} \cdot C_{A^*} - k_{A,sr,f} \cdot C_{A^*} + k_{B,sr,r} \cdot C_{B^*} \tag{4-28}$$

C* is then replaced with $C^* = C_{tot} - C_{A^*} - C_{B^*} - C_{C^*}$:

$$\frac{dC_{A^*}}{dt} = k_{A,a} \cdot C_A \cdot (C_{tot} - C_{A^*} - C_{B^*} - C_{C^*}) - k_{A,d} \cdot C_{A^*} - k_{A,sr,f} \cdot C_{A^*} + k_{B,sr,r} \cdot C_{B^*} \quad (4\text{-}29)$$

C_{tot} is also factored out of all terms on the right hand side of the equation:

$$\frac{dC_{A^*}}{dt} = k_{A,a} \cdot C_{tot} \cdot C_A \cdot (1 - \theta_A - \theta_B - \theta_C) - k_{A,d} \cdot C_{tot} \cdot \theta_A - k_{A,sr,f} \cdot C_{tot} \cdot \theta_A + k_{B,sr,r} \cdot C_{tot} \cdot \theta_B \quad (4\text{-}30)$$

Both sides are then divided by C_A^0 to get the differential equation in terms of F_A:

$$\frac{1}{C_A^0} \cdot \frac{dC_{A^*}}{dt} = k_{A,a} \cdot C_{tot} \cdot F_A \cdot (1 - \theta_A - \theta_B - \theta_C) - \frac{k_{A,d} \cdot C_{tot}}{C_A^0} \cdot \theta_A - \frac{k_{A,sr,f} \cdot C_{tot}}{C_A^0} \cdot \theta_A + \frac{k_{B,sr,r} \cdot S_{tot}}{C_A^0} \cdot \theta_B \quad (4\text{-}32)$$

Up to this point, the same steps have been taken as above. However, the left hand side of the equation is still in terms of C_{A*}. The definition of θ_A is invoked here to make the transformation to the differential for θ_A:

$$C_{A^*} = \theta_A \cdot C_{tot} \;\; \therefore \;\; \frac{dC_{A^*}}{dt} = C_{tot} \cdot \frac{d\theta_A}{dt} \quad (4\text{-}33)$$

Plugging the equality from Equation 4-33 into equation 4-32 yields:

$$\frac{C_{tot}}{C_A^0} \cdot \frac{d\theta_A}{dt} = k_{A,a} \cdot C_{tot} \cdot F_A \cdot (1 - \theta_A - \theta_B - \theta_C) - \frac{k_{A,d} \cdot C_{tot}}{C_A^0} \cdot \theta_A - \frac{k_{A,sr,f} \cdot C_{tot}}{C_A^0} \cdot \theta_A + \frac{k_{B,sr,r} \cdot C_{tot}}{C_A^0} \cdot \theta_B \quad (4\text{-}34)$$

Multiplying both sides by C_A^0 and then dividing both sides by C_{tot} gives:

$$\frac{d\theta_A}{dt} = k_{A,a} \cdot C_{tot} \cdot \frac{C_A^0}{C_{tot}} \cdot F_A \cdot (1 - \theta_A - \theta_B - \theta_C) - k_{A,d} \cdot \theta_A - k_{A,sr} \cdot \theta_A + k_{B,sr} \cdot \theta_B \quad (4\text{-}35)$$

Finally absorbing multiplicative terms to form the same rate constants $k_{A,a}$' gives:

$$\frac{d\theta_A}{dt} = k_{A,a}{}' \cdot \frac{C_A^0}{C_{tot}} \cdot F_A \cdot (1 - \theta_A - \theta_B - \theta_C) - k_{A,\mathrm{d}} \cdot \theta_A - k_{A,sr} \cdot \theta_A + k_{B,sr} \cdot \theta_B \quad (4\text{-}36)$$

It becomes clear here why the above ratio of C^0_A/C_{tot} was not absorbed into the rate constant above. The ratio is an important parameter and is defined as a new constant R_{As} =

C^0_A/C_{tot}. In summary, the differential equations for the mechanism shown in Figure 4-1 with the additional mechanism of B* → C* → C are:

$$\frac{dF_A}{dt} = -k_{A,a} \cdot F_A \cdot (1 - \theta_A - \theta_B - \theta_C) + \frac{k_{A,d}}{R_{As}} \cdot \theta_A \quad (4\text{-}37)$$

$$\frac{d\theta_A}{dt} = k_{A,a} \cdot R_{As} \cdot F_A \cdot (1 - \theta_A - \theta_B - \theta_C) - k_{A,d} \cdot \theta_A + k_{B,sr,r} \cdot \theta_B - k_{A,sr,f} \cdot \theta_A \quad (4\text{-}38)$$

$$\frac{dF_B}{dt} = -k_{B,a} \cdot F_B \cdot (1 - \theta_A - \theta_B - \theta_C) + \frac{k_{B,d}}{R_{As}} \cdot \theta_B \quad (4\text{-}39)$$

$$\frac{d\theta_B}{dt} = k_{B,a} \cdot F_B \cdot R_{As} \cdot (1 - \theta_A - \theta_B - \theta_C) - k_{B,d} \cdot \theta_B + k_{A,sr,f} \cdot \theta_A - k_{B,sr,f} \cdot \theta_B + k_{C,sr,r} \cdot \theta_C - k_{B,sr,r} \cdot \theta_B \quad (4\text{-}40)$$

$$\frac{dF_C}{dt} = -k_{C,a} \cdot F_C \cdot (1 - \theta_A - \theta_B - \theta_C) + \frac{k_{C,d}}{R_{As}} \cdot \theta_C \quad (4\text{-}41)$$

$$\frac{d\theta_C}{dt} = k_{C,a} \cdot F_C \cdot R_{As} \cdot (1 - \theta_A - \theta_B - \theta_C) - k_{C,d} \cdot \theta_C + k_{B,sr,f} \cdot \theta_B - k_{C,sr,r} \cdot \theta_C \quad (4\text{-}42)$$

The new rate constants are:

$$k_{A,a} = k_{A,a} \cdot C_{tot} \quad (4\text{-}43)$$

$$k_{B,a} = k_{A,a} \cdot C_{tot} \quad (4\text{-}44)$$

$$k_{C,A} = k_{A,a} \cdot C_{tot} \quad (4\text{-}45)$$

As noted, there are eleven parameters (the ten rate constants and R_{As}) and six differential equations shown in Equations 4-37 to 4-42 for predicting A, B, and C with time. Since the fractions of A, B, and C (F_A, F_B, and F_C), the fractional coverage (θ_A, θ_B, and θ_C), and R_{As} are unitless terms, all rate constants have units of 1/s (unlike the pseudo steady state model previously described). For the sake of simplification, the prime symbols (') have been dropped from the rate constants. However, it is important to make the reader aware that the rate constants

here do not have the same definition as those that have been listed in sections previous to this one.

It becomes very important at this point to get an idea of what value R_{As} should be. If each molecule is approximated as a perfect sphere, it can be estimated how many molecules of A would be able to fit on the surface of the electrode in a closed-pack structure. All of the molecules utilized as electron mediators in this work (AQDS, MV, BV, and NR) have benzene-like ring structures. The molecular diameter of a benzene ring, which should be a lower limit for the molecular diameter of the electron mediators, is 280 picometers [53]. For instance, the smallest electron mediator molecule is methyl viologen, which is approximately 2.5 times the size of benzene. The benzene ring approximation gives a surface area per molecule of 4.90×10^5 pm^2 per molecule. The surface area of the electrode in this study is 62.5 cm^2. Assuming a closed-pack structure, $S_{tot} = 1.28 \times 10^{16}$ molecules, or 2.12×10^{-5} millimoles of electron mediator would be on the surface if no mediators were present in any porous component of the electrode. For this study, the minimum amount of electron mediator added during experimental work was N^0_A = 0.02 millimoles. Therefore, an approximation for $R_{As} = C^0_A/C_{tot} = N^0_A/S_{tot}$ for this study is 944 (at least three orders of magnitude greater number of initial moles of A than molar surface sites available). This ratio could be smaller if there are pores within the electrode in which A can absorb. This ratio could be larger if the electron mediator is larger than a benzene ring or if the electrode does not have uniform active sites covering the entire surface.

4.4.5 **Example Characteristic Curves and Discussion**

The following example shows how the model can be used for predicting F_B. Assuming that only A converts to B (i.e. no C product is formed such that $\theta_C = 0$ and $k_{B,sr,r} = 0$), Equations

4-37 to 4-40 were used to predict F_B with time. Figure 4-2 and Figure 4-3 show characteristic curves for F_B using kinetic data in each of these control regimes. F_B of unity means that all of A has converted to B. Figure 4-2 shows curves for a reversible reaction and Figure 4-3 shows curves for an irreversible reaction. To generate the curves shown in Figure 4-2 and Figure 4-3, the initial value of F_A was set equal to one whereas initial values of θ_A, F_B, and θ_B were set equal to zero. The forward rate constant of the rate limiting step (either $k_{A,a}$, $k_{A,sr,f}$ or $k_{B,d}$) was set equal to 0.1 s^{-1}. For reversible reactions, the reverse rate of the rate-limiting step (either $k_{A,d}$, $k_{B,sr,r}$ or $k_{B,a}$) was set to 0.025 s^{-1}. For irreversible reactions, the reverse rate constant of the rate-limiting step was set to 0 mol/s. The forward and reverse rate constants of the non-rate limiting steps were set equal to 100 s^{-1}. R_{As}, in all cases, was set to 1000. As seen in the above equations, the equilibrium constants are not required for the predictions, although they can be calculated from kinetic rate constants.

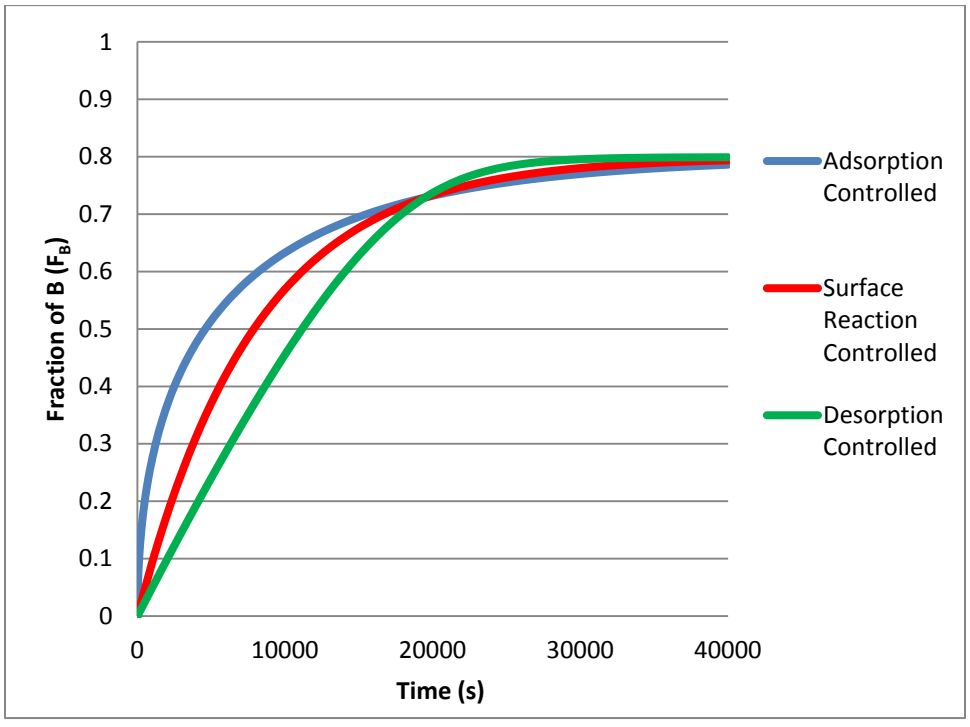

Figure 4-2 - Example graphs for a reversible reaction

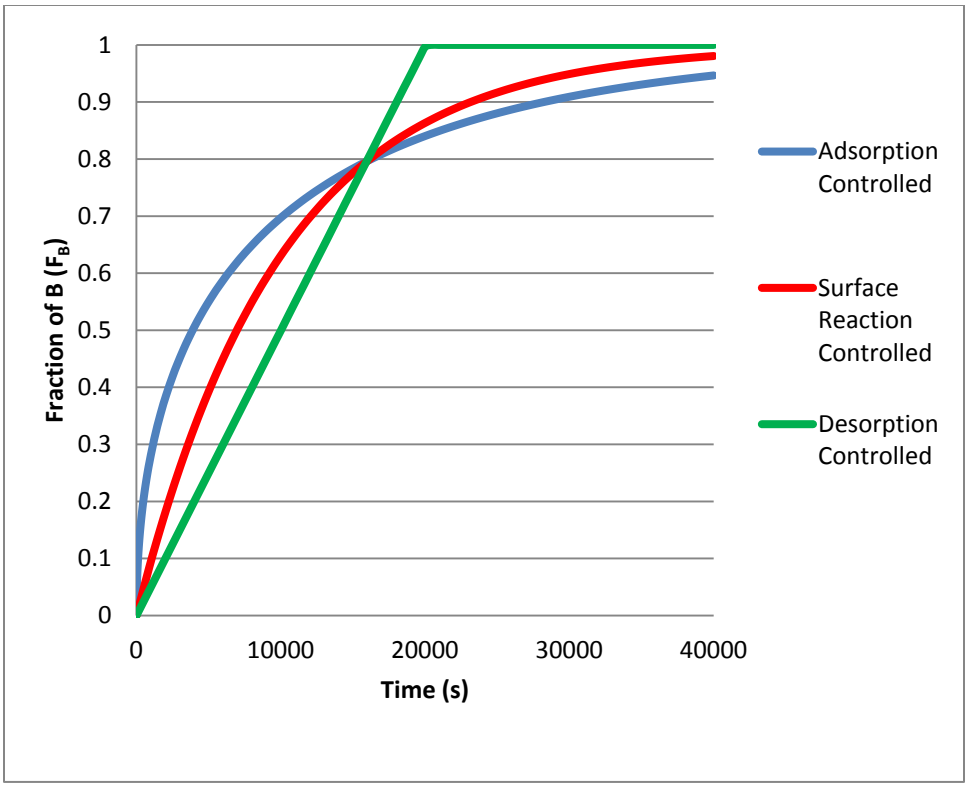

Figure 4-3 - Example graphs for an irreversible reaction

These curves show visually what the curves look like for each rate determining step. In comparison with the pseudo steady state model, the adsorption controlled rate is first order throughout for both reversible and irreversible reactions, giving its curves an exponentially decaying shape. The desorption controlled curves are zeroth order and remain at this order until either approaching equilibrium for the reversible reaction or approaching unity for the irreversible reaction. Finally, the surface reaction controlled curves for both reversible and irreversible reactions are essentially a combination of both zero and first order reactions. At low F_B, the curve is linear in nature, but it takes on the nature of the adsorption controlled rate as it gets closer to equilibrium. How long the linearity of the surface reaction controlled curve persists is dependent upon the relative values of the rate constants.

The understanding gleaned from the pseudo steady state model and the characteristic curves shown above (no pseudo steady state assumption) aided in the analysis of experimental data presented in Chapter 5. Specifically, the shape of the experimental curve was used to determine which step of the reaction mechanism was the rate limiting step. Once the rate determining step was correctly identified, rate constants were regressed from the kinetic data to gain a better understanding of the process. Identification of the rate limiting step and quantification of the corresponding rate constants are among the first steps that will allow for an engineering analysis of BER technology and identify strategic pathways for improvement moving forward towards implementation.

4.4.6 **Value of Ordinary Differential Equation Model over Pseudo Steady State Model**

The pseudo steady state model makes the assumption that the value of the intermediates (θ_A, and θ_B) are constant. Utilizing the ordinary differential equation model, the validity of pseudo steady state was tested. Figure 4-4 shows the plot for the corresponding values of θ_A and θ_B for the exact same model as the reversible reaction curves generated in Figure 4-2.

It is immediately apparent that the assumption is valid if the rate limiting step is adsorption or desorption. This is because the amount of adsorbed A and adsorbed B, in these cases, is dependent on the ratio of the forward rate of surface reaction and the reverse rate of surface reaction. However, the assumption is invalid if the rate limiting step is the surface reaction. This is because the amount of adsorbed A and adsorbed B, in these cases, becomes dependent on the bulk concentration, a dependence that will be explored further in later sections. Therefore, the added value of the ordinary differential equation model without the pseudo steady state assumption is its ability to model a surface reaction controlled rate law more accurately.

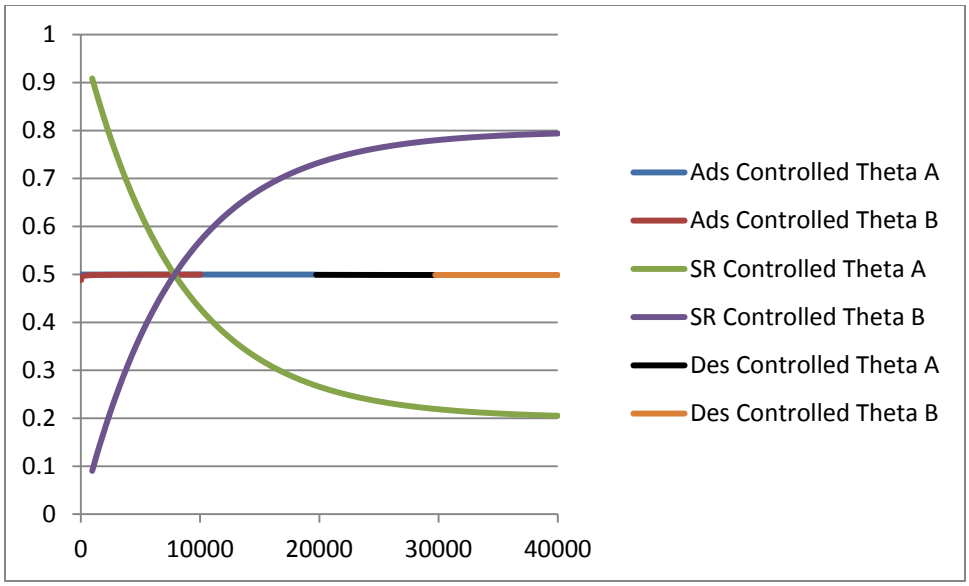

Figure 4-4 - Plots of θ_A and θ_B for different rate controlling steps. All data is plotted for the entire time range, but different portions have been brought to the front to show overlap.

5 EXPERIMENTAL DETERMINATION OF KINETIC MECHANISM AND DEFINITION OF KEY KINETIC CONSTANTS

5.1 Introduction

As discussed in the previous chapter, one of the most important variables in implementation of the BER is to understand the kinetics of electron mediator oxidation-reduction reactions. Chapter 4 was included to define the model by which these reactions are characterized and explained. However, complete understanding of the system cannot be achieved by modeling alone. Experimental results become necessary in order to understand which of the proposed steps is rate-limiting and therefore defines the rate law.

Experimental validation is the only true way to determine parameters that are important moving forward in reaction design. Performance of the BER is almost completely determined by how effectively the transfer of electrons occurs. Experimental determination of the rate law adds key information to the knowledge base that is important for future optimization of the reactors. Any understanding gained in regards to the mechanism will also further aid development and give clarity to the path to industrial implementation.

5.1.1 Materials and Methods

The BER (Figure 5-1) is constructed of two jacketed 50 mm ID glass chambers (University of Utah Scientific Glassblowing Shop, UT) connected by a pinch clamp assembly.

The chambers are separated by a cation exchange Nafion membrane (Fuel Cell Store, CA). Each chamber contains two liquid sampling points sealed with rubber stoppers and two gas sampling ports sealed with rubber stoppers threaded with 1/8" stainless steel tubing for continuous gas purging. The electrodes are unpolished graphite that measure 2.5 x 1.25 x 7.5 cm^3 (G-10 Graphite Engineering and Sales, MI). Electrodes are connected with watertight threaded fittings (Impulse, CA) to wires and sealed with conductive silver epoxy (Epoxy Technology, MA). Wires are threaded through stoppers in the top of each chamber. Prior to initial use and before each use thereafter, the electrodes were washed repeatedly in 1 N HCl to remove residual minerals, any biomass buildup, and adsorbed electron mediators, followed by a thorough rinse with sterile deionized water. The silver (Ag/AgCl) reference electrode (Warner Instruments, CT) is threaded through the butyl stopper of the liquid sampling point in the cathode chamber for AQDS experiments. This was later replaced with a non-leaking Ag/AgCl reference electrode for the MV experiments. A continuous flow-through spectrophotometric system composed of Viton® pump tubing utilizing a peristaltic pump (Masterflex, IL) connected to a flow-through cuvette (Starna Cells, CA) was threaded through one of the butyl rubber stoppers in the liquid sampling port in the anode chamber. Continuous data was taken using a Shimadzu PharmaSpec UV-1700 spectrophotometer (Tokyo, Japan).

The prepared solution was buffered at pH 7 with a 100 mM phosphate buffer with KOH added until pH 7 was reached. The pH was measured at the beginning and end of each experiment, and no measurable difference was seen (data not shown). pH control is important for two reasons. The first is that hydrogen ions participate in the reaction, so availability of hydrogen ions can affect the overall rate of reaction. Second, the photometric spectrum of the electron

mediators also depends on pH. Therefore, in order to have consistent data, the solution must be buffered. 100 mM KCl was dissolved as a standard for the reference electrode into the media of

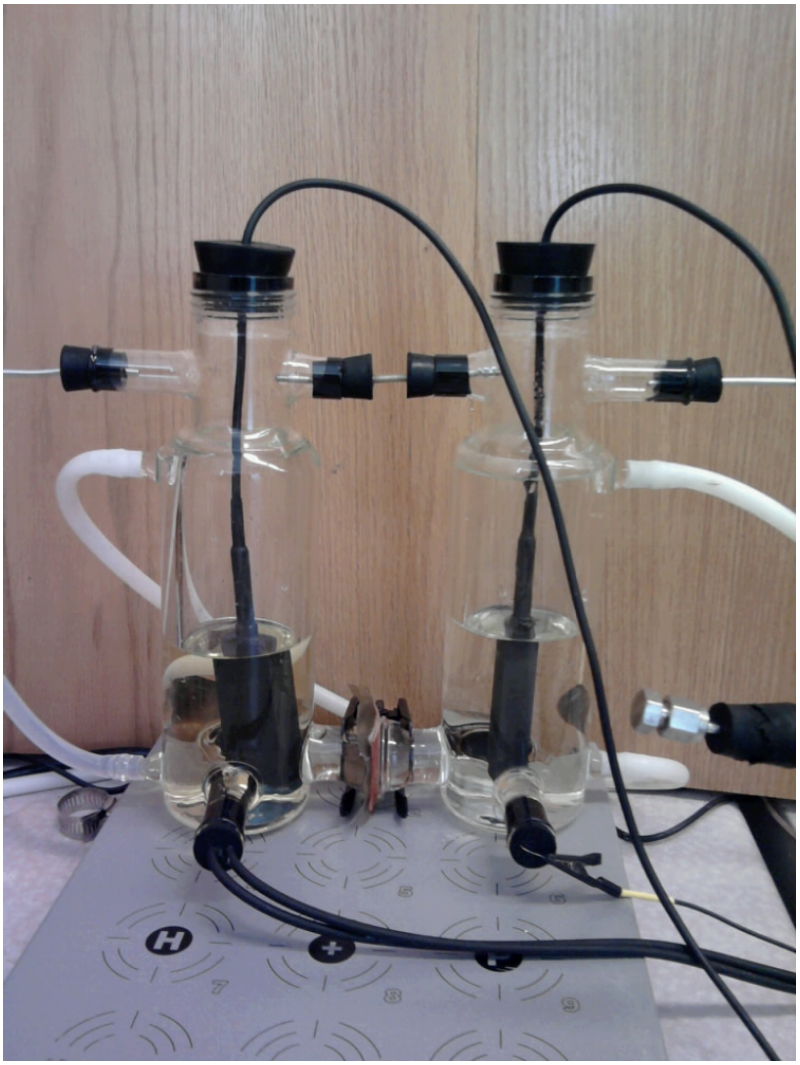

Figure 5-1 - Experimental BER reactor

both chambers for AQDS experiments and only the anodic chamber in MV experiments. 1 mM oxidized electron mediator was dissolved into the anode chamber for AQDS runs and some preliminary MV runs. For later MV runs, 0.1 mM of oxidized electron mediator was used because dimerization of MV occurs at greater concentrations [54] [55]. 20 mL of dimethylformamide (DMF) was also included in MV runs to minimize the occurrence of

dimerization. Each chamber was filled with 200 mL of the prepared solution and the system was purged with N_2 for at least 12 hours in order to purge out any remaining O_2. Continuous purging continued throughout the experiment. The temperature of the reaction chambers were maintained by continuous pumping of 37 °C water from a temperature controlled water bath through the outer jackets of the reaction chambers. Control of voltage potential was maintained using a Potentiostat and eCorder controlled by Chart software, all manufactured by eDAQ (Potentiostat EZ161, and Ecorder ED821, Colorado Springs, CO). Reaction chambers were stirred with magnetic stir bars at 400 rpm to maintain uniform concentration in the reaction chamber. Tests were also run at 600 rpm to validate that stirring was sufficient and that potential mass transfer limitations did not affect the kinetics. This data is shown in Figure 5-2, where runs 1-3 were run at 990 rpm, and run 4 was run at 600 rpm.

After purging occurred, the potential was set to its predetermined value. For AQDS, experiments were run at -2000 mV relative to the Ag/AgCl reference electrode to maximize rate and conversion. The voltage differed for MV runs. It was varied at -800 mV, -900 mV, and -1000 mV. With lower concentrations of electron carrier, voltages greater than -1000 mV resulted in the formation of hydrogen gas, an undesired side reaction. Higher voltages also increase the rate of dimerization in NADH reduction [5], and a similar result in our experiments would be undesirable. The voltage was applied at the instant that the spectrophotometric first point of datum was taken. Runs lasted varying lengths from 7-24 hours depending on the run. Data were taken at varying time intervals depending on the experiment, but on a scale much shorter than that of the reactions taking place within the chambers.

Calibration standards for fully reduced media were prepared as follows. Since the photometric spectra of the individual electron mediators depends on the pH, 100 mM phosphate

buffer was added to deionized water and buffered to pH 7 using KOH. 1 mM electron buffer was added to the system and dissolved. The solution was boiled and purged with N_2 gas to remove any nitrogen from the system. After cooling to room temperature, and during continuous purging of nitrogen, excess sodium dithionite was used to chemically reduce the electron mediator. The calibration standard was pumped through the flow-through spectrophotometric system previously described and optical density was read and recorded.

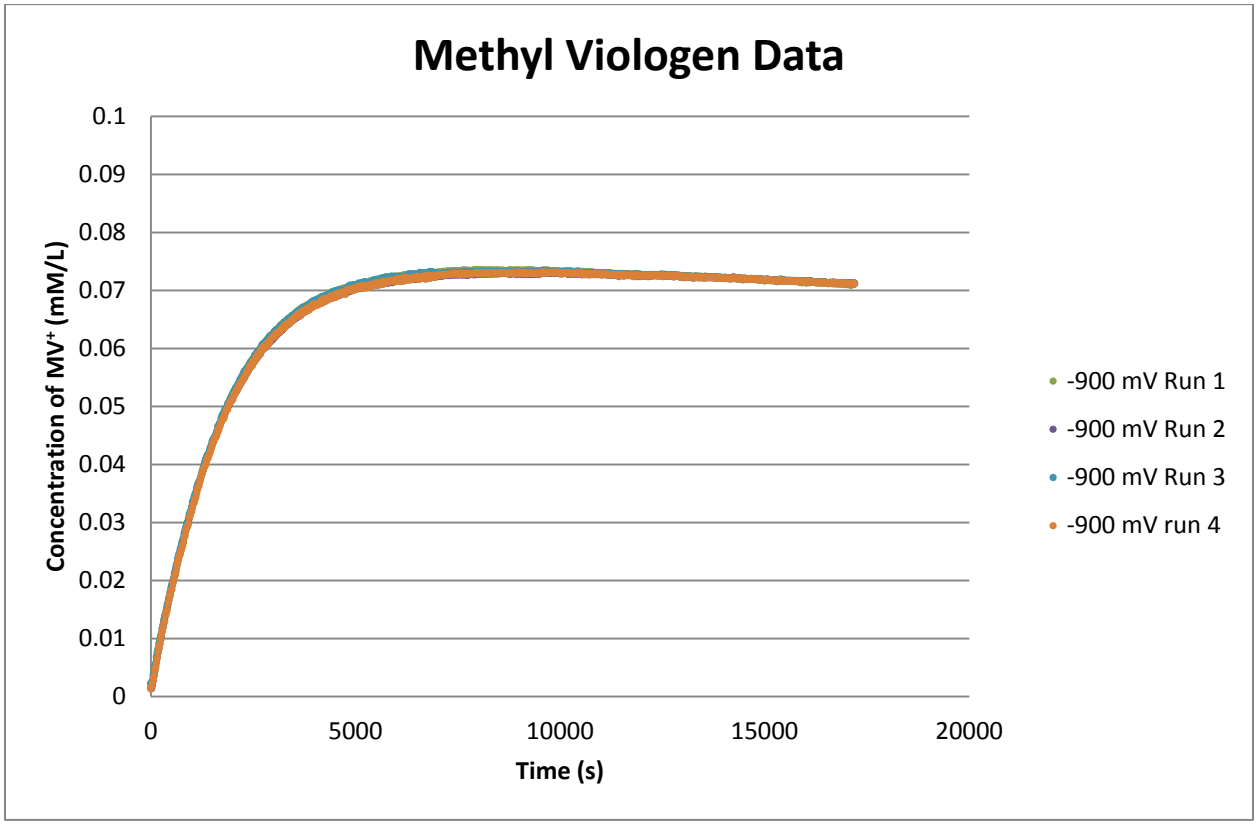

Figure 5-2 - Methyl viologen kinetic data performed at -900 mV. Data overlaps so it is difficult to see individual runs.

5.2 Problems Encountered During Experimentation

5.2.1 Buffer Interference

The first experiments took place in the exact same manner as described above except MES was used as a buffer instead of phosphate. MES buffer was used because it is a standard buffer for our biological systems. Initial data were taken in the same exact manner as described above in the materials and methods sections with the buffer exception as noted. Experimental results were varied and showed a zero-order rate law for the overall rate of reaction. However, as multiple runs of this experiment were performed, the rates varied greatly (see Figure 5-3) and formation of a green precipitate occurred irregularly toward the end of some of the experimental runs. Previous calibrations had made clear that the solubility of the reduced species (which in all cases using MES was AH_2DS) had not been reached. Additionally, the solution in the oxidation (anode) chamber, which did not include any other species besides MES buffer, KOH, and KCl, changed from clear to yellow, indicating that a reaction had occurred other than hydrolysis.

Upon delving more deeply into the literature, it becomes apparent that synthetic zwitterionic buffers such as MES, HEPES, and PIPES, which have been developed for and utilized in biological studies, can cause interference in the chemical reactions in the media they are buffering. This undesirable effect has been observed in other oxidation-reduction reactions. For example, zwitterionic buffer also interfered in the oxidation-reduction reactions taking place in peroxidase reactions in plant assays [56]. Solid precipitate formation in the cathode chamber and the oxidation of MES characterized by an observable color change of the solution in the cathode chamber indicate that MES interference also occurs in electrochemical reactions taking place within a BER.

In order to overcome this interference for the kinetic experimentation, a suitable buffer had to be found that would not interact with the chemistry of the system. It seems that none of the zwitterionic buffers would be suitable because of their propensity to interact in oxidation-reduction reactions. A simple inorganic molecule with only a single oxidation state, however, would be suitable for this application. However, inorganic buffers are usually unsuitable for biological experimentation because they interfere greatly with the metabolism of the biological species being studied. Since no biological species is present in these particular experiments, and since phosphate has only one oxidation state, phosphate buffer was chosen and utilized during all further experimentation. In cellular BER systems, careful consideration must occur when choosing a buffer to assure a suitable buffer is in place to avoid the issues noted above.

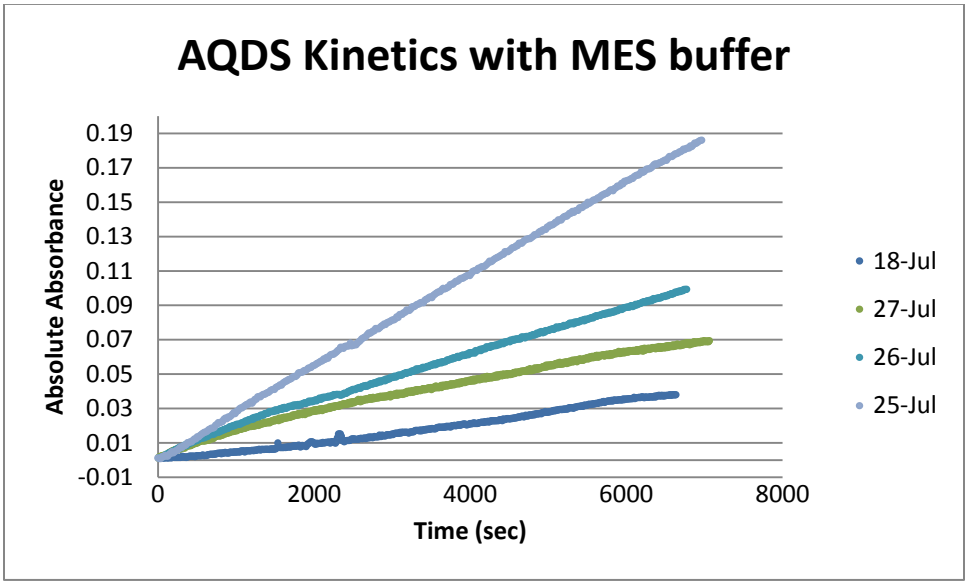

Figure 5-3 - Note that all data has been modified so that the first sign of reduction occurs at time zero although this is not actually the case (see section 5.3.1)

5.2.2 Oxygen Contamination

A significant problem with the original setup was contamination of the samples or system with oxygen. The first experiments were run without a continuous flow-through system in place

to take spectrophotometric data. Indeed, individual samples of approximately 1 mL were taken in triplicate at regular intervals to determine the rate of reaction. Samples were taken through the butyl rubber stoppers in the liquid ports of the reaction chambers via a syringe with an attached sterile needle. The samples were then placed into disposable plastic cuvettes to read the OD with the spectrophotometer. This was performed for both runs with both AQDS and MV acting as the electron acceptors. During these initial runs, visual inspection of the reaction chambers revealed that the reduction was taking place, however, the triplicates had a large amount of scatter, particularly with the MV. It was revealed that although AH_2DS was somewhat stable even when exposed directly to atmospheric oxygen, MV^+ is highly unstable and oxidizes almost immediately upon exposure to even small amounts of oxygen. A change in the sampling procedure was immediately decided upon and implemented.

The next sampling procedure involved purging of sealed cuvettes in an attempt to introduce the samples into an oxygen-free environment. Quartz cuvettes sealed with plastic caps containing septa were utilized for this process. The septum was pierced with a needle connected to an N_2 inlet and also pierced with a vent needle. The cuvette was purged of any oxygen, and care was taken to ensure that the vent needle was removed and a slight over pressurization of the cuvette with N_2 occurred. The sample was taken through butyl rubber stoppers with a syringe and needle as described above. The sample was then injected through the septum into the purged oxygen-free environment of the quartz cuvette. Although great care was taken during this procedure, variability and reliability of the results were still compromised, especially during the MV runs. It was revealed that the rate of withdrawal of the sample from the chamber had a significant impact on the amount of oxidation which occurred in the sample. If the sample was drawn quickly, developing a vacuum within the syringe, larger amounts of oxygen contaminated

the sample. However, even with long purging times of the sealed cuvettes and careful extraction of the liquid sample, oxygen contamination continued to render all data unreliable. All runs were abandoned after only a few hours due to the contamination of the samples.

It was decided that a continuous flow-through system would be necessary in order to avoid oxygen contamination. The original flow-through system was constructed using a combination of Teflon and silicone tubing. All other aspects of the system were identical with the exception of the addition of the flow-through system which was threaded through butyl rubber stoppers. However, initial experiments resulted in no reduction, even when run for extended periods of time greater than 24 hours. All aspects of the experimental setup were tested and retested to ensure that the electrical connections were made correctly, that the reaction solution was mixed and buffered correctly, and that continuous gas purging was occurring. After multiple failed attempts, the flow through system was removed and a standard butyl rubber stopper was used in place of the stopper threaded with tubing connected to the flow-through system. The system again performed as expected and reduction occurred, indicating that the flow-through system was somehow interfering with the system.

No decomposition of the electron mediator should have occurred through the peristaltic pump because it was in a fully dissolved aqueous state. It became fairly obvious that oxygen contamination was the most probably cause of system failure. The flow-through system had to be inspected to ensure that any possible oxygen contamination pathways were investigated and removed. The first element to be inspected was the cuvette itself. If the cuvette and its fittings were not air-tight, then oxygen could be introduced into the system and reverse any reduction that occurred. Chemically reduced MV was placed inside the sealed cuvette and left over 1 hour. Although an initial drop in OD occurred due to oxygen contamination from the sampling

process, the OD remained level for the remainder of the time, indicating that no oxygen was being introduced through the cuvette. Since so many other pieces of equipment were also threaded through butyl rubber stoppers (e.g. gas tubing, wiring, and reference electrode), it seemed unlikely that the contamination was occurring through the stopper.

The only option left was the pump tubing itself. Leak checks were performed and no leaks were detected. Finally, the oxygen permeability of both Teflon and Silicone were taken into consideration. According to the Cole Parmer catalogue, silicone and Teflon have oxygen permeabilities of 7961 and 1345 in units of (cc-mm) / (sec-cm^2cmHg)*10^{-10}. While this may seem like a very small number, it is significant enough to completely eliminate all reduction in the anode chamber. The decision was made to replace all pump tubing with Viton, which has an oxygen permeability of 15 (cc-mm) / (sec-cm^2cmHg)*10^{-10}. Once this change was made, oxygen contamination ceased to be a problem and the reactors ran as expected and as seen in the experiments performed prior to implementation of the flow-through system.

5.3 Experimental Results with Anthraquinone-2,6-Disulfonate (AQDS)

5.3.1 AQDS Kinetic Experimental Results

The first tests that were run took place with AQDS as the electron acceptor. Three independent runs are included in the data set. Figure 5-4 shows the raw data from these tests. It becomes immediately apparent that run 3 differs a great deal from the other two. Unfortunately, since the process was still being optimized, spectrophotometric data were taken at different wavelengths for the first two runs as for the third run. Additionally, the Shimadzu spectrophotometer has proven to be unreliable at elevated optical density, and a linear calibration is not guaranteed across the total range of 0-4 OD that is available.

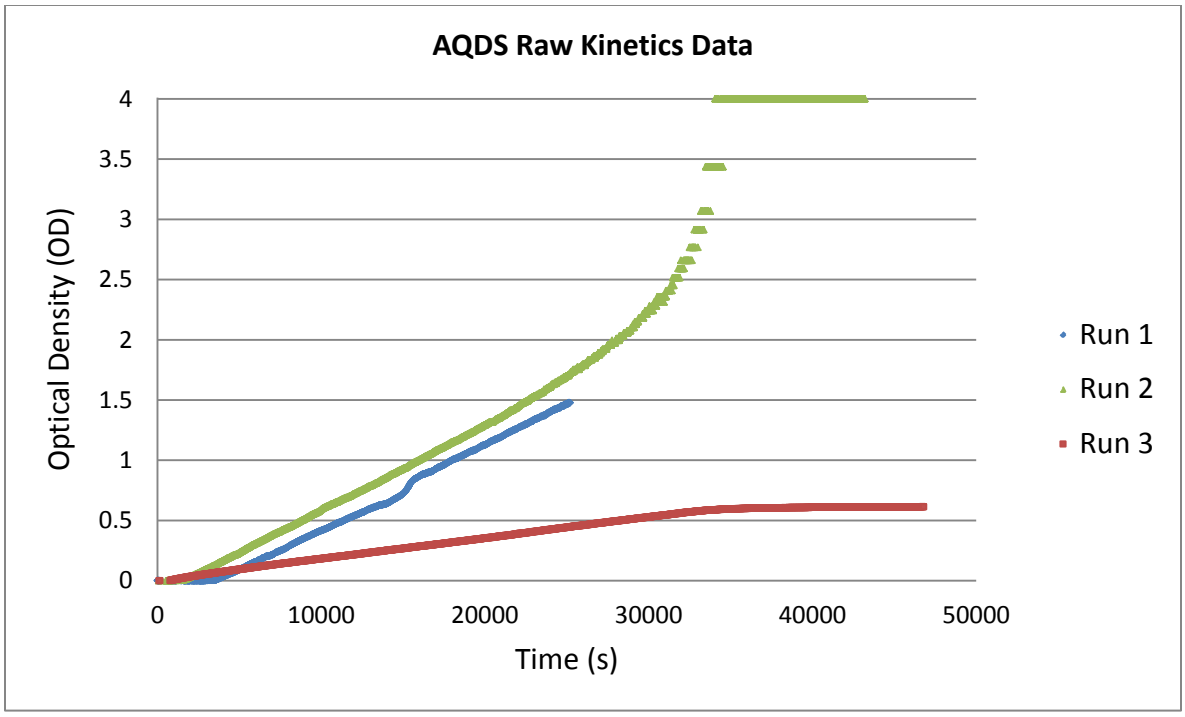

Figure 5-4 - Raw kinetic data from three separate runs with AQDS

The data must also be adjusted in order to be graphed on the same scale. The first adjustment made was to eliminate all points of data with an absolute OD greater than 1.5. The reliability of the device becomes suspect above these levels. Additionally, there are in these experiments, and in all experiments run, a time period of no activity at the beginning of the run. Although each run was purged continually with nitrogen as noted above, it is believed that this delay is caused by residual oxygen that must be eliminated from the system before electron mediator reduction occurs. Therefore, the second adjustment was to remove this delay from the beginning of the experiment and adjust the start time as if it were at time zero when the first notable detection of reduction occurred.

The final adjustment that had to occur was to convert the data to the fraction of reduced AH_2DS (species B) relative to the initial amount of oxidized AQDS (species A) added to the system (i.e. F_B discussed in Chapter 4). Thus, F_B could be graphed as a function of time. In order

to do so, calibration of reduced AH_2DS at 1 mM concentration and 0.5 mM concentration was performed at the given wavelengths. Fully reduced 1mM AH_2DS, ran in triplicate, was 0.620 OD at a wavelength of 520 nm and was above 2 at a wavelength of 450 nm. Fully reduced .5 mM AH_2DS, ran in triplicate, was 0.309 OD at a wavelength of 520 nm and 1.142 OD at a wavelength of 450 nm. If the calibration were to continue to be linear above 1.5 OD, then fully reduced AH_2DS would be 2.284 OD. Therefore, all data shown in Figure 5-4 was adjusted accordingly and F_B was plotted as seen in Figure 5-5. These changes showed that the data was actually consistent between the three runs.

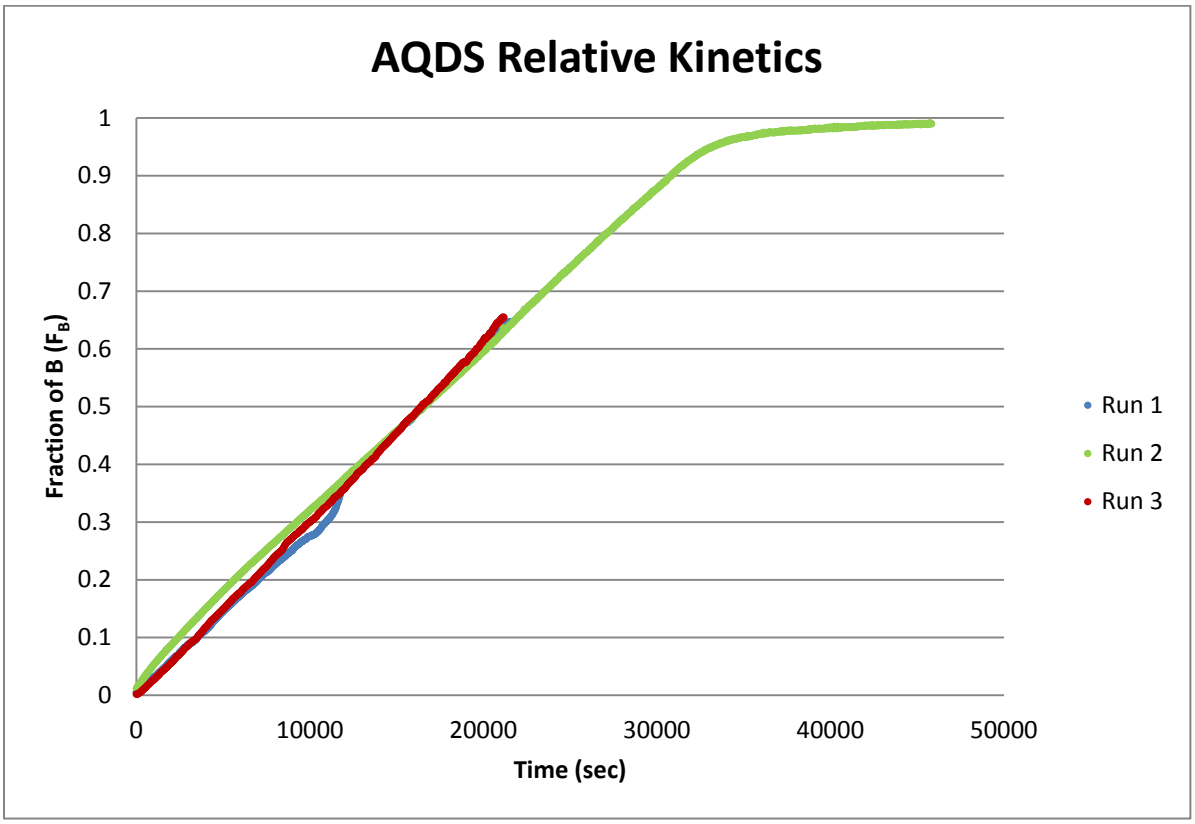

Figure 5-5 - Adjusted relative kinetic data for AQDS

5.3.2 **Methodology for Fitting of Kinetic Data to Kinetic Model**

The purpose of the model presented in Chapter 4 was to gain greater understanding of the rate limiting step in BER reduction reactions. Additionally, it presents a way to analyze, understand, and characterize the reactions that take place within the BER. In the absence of species C, the four dependent variables in Equations 4-37 through 4-40 are F_A, F_B, θ_A, and θ_B. The six rate constants, $k_{A,a}$, $k_{A,d}$, $k_{A,sr,f}$, $k_{B,a}$, $k_{B,d}$, and $k_{B,sr,r}$, are unknowns which must be fit to the data. The ratio parameter, R_{As}, is also an unknown, but its value was estimated as 10^3. The data, in all cases, to which the model was fit was converted to F_B as determined by the measured moles of B (reduced AH_2DS, or MV^+) relative to the known initial amount of A (oxidized AQDS, or MV^{2+}). For all data, there exist constraints which give a starting point for estimating rate constants prior to determining the rate constant values that provide the best fit.

However, before looking at the rate constants, it was important to determine the effect of the ratio parameter, R_{As}, on the model. It turns out that increasing the value of the R_{As} results in a slower approach to conversion of A to B, while decreasing the value of R_{As} results in a faster approach to conversion. This is illustrated in Figure 5-6, which shows the reversible model solved in Section 4.4.5 with surface reaction limiting (Example 1 with R_{As}= 1000) with the only difference being the value of R_{As} was halved (500) for Example 2 and increased by a full order of magnitude (10,000) for Example 3.

This scenario was run for a surface reaction limited rate, although the same trend applies no matter which rate limiting step is chosen. The results are explained by the fact that since the starting value of the oxidized electron mediator, C_A^0, is fixed, varying R_{As} is equivalent to varying C_{tot}. Since the actual value of C_{tot} is unknown, and cannot be gleaned simply from kinetic data, this could present a problem. However, R_{As} does not need to be known nor

regressed in order to have a model that yields useful information. This is because if the value of the rate constants of the rate limiting step are changed in the exact same manner as that of the R_{As}, then the resulting model is unchanged. This is shown in Figure 5-7 for the surface reaction rate-limiting scenario, which was generated from the rate constants shown in Table 5-1. The first curve, Example 1, is the same as Example 1 in Figure 5-6. As noted in Examples 4 and 5, the ratio of $k_{A,sr,f}$ to R_{As} and the ratio of $k_{B,sr,r}$ to R_{As} were maintained the same. Again, this data is plotted using surface reaction as the rate limiting step, but the results are the same no matter which rate limiting step is used.

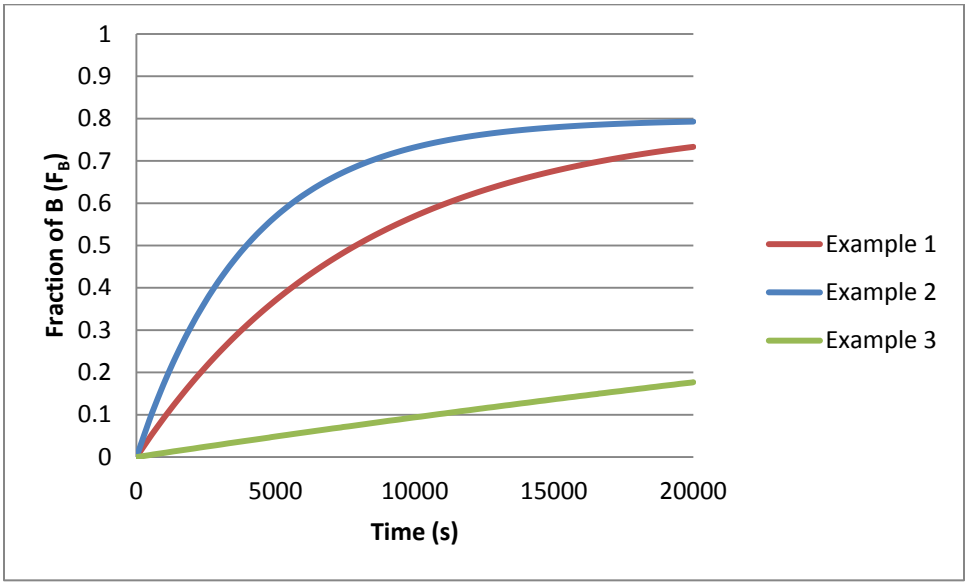

Figure 5-6 - Example model results with varying values of R_{As}

What is important, therefore, is not just the value of R_{As} or the rate constants of the rate limiting step, but rather the ratio of the rate constants of the limiting step to R_{As}. The ratio, which is fit to a given set of data, gives a rate constant that is normalized to the starting concentration of electron mediator (C_A^0). For all of the examples noted above, the ratio is equal to 1×10^{-4} s^{-1} even though the rate-limiting constants and R_{As} differ between examples. Since C_A^0 is known, a

rate constant could also be obtained that is the rate constant multiplied by C_{tot}. Although the value of R_{As} was fixed at 1000 in all data fitting noted below, the kinetic values of the rate limiting steps are reported as the ratio of the rate-limiting rate constants divided by R_{As}.

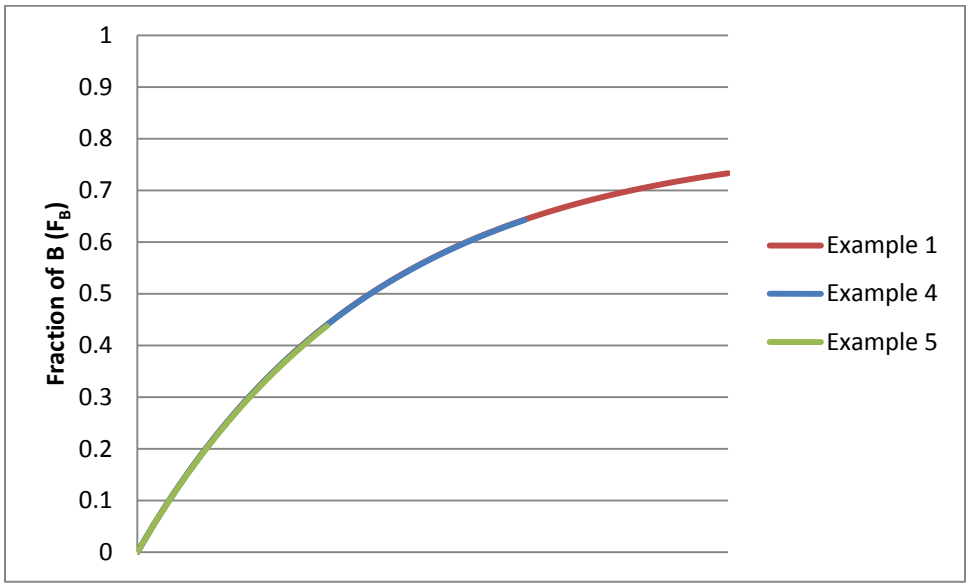

Figure 5-7 - Example model results varying R_{rb}, $k_{A,sr}$, and $k_{B,sr}$. Models were so close to identical that different portions had to be brought to the front in order to show that they are overlapping. Data from all models over the entire range are included in the graph.

Table 5-1 - Values of the rate constants used in Figure 5-7

	Example 1	Example 4	Example 5
$k_{A,a}$ (1/s)	1.000E+02	1.000E+02	1.000E+02
$k_{A,d}$ (1/s)	1.000E+02	1.000E+02	1.000E+02
$k_{A,sr,f}$ (1/s)	1.000E-01	5.000E-02	1.000E+00
$k_{B,a}$ (1/s)	1.000E+02	1.000E+02	1.000E+02
$k_{B,d}$ (1/s)	1.000E+02	1.000E+02	1.000E+02
$k_{B,sr,r}$ (1/s)	2.500E-02	1.250E-02	2.500E-01
R_{As}	1.000E+03	5.000E+02	1.000E+04

The first constraint for fitting the data is the identification and valuation of the rate limiting step. The rate constant of the rate-limiting step is, by definition, the smallest of the forward rate constants. . For all data, the initial data points were taken, linear regression was applied, and a slope was taken which was assumed to be equal to the initial rate. The initial rate is directly correlated to the forward rate constant of the rate limiting step. However, this correlation is not directly identifiable by use of Equations 4-37 through 4-40 because it is buried deep within the interaction of the equations. It is instructive, once again, to look at the pseudo steady state model equations to identify how this constraint can be used. The following analysis is performed on the surface reaction limited pseudo steady state rate law, Equation 4-19, but a similar analysis can also be performed for both adsorption and desorption limited rate laws.

Equation 4-19 must be converted from its current form, which is in terms of species concentrations, to a form analogous to the differential equation model, which is in terms of relative concentration. Initial simplification is performed by plugging in the values at time 0:

$$-\left[\frac{dC_A}{dt}\right]_0 = \left[\frac{dC_B}{dt}\right]_0 = r_{A0} = \frac{k_{sr}\cdot C_{tot}\left[C_A^0 - 0/K\right]}{\frac{1}{K_a}+C_A^0+0} = \frac{k_{sr}\cdot C_{tot}\cdot C_A^0}{\frac{1}{K_a}+C_A^0} \tag{5-1}$$

Next, the assumption that K_a is much greater than one is made. This is justified by the existence of the zeroth order character near the beginning of the experimental runs. Also, the initial rate is converted to the initial relative rate of F_B by factoring out a C_A^0 from the left hand side of the equation:

$$C_{A0}\left[\frac{dF_B}{dt}\right]_0 = \frac{k_{sr}\cdot C_{tot}\cdot C_A^0}{\cancel{\frac{1}{K_a}}+C_A^0} = \frac{k_{sr}\cdot C_{tot}\cdot C_A^0}{C_A^0} = k_{sr}\cdot C_{tot} \tag{5-2}$$

And finally, both sides are divided by C_A^0:

$$\left[\frac{dF_B}{dt}\right]_0 = \frac{k_{sr}\cdot C_{tot}}{C_A^0} = \frac{k_{sr}}{C_A^0/C_{tot}} = \frac{k_{sr}}{R_{AS}} \tag{5-3}$$

Therefore, the rate limited ratio of the forward rate (the rate constant of the forward rate of the rate limiting step divided by R_{As}) can be determined by analyzing the initial slope of the experimental data.

The next system constraint is equilibrium. Tests were run for a long enough period of time to measure an equilibrium value of $K = C_B/C_A = F_B/(1-F_B)$ at a given potential. While Equations 4-37 through 4-40 make no mention of K, K can be defined in terms of rate constants as follows:

$$K = \frac{C_B}{C_A} = \frac{K_a \cdot K_{sr}}{K_r} = \frac{\frac{k_{A,a}}{k_{A,d}} \cdot \frac{k_{A,sr,f}}{k_{B,sr,r}}}{\frac{k_{B,a}}{k_{B,d}}} \tag{5-4}$$

Therefore, none of the rate constants can be varied independently since this equality must be satisfied in order for the correct equilibrium to be reached. Since this is the case, an initial guess for the reverse rate of the limiting step (in terms of a rate constant divided by R_{As}) is obtained by dividing the forward rate of the limiting step (in terms of a rate constant divided by R_{As}) divided by the value of the overall equilibrium constant K. For example, if the reaction is surface reaction controlled, then the initial guess for $k_{B,sr,r}/R_{As}$ would be equal to $k_{A,sr,f}/R_{As}$ divided by K. If the reaction is adsorption controlled, then $k_{A,d}/R_{As}$ would be equal to $k_{A,a}/R_{As}$ divided by K. This results in the equilibrium constant of the rate limiting step being equal to the overall equilibrium constant. Although this is not completely true, it does provide a good initial estimate for the reverse rate constant. The other rate constants are defined in such a way as to require Equation 5-4 to be correct while assuring that value of the smallest rate constant other than the rate limiting rate constant is at least two orders of magnitude greater than the rate constant of the rate limiting step. The reason for this decision is described below.

This is best illustrated with an example. A hypothetical oxidized molecule A is reduced to B and conversion is equal to 80%, giving an overall K of 4. Additional data interpretation leads to the hypothesis that the rate limiting step is the surface reaction step and that initial rate in terms of relative concentration is 0.1 s^{-1}. In this case, the initial guess for the forward rate limiting ratio, $k_{A,sr,f}/R_{As}$ would be equal to $0.1s^{-1}$. The initial guess for the reverse rate limiting ratio, $k_{B,sr,r}/R_{As}$, would be equal to $0.025s^{-1}$, or $k_{A,sr,f}/R_{As}$ divided by K.

The other rate constants actually become arbitrary as long as the equality in Equation 5-4 holds true and as long as they are more than two orders of magnitude greater than the rate constant of the rate limiting step. If they are not two orders of magnitude greater, a regime begins to appear where multiple steps begin to control the overall rate. The reason the actual values are arbitrary is dependent upon the assumption that the number of molecules in the bulk is much greater than the number of available surface sites, or, in other words, that the value of R_{As} is large. As long as the other rate constants are fast enough such that the number of vacant surface sites remains very close to zero, the shape of the curve is dependent only on the ratio of the equilibrium constants for non-rate controlling steps, rather than the values of their rate constants.

This point, that the value of the rate constants becomes arbitrary, is illustrated in the following example for a surface reaction controlled model. In this model, the desorption and adsorption rate constants are described here in Table 5-2. The rate constants for the non-rate limiting steps were varied by an order of magnitude, but the model results, as seen in Figure 5-8, were completely unaffected.

Table 5-2 - Kinetic rate constants for example models

	Example 6	Example 7	Example 8
$k_{A,a}$ (1/s)	1.000E+02	1.000E+03	1.000E+02
$k_{A,d}$ (1/s)	1.000E+02	1.000E+02	1.000E+03
$k_{A,sr,f}/R_{As}$ (1/s)	1.000E-04	1.000E-04	1.000E-04
$k_{B,a}$ (1/s)	1.000E+02	1.000E+03	1.000E+02
$k_{B,d}$ (1/s)	1.000E+02	1.000E+02	1.000E+03
$k_{B,sr,r}/R_{As}$ (1/s)	2.500E-05	2.500E-05	2.500E-05

In fact, the only way to change the shape of the curve is to vary the value of the reverse rate constant of the rate-limiting step. Doing this necessitates the adjustment of one of the other rate constants to satisfy equilibrium conditions. What is interesting is that it does not matter which other rate constant is selected, the models all result in the same curve. This is illustrated in Figure 5-9. A baseline model was generated using the same rate constants used in Example 1 of Table 5-2. Then the reverse rate constant of the rate limiting step (in this case $k_{B,sr,r}$) was doubled or halved. Other rate constants were either doubled or halved independently, but always resulting in an overall equilibrium constant K of 4. The curves went unchanged regardless of which other rate constant was modified. When the value of the reverse rate constant is increased, even though the initial rate is the same, this rate is maintained for a longer period of time, resulting in a steeper ascent to equilibrium. When the value of the reverse rate constant of the rate limiting step is decreased, the result is a slower ascent to equilibrium.

Thus, the steps for data fitting are as follows:

1. Visual inspection for identification of possible rate determining steps.
2. Interpret the data for identification of overall equilibrium constant, K, and initial rate of reaction.

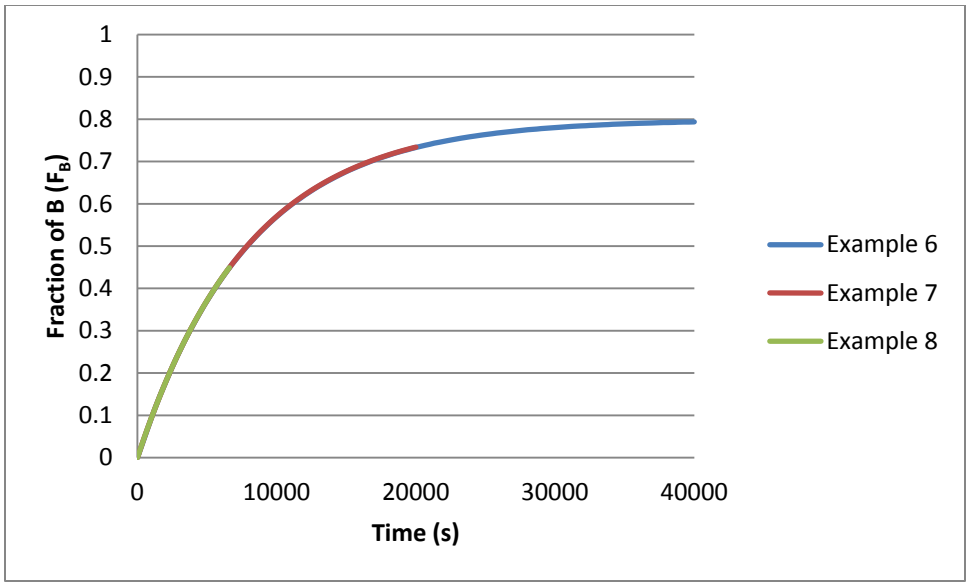

Figure 5-8 - Example model results. Models were so close to identical that different portions had to be brought to the front in order to see that they are overlapping. Data from all models over the entire range are included in the graph.

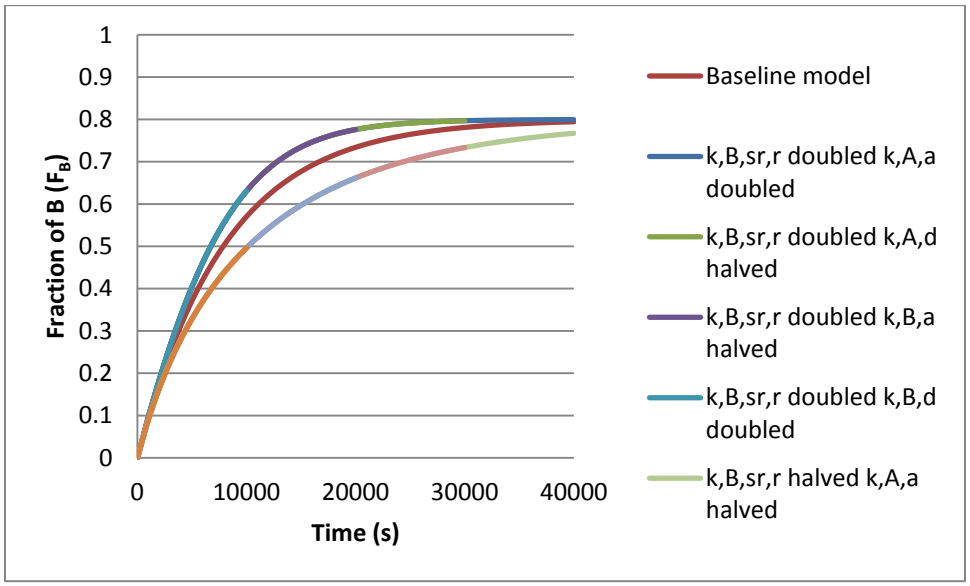

Figure 5-9 - Results of rate constant variations. As in Figure 5-8, models were so close to identical that different portions had to be brought to the front in order to see that they are overlapping. Data from all models over the entire range are included in the graph.

3. Set forward rate limited ratio (the rate constant of the forward rate of the rate limiting step divided by R_{As}) equal to the initial rate of reaction of F_B.

4. Set the reverse rate limited ratio (the rate constant of the reverse rate of rate limiting step divided by R_{As}) equal to the forward rate limited ratio divided by the overall equilibrium constant.
5. Set all other rate constants equal to a value at least two orders of magnitude greater than the magnitude of the rate limiting step and such that their combined product satisfies Equation 5-4 for K.
6. Adjust the reverse rate limited ratio accordingly to modify the speed of ascent to equilibrium, adjusting one of the non-rate limiting rate constants from step 5 in tandem to assure that Equation 5-4 remains satisfied.
7. Repeat step 6 until the model has converged on the experimental data.

5.3.3 **AQDS Kinetics Results Analysis**

Both the raw and relative data indicate that the reaction proceeds in zeroth order fashion until very high conversion occurs. Referring back to the model that was derived in Chapter 4, it becomes apparent that the rate-limiting step cannot be adsorption. The only possibilities are surface reaction controlled and desorption controlled because both of these options include the possibility of a zeroth order reaction rate law. Therefore, the data was modeled as surface-reaction limited and desorption limited using Polymath 6.10 Professional software's STIFFBS ordinary differential equation solver method. Varying the six unknowns with both models leads to a good fit for both possible rate-limiting step kinetic models. Therefore, it becomes impossible to decipher from this data set alone which of these two steps controls the overall rate. Figure 5-10 below shows the data fitted with a surface reaction controlled rate law and a desorption controlled rate law. Both are almost carbon copies of each other until high conversion, and neither model is conclusively superior.

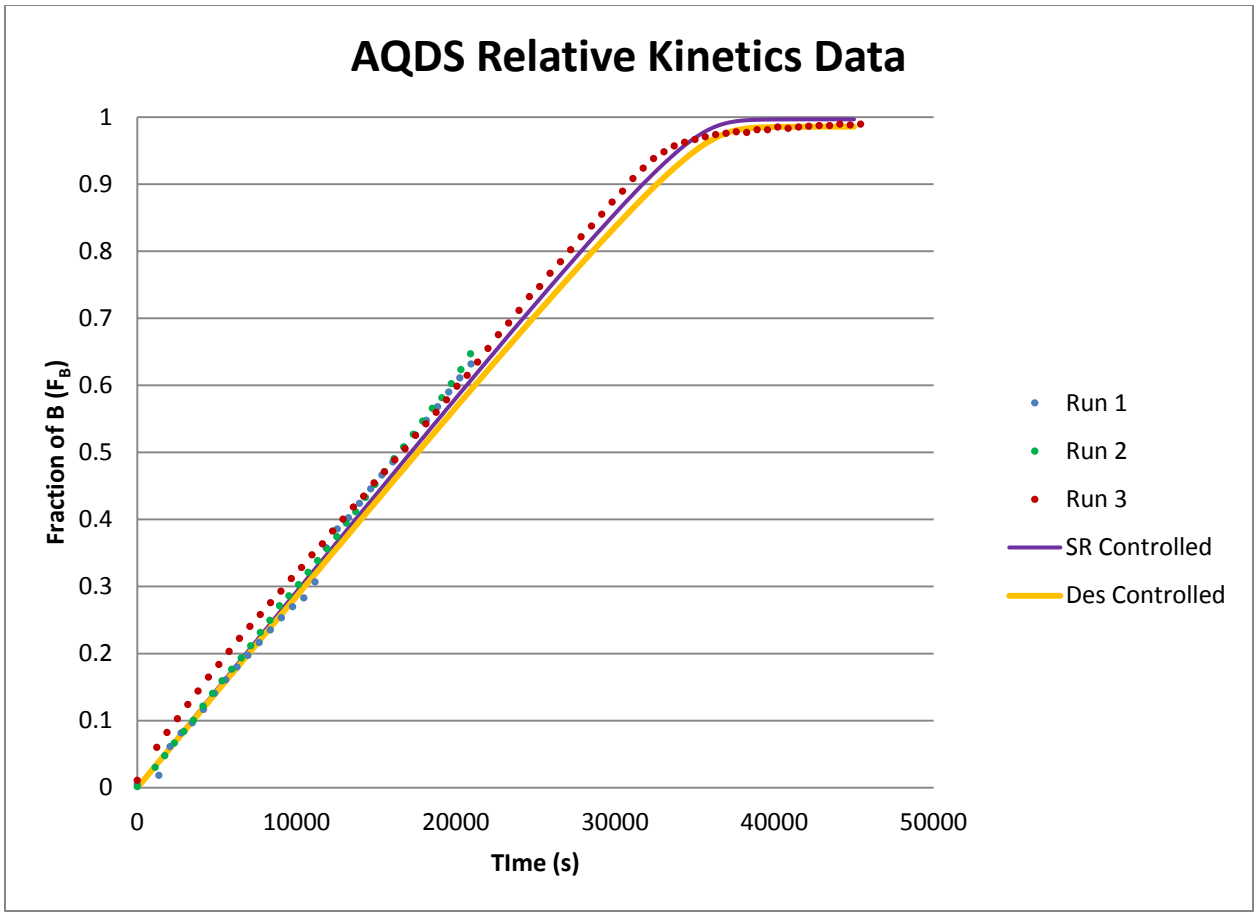

Figure 5-10 - Adjusted kinetic data plotted with a fitted surface reaction controlled model and a fitted desorption controlled model. Data has been thinned to 1 plotted point for every 25 experimental points to allow the model to be shown.

The most important message that can be gleaned from this data is the zeroth order rate of reaction. Using the relativized data, this rate can be calculated independently for each of the three runs and then analyzed to determine the average rate of reaction. A statistical analysis of the presented data was performed for the linear portion of the reactions. The results of this analysis are presented in Figure 5-3.

Table 5-3 - Summary of rate of reaction for AQDS runs

	Rate of Reaction (mM/s)	Rate of Reaction (mM/hr)	R^2 (unitless)
Run 1	3.054E-05	1.099E-01	0.9975
Run 2	3.081E-05	1.109E-01	0.9998
Run 3	2.823E-05	1.016E-01	0.9997
Average	2.986E-05	1.075E-01	n/a
Standard Deviation	1.418E-06	5.105E-03	n/a

It becomes apparent that over the linear portion of the model, the behavior of the model is highly predictive of the trend seen. The fact that the coefficient of determination, R^2, is greater than 0.99 for each of the three data sets illustrates the reliability of the model. Additionally, the standard deviation across the three runs is only 4.8% of the average value, indicating that repeatability is not a key issue in this set of data.

5.3.4 **Regression of Parameters for AQDS Experiments**

Revisiting Equations 4-22 through 4-25, it is apparent that there are six unknowns that need to be solved for from the data. These unknowns are $k_{A,a}$, $k_{A,d}$, $k_{A,sr}$, $k_{B,a}$, $k_{B,d}$, $k_{B,sr,r}$. From the data, we can only define the rate-constant of what we expect to be the rate-limiting step, in this case either the forward surface reaction rate constant ($k_{A,sr,f}$) or the desorption rate constant of the reduced species ($k_{B,d}$). All other parameters can be fine-tuned to fit the data since no other constraints can be placed on the system. Table 5-4 below gives values for the models that were used in Figure 5-10. It should be noted that the forward and reverse rate constants of the limiting

step (highlighted in the table) are the only parameters of significance since the values of the other parameters can be arbitrarily chosen as long as the meet the equilibrium constraint.

Table 5-4 - Summary of rate constants from fitted models

	Surface Reaction Controlled		**Desorption Controlled**
$k_{A,a}$ (1/s)	1.000E+03	**$k_{A,a}$ (1/s)**	1.000E+03
$k_{A,d}$ (1/s)	1.000E+00	**$k_{A,d}$ (1/s)**	1.000E+00
$k_{A,sr,f}/R_{As}$ (1/s)	2.986E-05	**$k_{A,sr,f}$ (1/s)**	2.500E+01
$k_{B,sr,r}/R_{As}$ (1/s)	3.318E-06	**$k_{B,sr,r}$ (1/s)**	1.000E+00
$k_{B,d}$ (1/s)	2.000E+00	**$k_{B,d}/R_{As}$ (1/s)**	2.986E-05
$k_{B,a}$ (1/s)	4.000E+01	**$k_{B,a}/R_{As}$ (1/s)**	1.000E-03

5.3.5 AQDS Kinetics Results Discussion

Although this data set cannot on its own merits determine which step of the three-step mechanism is the rate-limiting step, important information can nevertheless be gleaned from the results and data presented. Since the rate is clearly zeroth order, the possibility of increasing the rate simply by increasing the bulk concentration of the electron mediator can be ruled out. This means that a great emphasis will need to be placed on reactor design. Referring back to Equations 4-19 and 4-21, the apparent rate constant during the portion can be defined as follows for a surface reaction controlled rate:

$$k_{sr'} = \frac{K_a \cdot k_{sr} \cdot C_{tot}}{K_a} = k_{sr} \cdot C_{tot} \tag{5-5}$$

For a desorption controlled rate, the apparent rate constant is defined as follows:

$$k_{d'} = \frac{K_a \cdot k_d \cdot C_{tot}}{K_a + \frac{1}{K_r}} \approx k_d \cdot C_{tot} \tag{5-6}$$

These two equations are remarkably similar. The approximate equality in Equation 5-6 can be justified using the assumptions that are inherent in a desorption controlled rate-limiting

step. K_a is simply the quotient of the rate of adsorption of A over the rate of desorption of A. Since the rate-limiting step is not the adsorption step, it seems reasonable to assume that K_a is much greater than one. Additionally, if it is desorption limited then the adsorption of the reduced species, B, is more favorable than the desorption, which suggests that the value of K_r would also be much greater than one. Since both adsorption coefficients, K_a and K_r are both much greater than one, Equation 5-6 collapses in a similar fashion to Equation 5-5, meaning that the apparent rate of desorption, k_d', is simply the product of k_d and C_{tot}.

The simple reliance of the rate of reaction on the kinetic rate constant and total sites available for binding means that few options are available in order to speed up the reaction. The simplest and most effective way to increase the rate of reaction is to increase surface area of the electrode. Total adsorption sites are proportional to the surface area available for adsorption. Designing a reactor that would maximize the surface area to volume ratio would result in a large increase in the rate of reaction. The rate constant, k_d, is a function of temperature and electrode material. Temperature is somewhat limited in enzyme or whole cells systems because the cells may have a difficult time adapting to elevated temperatures and most proteins have an upper limit in temperature above which they become denatured and lose functionality. There will always be an upper limit to the temperature that is tolerable for the experiments, although in some applications it may prove worthwhile to run them at elevated temperatures. In these experiments, only carbon electrodes were used and different materials may yield different kinetic rate laws. Future work could include similar kinetic studies performed on other electrode materials.

5.4 Experimental Results with Methyl Viologen (MV)

5.4.1 Experimental Results with MV

The next set of experimental data was taken with methyl viologen as the electron mediator. All data for the methyl viologen experiments were taken at 606 nm, where the extinction coefficient is 13000 M^{-1} cm^{-1} [57]. Data was taken at three different relative voltages, -800 mV, -900 mV, and -1000 mV.The majority of methyl viologen data was taken by Chang Chen [58], only Run 3 and Run 4 of the plotted data at -900 mV were performed by the author. Conversion to units of concentration has already occurred and, similar to AQDS, removal of the lag time during which no reaction occurs has also already been applied.

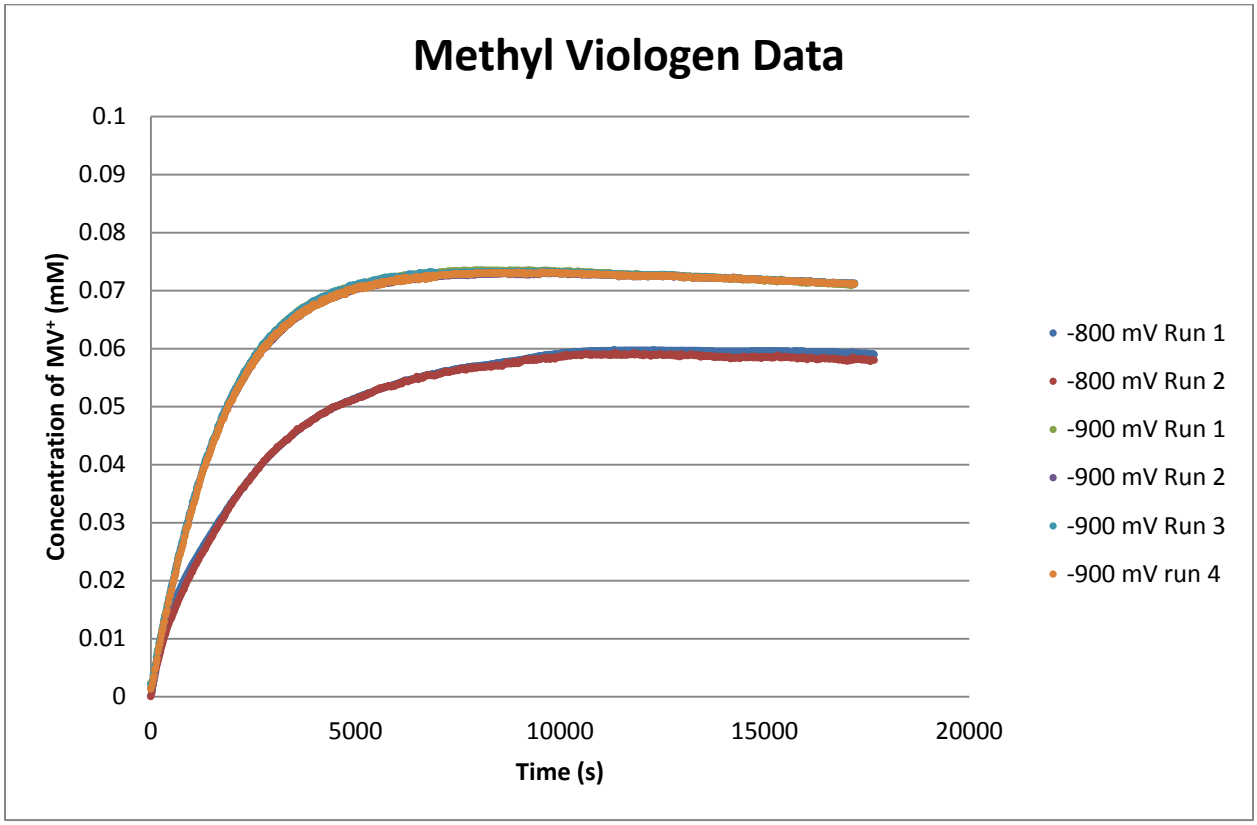

Figure 5-11 - Methyl viologen kinetic data for -800 mV and -900 mV. Data for -900 mV overlaps so it is difficult to see individual runs.

Preliminary kinetic analysis was also performed by Chang Chen[58]. The kinetic model utilized in that work was built on the same three step mechanism proposed here in Chapter 4. However, all reactions were assumed to be irreversible and the steady-state assumption for the intermediates was used. This resulted in a model which is less robust than the one that has been described in this text, and can only be applied to reactions which go to complete conversion. Also, no single set of parameters was able to provide an adequate fit for the entire range of kinetic data. Indeed, the kinetic data was split into 3 separate stages, and kinetic rate constants were regressed separately for each stage. The model used in this work requires no such splitting of data into different reaction stages. Figure 5-11 shows the data for the experiments run at -800 mV and -900 mV, while Figure 5-12 shows the data for experiments run at -1000 mV.

5.4.2 **MV Kinetics Results Initial Analysis**

What immediately becomes apparent when viewing Figure 5-11 is that it is vastly different from the AQDS data in that full conversion is not achieved. At -800 mV and -900 mV, the amount of MV^+ asymptotically approaches its equilibrium at that voltage potential. At -1000 mV, something drastically different happens. The data achieves a maximum and then begins to decrease, which is indicative of further reduction to MV^0. For the -800 mV and -900 mV cases, the curve appears to either be zeroth order until it approaches equilibrium or even first order in nature. For the -1000 mV case, each side of this maximum appears to be defined by zero order kinetics similar to the kinetics of the AQDS reduction, although some first order character is also apparent. Additionally, the visible color change associated with the entire reaction went from no visible color to a deep blue, which then faded to pale yellow at the end of the experiment. This interesting phenomenon was unobserved during initial experimentation where the voltage potential was set to -700 mV relative to the Ag/AgCl electrode, where the final product at the

end of the experiments was deep blue in color. However, all such experiments were performed before the implementation of the flow-through spectrophotometric system had occurred, so no spectrophotometric data exist for these runs. The final visible color of the -800 mV and -900 mV experiments was also a deep blue.

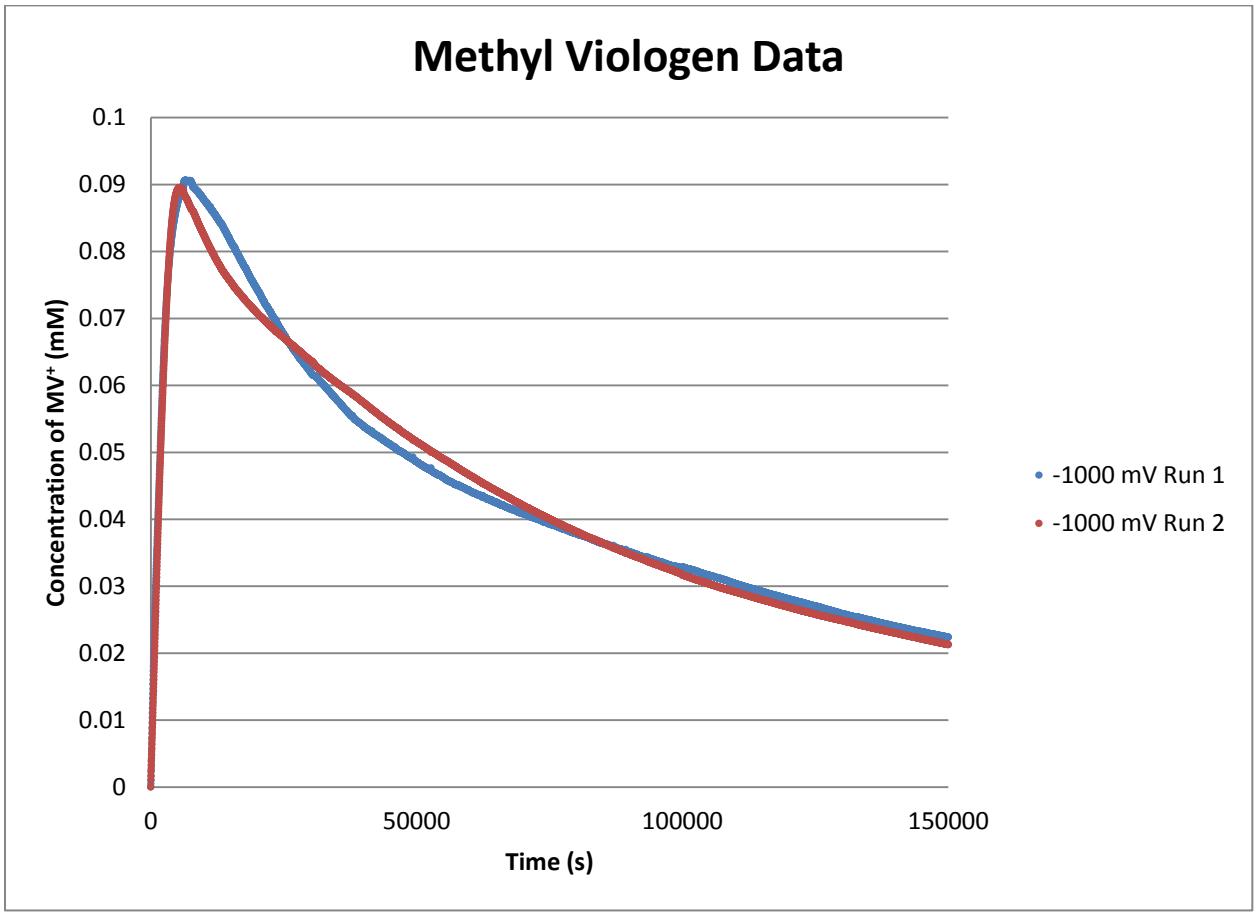

Figure 5-12 - Methyl viologen kinetic data for -1000 mV

A review of the literature finds that methyl viologen exhibits three separate oxidation states. The parent dication, MV^{2+}, can undergo a single reduction to MV^{+}, a blue monocation. This monocation is further reduced to the colorless uncharged form MV^{0}. The standard redox potential for these two respective reactions are -446 mV and -772 mV relative to the NHE (which are -646 mV and -972 mV relative to the Ag/AgCl electrode) [6]. Therefore, at -700, -

800, and -900 mV relative to the Ag/AgCl electrode, the overpotential is not great enough for the second reduction to be seen in abundance (some conversion can be seen at the end of the -800 mV and -900 mV runs, but only very little due to very slow kinetics). At -1000 mV however, there is more than sufficient driving force for the second reduction to occur.

5.4.3 **Modeling of Methyl Viologen Single Reduction Experiments**

Using the non-simplified model described in section 4.4.4, the data displayed in Figure 5-11 was modeled. Visual inspection of the data does not lead to immediate interpretation of the rate-limiting step. Therefore, the data was modeled as surface-reaction limited and adsorption limited using Polymath 6.10 Professional software's STIFFBS ordinary differential equation solver method. Careful fitting of the data utilizing both rate-limiting steps was performed. The results are presented Figure 5-13 and Figure 5-14.

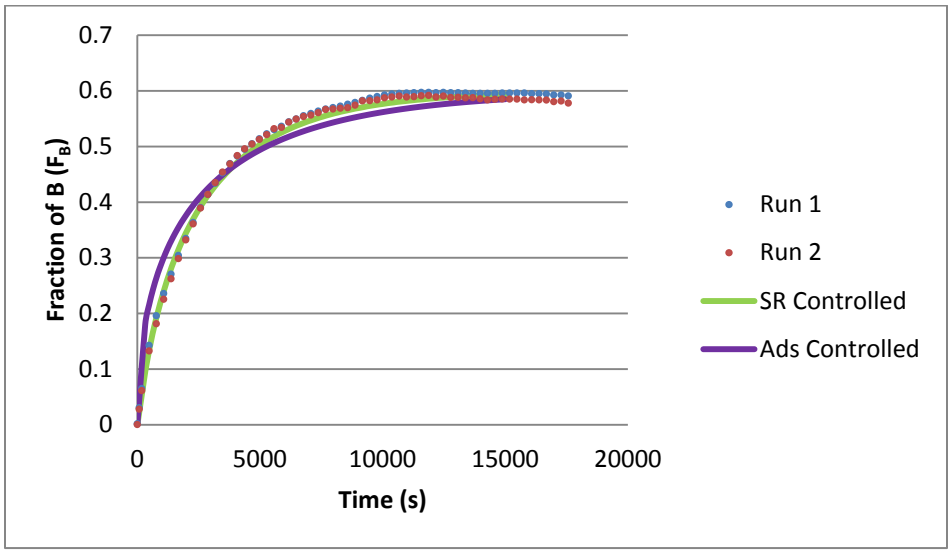

Figure 5-13 - Methyl viologen reduction data and model. Data from experiments performed at -800 mV. Data has been thinned to 1 plotted point for every 15 experimental points to allow the model to be shown.

Although both models provide a good fit to the data, it is obvious that the model with surface reaction as the rate-limiting step provides an almost exact fit, while the model with

adsorption as the rate-limiting step leads the data initially and then lags the data later on. No matter how the constants are massaged, the adsorption-controlled model displays this tendency. This model provides strong evidence that surface reaction is the rate-limiting step for methyl viologen reduction.

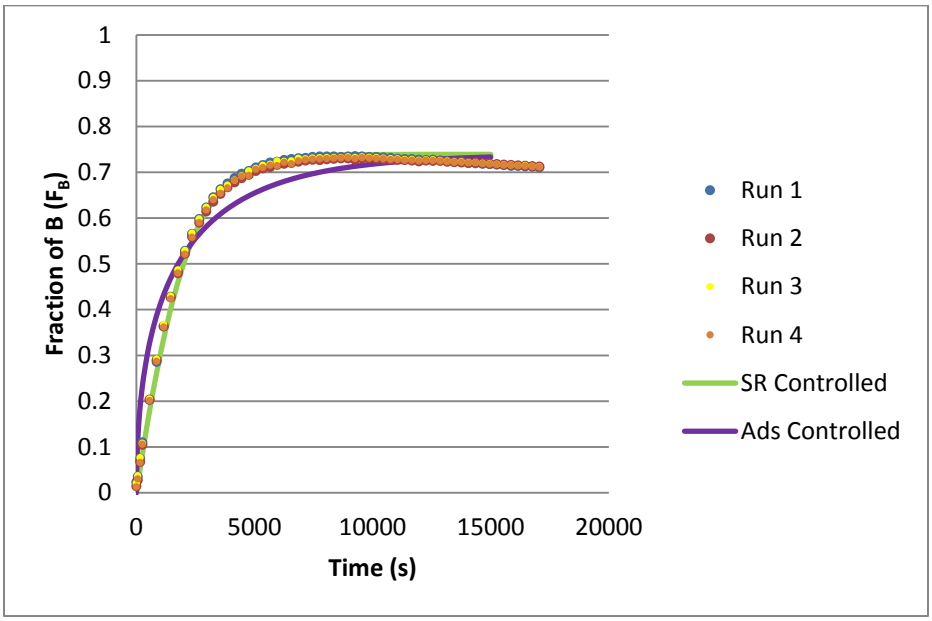

Figure 5-14 - Methyl viologen reduction data and model. Data from experiments performed at -900 mV. Data has been thinned to 1 plotted point for every 15 experimental points to allow the model to be shown.

5.4.4 Regression of Parameters for Methyl Viologen Single Reduction Experiments

As was the case when modeling the AQDS experimental data, there are six unknowns for the reactions in which only MV^{2+} is converted to MV^{+} (no MV^{0} is formed). The constraint for the forward reaction of the rate-limiting step, be it surface reaction or adsorption, is applied in the same manner described in section 5.3.4. The fact that the conversion of methyl viologen does not approach full conversion provides one additional constraint that was not available when fitting the AQDS experimental data. Conversion provides a constraint in the form of the overall equilibrium constant, which was defined above in Equation 4-14. Since the overall equilibrium

constant is a ratio of the kinetic rate constants, none of the rate constants can be varied independently, as each change necessitates a corresponding change to assure that the final conversion remains the same.

5.4.4.1 Regression of Initial Rate

Determination of the initial rate for the AQDS results was simplified due to the obvious linearity of the data. Unfortunately, the MV data is only zeroth order in nature for the very beginning of the data set. In order to ensure that the initial rate was calculated correctly, only the initial few data points were utilized. The data utilized to calculate these initial rates is presented here for -800 mV in Figure 5-15 and for -900 mV in Figure 5-16.

Data for the -800 mV experiment loses its linearity very quickly, which is why a smaller number of data was used to determine the initial rate. The initial rates that were used for the kinetic model, as well as averages and standard deviations, are summarized below in Table 5-5.

5.4.4.2 Model Parameters Determined by Best Fit

All parameters have been fit as described above in section 5.3.4 and are presented in Table 5-6 for -800 mV data and Table 5-7 for -900 mV data. The non-arbitrary parameters are highlighted. All other parameters are arbitrary except these parameters are consistent with the equilibrium constant.

Although the initial forward rates are very similar, the reverse rate increases at higher overpotential. This increase in the reverse rate leads to the observation that the initial rate of reaction persists for a longer period of time in the -900 mV experiments than the -800 mV experiments. A greater value of $k_{B,sr,r}$ leads to higher values of θ_A throughout the experiment, and higher values of θ_A lead to a faster observed rate.

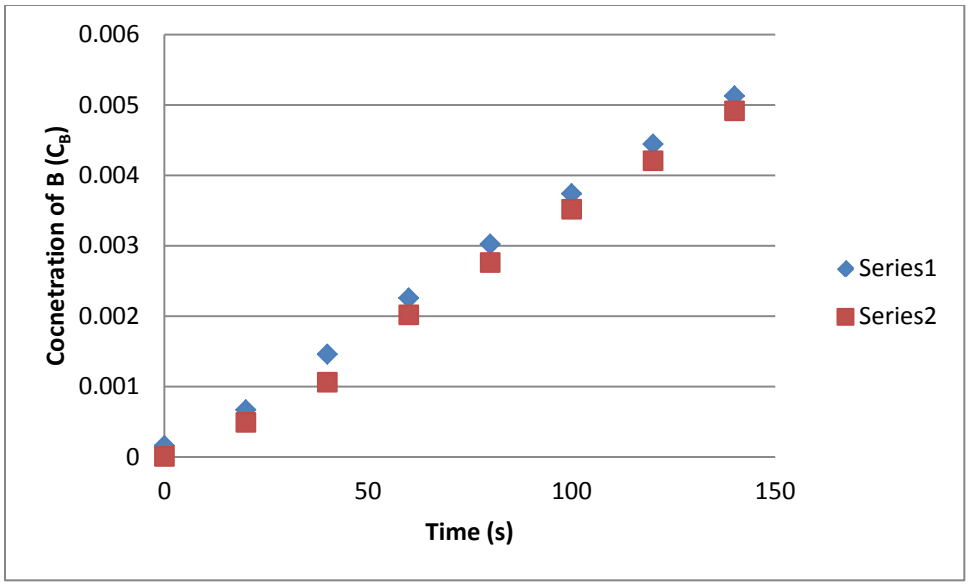

Figure 5-15 - Data utilized for initial rate of -800 mV methyl viologen experiment

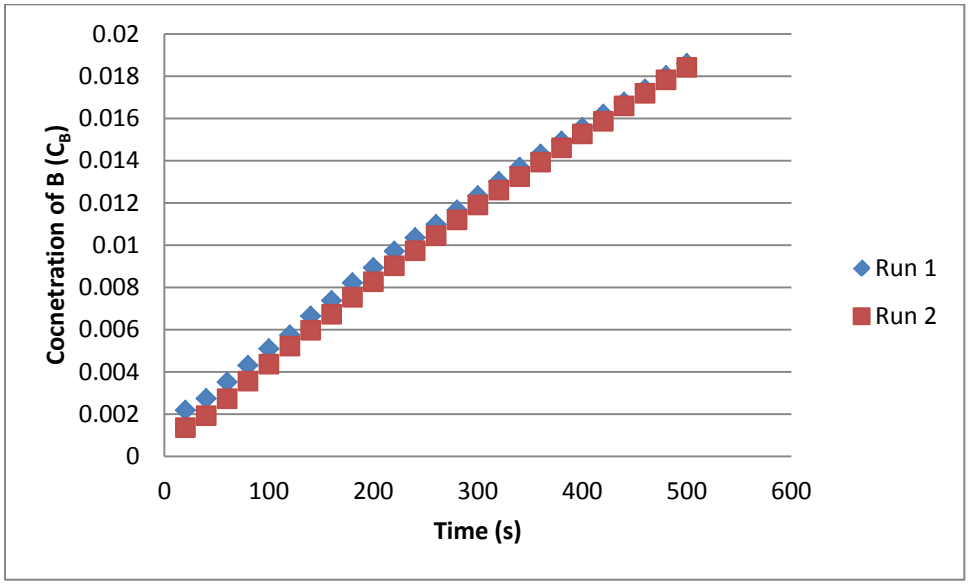

Figure 5-16 - Data utilized for initial rate of -900 mV methyl viologen experiment

Table 5-5 - Summary of initial rates of reaction for methyl viologen

	Apparent Initial Rate (mM/s)	Apparent Initial Rate (mM/hr)	R-squared (unitless)
Run 1 at -800 mV	3.647E-05	1.313E-01	0.9985
Run 2 at -800 mV	3.635E-05	1.309E-01	0.996
Average at -800 mV	3.641E-05	1.311E-01	n/a
Standard Deviation at -800 mV	8.485E-08	3.055E-04	n/a
Run 1 at -900 mV	3.456E-05	1.244E-01	0.9977
Run 2 at -900 mV	3.596E-05	1.295E-01	0.9983
Average at -900 mV	3.526E-05	1.269E-01	n/a
Standard Deviation at -900 mV	9.899E-07	3.564E-03	n/a

Table 5-6 - Kinetic rate constants used for modeling -800 mV experimental data

	Surface Reaction Controlled		Adsorption Controlled
$k_{A,a}$ (1/s)	3.333E+01	**$k_{A,a}/R_{As}$ (1/s)**	3.641E-04
$k_{A,d}$ (1/s)	1.000E+02	**$k_{A,d}/R_{As}$ (1/s)**	6.935E-05
$k_{A,sr,f}/R_{As}$ (1/s)	3.641E-04	**$k_{A,sr,f}$ (1/s)**	5.714E+01
$k_{B,sr,r}/R_{As}$ (1/s)	8.091E-05	**$k_{B,sr,r}$ (1/s)**	1.000E+02
$k_{B,d}$ (1/s)	1.000E+02	**$k_{B,d}$ (1/s)**	1.000E+02
$k_{B,a}$ (1/s)	1.000E+02	**$k_{B,a}$ (1/s)**	1.000E+02
K (unitless)	1.500E+00	**K (unitless)**	1.500E+00

Table 5-7 - Kinetic rate constants used for modeling -900 mV experimental data

	Surface Reaction Controlled		Adsorption Controlled
$k_{A,a}$ (1/s)	2.200E+02	**$k_{A,a}/R_{As}$ (1/s)**	3.526E-04
$k_{A,d}$ (1/s)	1.000E+02	**$k_{A,d}/R_{As}$ (1/s)**	2.478E-04
$k_{A,sr,f}/R_{As}$ (1/s)	3.526E-04	**$k_{A,sr,f}$ (1/s)**	4.000E+02
$k_{B,sr,r}/R_{As}$ (1/s)	2.726E-04	**$k_{B,sr,r}$ (1/s)**	1.000E+02
$k_{B,d}$ (1/s)	1.000E+02	**$k_{B,d}$ (1/s)**	1.000E+02
$k_{B,a}$ (1/s)	1.000E+02	**$k_{B,a}$ (1/s)**	2.000E+02
K (unitless)	2.846E+00	**K (unitless)**	2.846E+00

5.4.5 Discussion of Rate Limiting Steps

Before continuing, it must be determined which step is the rate-limiting step. The first piece of evidence is the AQDS reaction, which visually indicate the possibility of both surface reaction and desorption as possible rate limiting steps. Modeling cannot conclusively decide which of these two steps is in fact rate limiting, but adsorption is not an option for this set of conditions. The single reduction MV data visually indicate the possibility of surface reaction and adsorption as possible rate limiting steps. Modeling further makes it apparent that a surface reaction limiting assumption provides a significantly better fit for the data than an adsorption model. It seems, therefore, that the only explanation under those conditions is that the reaction of MV^{2+} to MV^{+} is limited by the rate of the surface reaction. Furthermore, the existence of measurable MV^{+} in the bulk suggests that adsorption is not the rate-limiting step for the reaction of MV^{+} to MV^{0} since the MV^{+} is already adsorbed to the electrode surface the instant that it is formed.

Finally, as stated in section 5.1.1, preliminary MV experiments were run with initial concentrations of 1 mM. Figure 5-17 presents the data from these preliminary experiments,

which were run at -2000 mV. While they are not useful for kinetic modeling due to the side-reaction of dimerization, the characteristic shape of the curve is another piece of evidence suggesting that the overall reaction is surface reaction limited. The curves are obviously zeroth order in nature, and the existence of MV^+ in the bulk solution cannot be explained by a desorption controlled rate law. If the reaction of MV^+ is desorption controlled, then it would immediately undergo the non-limiting surface reaction and be reduced to MV^0 without ever being released into the bulk to be detected by the spectrophotometer. Due to all of this overwhelming evidence, the conclusion has been drawn that the MV bioelectrical reactor experiments of this study are limited by the rate of the surface reaction at all applied potentials that were studied.

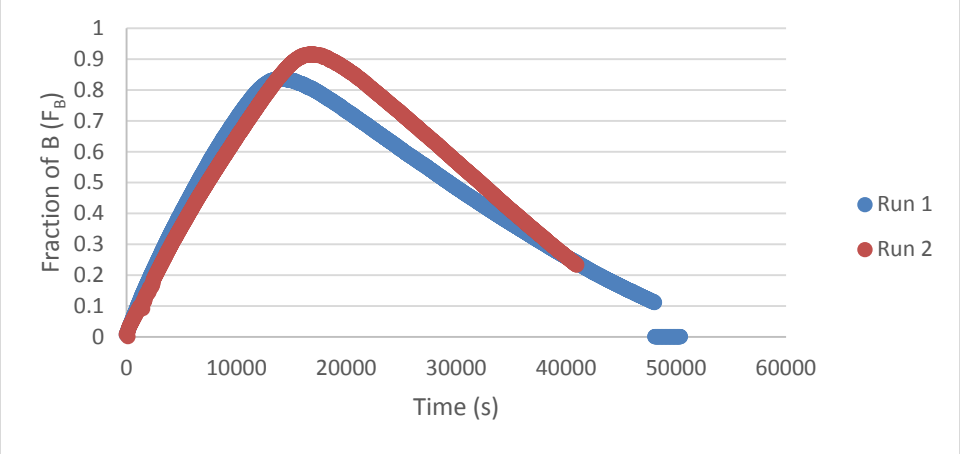

Figure 5-17 - Methyl viologen experiments run at -2000 mV

5.4.6 **Overpotential Model**

Other kinetic models exist for electrochemical kinetic rates based on overpotential of the electrodes. These models are made in order to explain the effect of potential on the rate of reaction. The full derivation is not covered in this work, but the calculation of the rate constant is of the following form:

$$k = A_1 \cdot \exp(\frac{n \cdot F \cdot U \cdot \beta_1}{R \cdot T}) \quad (5\text{-}7)$$

In these equations, A_1 and β_1 are fitted constants, n is the number of electrons transferred, R is the ideal gas constant, T is temperature, and U is potential. The value of U is negative for reducing reactions and positive for oxidizing reactions. This model helps to explain some of the trends that were observed. The value of U is negative for the forward rate constant $k_{A,sr,f}$ and positive for the reverse rate constant $k_{B,sr,r}$. A large negative value within the exponent leads to the exponential term becoming negligible, which is why there is no observed increase in the forward rate constant of reaction with increasing overpotential. Conversely, an increase in the value of the reverse rate constant is observed which is consistent with the overpotential model with a positive value for U.

Utilizing Equation 5-7, the reverse rate constant $k_{B,sr,r}$ for -1000 mV can be predicted from the -800 and -900 mV experiments. The relationship of any two rate constants with a known difference in potential is as follows:

$$k_2 = k_1 \cdot \exp(\frac{n \cdot F \cdot \Delta U \cdot \beta_1}{R \cdot T}) \quad (5\text{-}8)$$

where ΔU is the difference in potential associated with the two constants . The values of n, F, A_1, R, and β_1 are constant, and T is also constant since the experimental apparatus was held at constant temperature. When ΔU = 100 mV (e.g. 900 - 800 = 100 mV) then Equation 5-8 collapses to:

$$k_2^{U+100} = k_1^U \cdot C \quad (5\text{-}9)$$

This relationship holds true for any rate constant as long as the potential difference associated with the two rates constants is 100 mV. Using this relationship with $k_1^{800} = k_{B,sr,r}/R_{As} = 8.091 \times 10^{-5}$ s^{-1} (Table 5-6) and $k_1^{900} = k_{B,sr,r}/R_{As} = 2.726 \times 10^{-4}$ s^{-1} (Table 5-7), C = 3.37. Thus, $k_2^{1000} = k_{B,sr,r}/R_{As}$ is predicted to be 9.184×10^{-4} s^{-1} at -1000 mV.

5.4.7 **Modeling of Methyl Viologen Multiple Reduction Experiments**

Utilizing a similar methodology as described in section 4.4.4, the data presented in Figure 5-12 was regressed and modeled. Because of the length of the experiment, and because Polymath does not allow for specification of the number of nodes, the modeling took place in three separate time periods. The first time period was from 0-8,000 seconds, the second covered the data from 8,000-20,000 seconds, and the third covered the data from 20,000 to 150,000 seconds. All rate constants were maintained the same throughout each time period. The second and third time periods were initialized by inputting the final values from the preceding time period. This means that the numerical methodology is the same as solving it as one single time period with triple the number of nodes, and those nodes condensed to where the greatest changes are occurring (near the beginning of the experiment).

For the reaction in which MV^{2+} can reduce to both MV^{+} and MV^{0}, there exist 10 unknowns rate constants from Equations 5-4 through 5-9 (with R_{As} set to 1000) which must be fit to the data. There are four constraints which must be maintained. The first constraint is the initial rate. The second is the overall conversion, which was taken from longer experiments run by Chang Chen[58]. The third is the peak concentration of MV^{+}. The fourth is the zeroth order portion of the reduction of MV^{+} to MV^{0}. Results of optimization can be seen in Figure 5-18. The existent of so many constraints means that none of the rate constants in this model are arbitrary, as all contribute to one of these constraints.

It is important to note that the regressed rate constants can differ based on the value chosen for the reverse rate limiting ratio ($k_{B,sr,r}/R_{As}$). At different values of this parameter, all other rate constants can then be optimized in order to provide a best fit curve. For this reason, the value was constrained to 9.184×10^{-4} s^{-1} as described in Section 5.4.6. This provides a fifth

constraint for the fitting of the model performed.

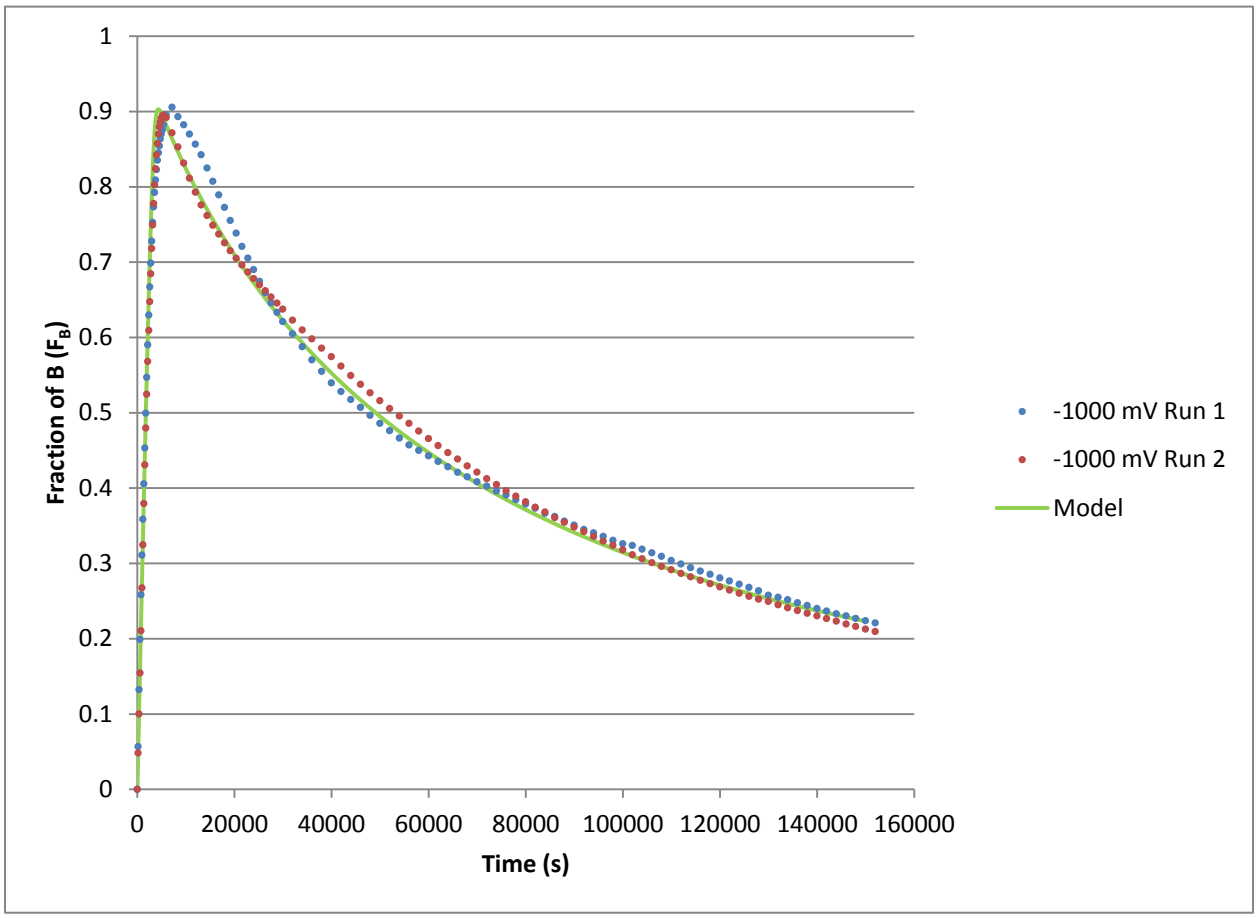

Figure 5-18 - Methyl viologen reduction data and model. Data from experiments performed at -1000 mV. Data has been thinned to allow the model to be shown.

The extent to which such a relatively simplistic model fits such a complex system is quite revelatory. This also provides the crowning piece of evidence that these reactions are in fact limited in their kinetic rate by the surface reaction of the species that is being reduced. The kinetic model optimization verifies the logical explanations that have been presented up to this point. It appears that there is no other explanation for the experimental data seen.

5.4.8 Regression of Parameters for Methyl Viologen Multiple Reduction Experiments

Regression for parameters was performed in like manner to the AQDS and single reduction MV experiments.

5.4.8.1 Regression of Zeroth Order Rates

Whereas in the above experiments only had zeroth order character near the beginning of the experiment, this data exhibits two sections defined by zeroth order kinetics. The first is the initial rate of MV^{2+} reduction. The second occurs just after the peak of MV^{+} is reached, and will be referred to as the zeroth order rate of MV^{+} reduction. Both of these portions of the data can be used as constraints for the kinetic model. The portions of data which were used to define these zeroth order experimental character are presented here in Figure 5-19.

While not as internally consistent as the data from the -800 mV and -900 mV duplicates, the rates are still extremely linear in nature. Due to the difference in the time it took to reach the peak MV^{+} conversion in the different runs, the data for the zeroth order portion of conversion from MV^{+} to MV^{0} are taken at different times for each run. Both figures are included here. A summary of all data presented in these three figures is presented in Table 5-8.

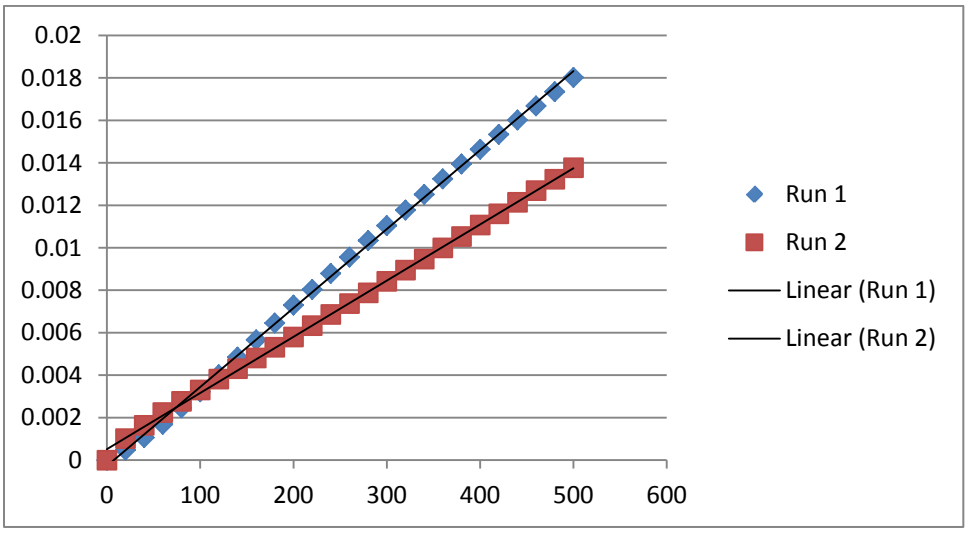

Figure 5-19 - Data utilized for determination of initial rate of the MV^{2+} of -1000 mV data

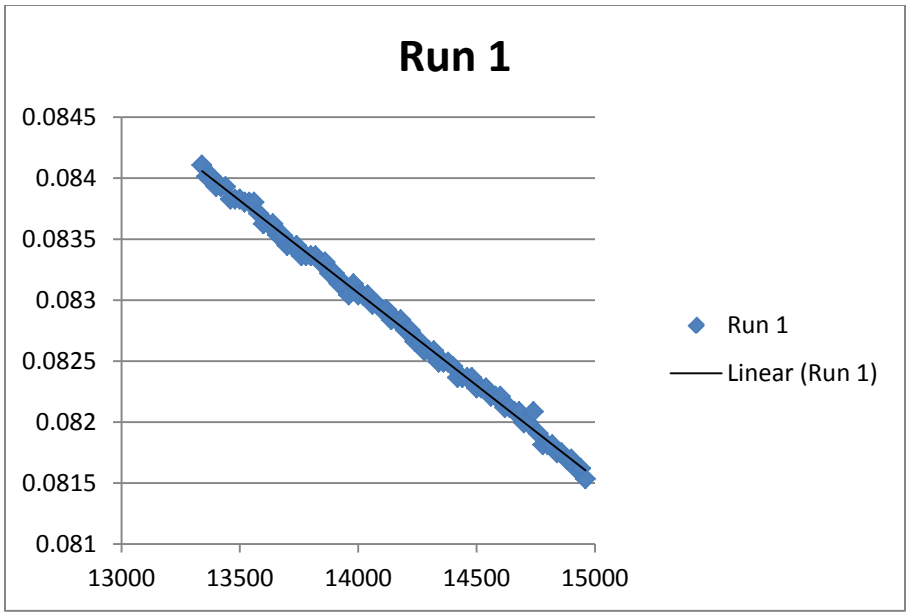

Figure 5-20 - Data utilized for determination of zeroth order rate of the MV^+ of -1000 mV data Run 1

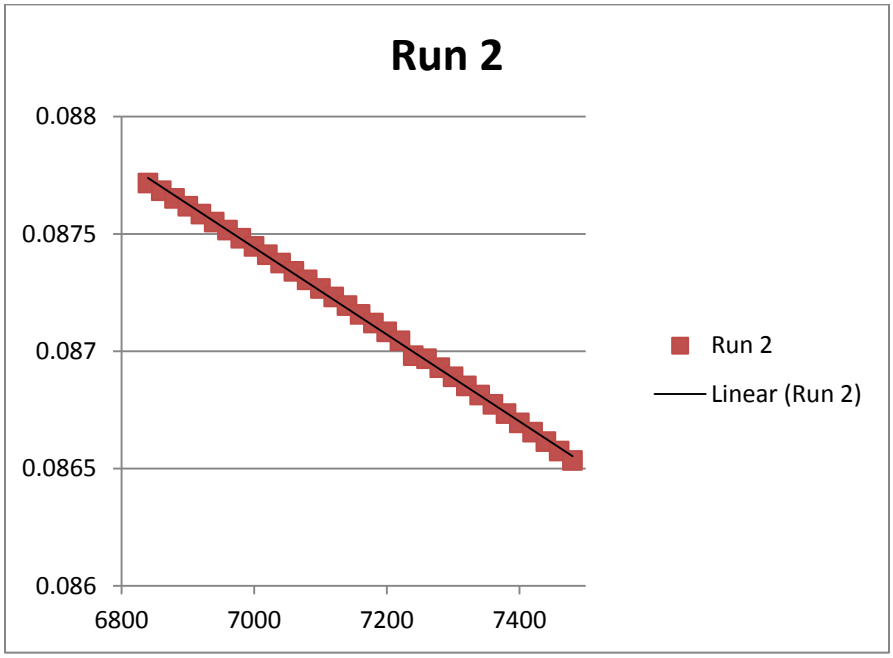

Figure 5-21 - Data utilized for determination of zeroth order rate of the MV^+ of -1000 mV data Run 2

Table 5-8 - Summary of initial rates of reaction for methyl viologen data at -1000 mV

	Zeroth Order Rate (mM/s)	Zeroth Order Rate (mM/hr)	R-squared (unitless)
Initial Rate of MV^{2+} Run 1	3.720E-05	1.339E-01	0.9991
Initial Rate of MV^{2+} Run 2	2.646E-05	9.526E-02	0.9991
Average Initial rate of MV^{2+}	3.183E-05	1.146E-01	n/a
Standard Deviation	7.594E-06	2.734E-02	n/a
Initial Rate of MV^{+} Run 1	1.854E-06	6.674E-03	0.9992
Initial Rate of MV^{+} Run 2	1.515E-06	5.454E-03	0.9973
Average Initial rate of MV^{+}	1.685E-06	6.064E-03	n/a
Standard Deviation	2.397E-07	8.630E-04	n/a

5.4.8.2 Model Parameters Determined by Best Fit

All parameters have been fit as described above in section 5.3.4. The values of all unknowns are presented here in Table 5-9.

Table 5-9 - Kinetic rate constants used for modeling -1000 mV experimental data

	Surface Reaction Controlled
$k_{A,a}$ (1/s)	1.212E+03
$k_{A,d}$ (1/s)	2.000E+01

Table 5-9 - Kinetic rate constants used for modeling -1000 mV experimental data

$k_{A,sr,f}/R_{As}$ (1/s)	3.183E-04
$k_{B,a}$ (1/s)	3.030E+01
$k_{B,d}$ (1/s)	2.000E+01
$k_{B,sr,f}/R_{As}$ (1/s)	7.3571E-05
$k_{B,sr,r}/R_{As}$ (1/s)	9.1840E-04
$k_{C,a}$ (1/s)	2.500E+02
$k_{C,d}$ (1/s)	2.000E+01
$k_{C,sr,r}/R_{As}$ (1/s)	9.9090E-07

5.4.9 MV Kinetics Results In-Depth Analysis and Discussion

5.4.9.1 Determination of Rate Limiting Step

This point was covered in section 5.4.5, but is highlighted and summarized again here. One of the most important purposes of this work was to discover which of the three steps of adsorption, surface reaction, and desorption in the three-step model was the rate determining step. The zeroth order nature of the curves from the AQDS experiments suggest that the rate limiting step is either the desorption or surface reaction steps. The data from the single reduction MV experiments visually indicate adsorption or surface reaction as the rate limiting step, but the kinetic model shows an unsatisfactory fit of the data for an adsorption controlled model. The presence of such a large amount of MV^+ rejected to the bulk in the multiple reduction MV experiments indicates that the surface reaction is the rate limiting step since both adsorption controlled and desorption controlled models would proceed directly from reduction of MV^{2+} to MV^0 without seeing any of the intermediate MV^+ in the bulk. Finally, the robustness of the

model to fit data from all four sets of experimental runs strongly suggests that the surface reaction is the slow step along the proposed mechanism, as neither an adsorption nor desorption controlled model can be fit to all four sets of data. The conclusion of this work, therefore, is that the surface reaction is the rate-limiting step in carbon electrode electron mediator reduction in the BER system described in this work.

5.4.9.2 Data Trends and the Influence of Thermodynamic Equilibrium

While a large amount of rate constant fitting has occurred, the importance of these parameters has yet to be addressed. Essentially, all six runs with MV start with similar apparent initial rates. This can be seen more clearly here in Figure 5-22, where the first 2000 seconds of each run are presented in one plot. Similar rates are also clearly shown in Table 5-10 where the fitted rate constant for the forward rate-limiting step ($k_{A,sr,f}/R_{As}$) characterizes the initial rate.

The similar initial rates indicate that the initial rate is independent of the overpotential, as stated in Section 5.4.6. In fact, a statistical analysis of the data presented in this chapter for initial rates shows that the difference between initial rates is statistically insignificant. A one-way ANOVA results in a p-value of 0.612, so even at a very conservative level of α=0.10, we fail to reject the null hypothesis that the mean value for the initial rates at each different potential are equal. The reverse rate constant is a determining factor in the shape of the curves that are generated, and is used as a key parameter for data fitting. This shift, it would also seem, is due to the change in thermodynamic states. A higher reverse reaction leads to the fractional coverage of A remaining high at greater overpotentials. This subsequently leads to a longer period of zeroth order nature at higher overpotentials.

Since the reactions are surface reaction limited, the electrode surface sites are essentially completely full at all times. Since the adsorption and desorption rates are faster than the rate of

surface reaction, there exists a quasi-equilibrium on the electrode surface since excess bulk ions are competing for limited surface sites. Since all surface sites are full at any given time, the fractional coverage of any species X, at any given time is approximately equal to the relation given in Equation 5-10.

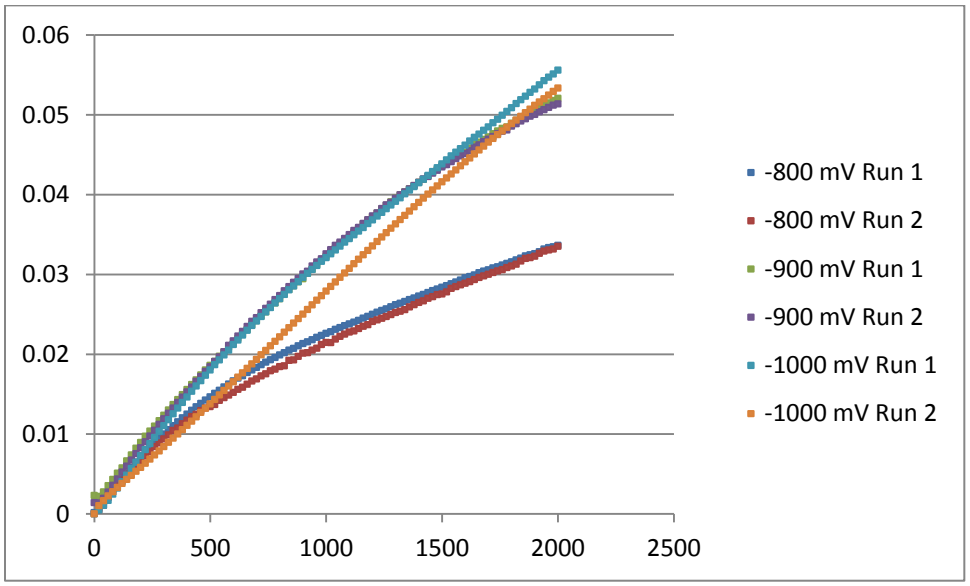

Figure 5-22 - First 2000 seconds of all six methyl viologen experimental runs

Table 5-10 - Fitted rate constants from experimental methyl viologen data

	-800 mV	**-900 mV**	**-1000 mV**
$\mathbf{k_{A,sr,f}/R_{As}}$ **(1/s)**	3.641E-04	3.526E-04	3.183E-04
$\mathbf{k_{B,sr,r}/R_{As}}$ **(1/s)**	8.091E-05	2.726E-04	9.1840E-04

$$\theta_X \approx \frac{K_{a,X} \cdot C_X}{\sum_{I=1}^{n} K_{a,I} \cdot C_I} \tag{5-10}$$

In this equation, X can be any adsorbed species (e.g. A, B, C, or any other species dissolved in the solution which can be adsorbed to the electrode surface). $K_{a,X}$ is the adsorption equilibrium constant for species X. $K_{a,I}$ is the adsorption equilibrium constant for species I. The sum on the bottom of the equation covers all species in the system which can be adsorbed to the

electrode surface. This indicates that at time 0, in the case where only A, B, and C are present as species which can be adsorbed to the electrode surface, the fractional coverage of A is approximately equal to one since only A is available in the bulk phase. This same evidence is also shown in Figure 4-4 for the surface reaction limited regime. This finding, combined with the observation that the initial rates for all experiments are approximately equal, means that the sustained initial rate at different potentials can be somewhat attributed to the shifting of the overall thermodynamic equilibrium constant caused by differences in potential. Essentially, the values of the adsorption equilibrium constants $K_{a,A,}$ $K_{a,B}$, and where applicable $K_{a,C}$, help to explain why the rate slows faster in the experiments at -800 MV than at -900 mV, and why it slows faster at -900 mV than at -1000 mV. At higher potentials, the ratio of $K_{a,A}$ to $K_{a,B}$ increases, which affects how long the initial rate persists before dropping off. From the regressed parameters, $K_{a,A}^{800}/K_{a,B}^{800} = 0.33$, $K_{a,A}^{900}/K_{a,B}^{900} = 2.2$, and $K_{a,A}^{1000}/K_{a,B}^{1000} = 40$. The persistence of the initial rate for longer periods of time at higher ratio values occurs because the rate-determining step is the product of the rate constant and fractional coverage, which is affected by the ratio of equilibrium constants as described in Equation 5-10.

5.4.9.3 Reactor Design Implications

The determination that the surface reaction is the rate determining step allows us better insight into possible reactor improvements that would lead to higher rates. The first and most obvious improvement would be to increase the total number of sites available for the reaction to occur since total adsorption sites are proportional to the surface area available for adsorption. Furthermore, electrode material could make a large difference on the observed rate of reaction. Finally, the zeroth order nature of the reactions persists at higher conversions with larger

overpotentials due to the thermodynamic considerations that were just discussed. This means that if side reactions such as dimerization could be mitigated, the reactor could be designed in such a way to have a constant rate of reduction over a wide range of electron mediator conversion, an important consideration for process control of BER technology.

5.5 Related Kinetic Considerations

5.5.1 Hydrogen Adsorption

One aspect that was not covered in the thermodynamic model is the adsorption of protons to the electrode surface. Since fractional coverage is such a key parameter in the kinetic rate laws, inclusion of the fractional coverage of protons, defined here as θ_H, is something that ought to be mentioned. Fortunately, work done with the same BER system indicates that the value of θ_H remains fairly consistent throughout the experiment [58]. This argument is based on an efficiency study performed to determine how many electrons are utilized to reduce MV. Electrons that are not utilized by MV are assumed to go to hydrogen production, since no other reducible species is available. Since efficiency is fairly consistent throughout the experiment, it follows that the rate of production of hydrogen, and therefore hydrogen rate constant and fractional coverage, can be initially approximated with a constant.

5.5.1.1 Modification of Kinetic Model to Include Hydrogen Adsorption

Inclusion of the hydrogen fractional coverage in the kinetic model modifies the equations for a single reduction three-step mechanism as follows for a single reduction mechanism (A → B only, with no further reaction to C). These would replace the equations listed in section 4.4.4.

$$\frac{dF_A}{dt} = -k_{A,a} \cdot F_A \cdot (1 - \theta_A - \theta_B - \theta_H) + \frac{k_{A,d}}{R_{As}} \cdot \theta_A \tag{5-11}$$

$$\frac{d\theta_A}{dt} = k_{A,a} \cdot R_{As} \cdot F_A \cdot (1 - \theta_A - \theta_B - \theta_H) - k_{A,sr,f} \cdot \theta_A - k_{A,d} \cdot \theta_A + k_{B,sr,r} \cdot \theta_B \quad (5\text{-}12)$$

$$\frac{d\theta_B}{dt} = k_{A,sr,f} \cdot \theta_A - k_{B,d} \cdot \theta_B + k_{B,a} \cdot F_b \cdot R_{As} \cdot (1 - \theta_A - \theta_B - \theta_H) - k_{B,sr,r} \cdot \theta_B \quad (5\text{-}13)$$

$$\frac{dF_B}{dt} = -k_{B,a} \cdot F_B \cdot (1 - \theta_A - \theta_B - \theta_H) + \frac{k_{B,d}}{R_{As}} \cdot \theta_B \quad (5\text{-}14)$$

5.5.1.2 Implications of Hydrogen Adsorption on Kinetic Model

As an example of what inclusion of a hydrogen fractional coverage term would do to the kinetic model, the data from the -800 mV runs have been refit using a surface reaction limited model and a θ_H of 50%. The data and a comparison of the thermodynamic and kinetic coefficients can be seen in Figure 5-23 and Table 5-11.

The adsorption and desorption rate constants did not change with the inclusion of the hydrogen term. The surface reaction rate constants doubled, as would be expected since only half the sites were available as would have been had there been no hydrogen. This points out that the actual rate constants might be significantly higher than those presented in section 5.4, depending on the value of θ_H. It also provides an explanation for the slightly decreasing forward rate of reaction with higher overpotentials. Higher overpotentials would lead to a greater value of θ_H, which would in turn lead to a slower apparent rate even if the rate constant remained the same at all overpotentials.

Table 5-11 - Kinetic rate constants used for hydrogen modeling

	$\theta_H = 0$	**$\theta_H = 0.5$**
$k_{A,a}$ (1/s)	3.333E+01	3.333E+01
$k_{A,d}$ (1/s)	1.000E+02	1.000E+02
$k_{A,sr}/R_{bs}$ (1/s)	3.641E-04	7.282E-04

Table 5-11 - Kinetic rate constants used for hydrogen modeling

$k_{B,a}$ (1/s)	1.000E+02	1.000E+02
$k_{B,d}$ (1/s)	1.000E+02	1.000E+02
$k_{B,sr}/R_{bs}$ (1/s)	8.091E-05	1.618E-04

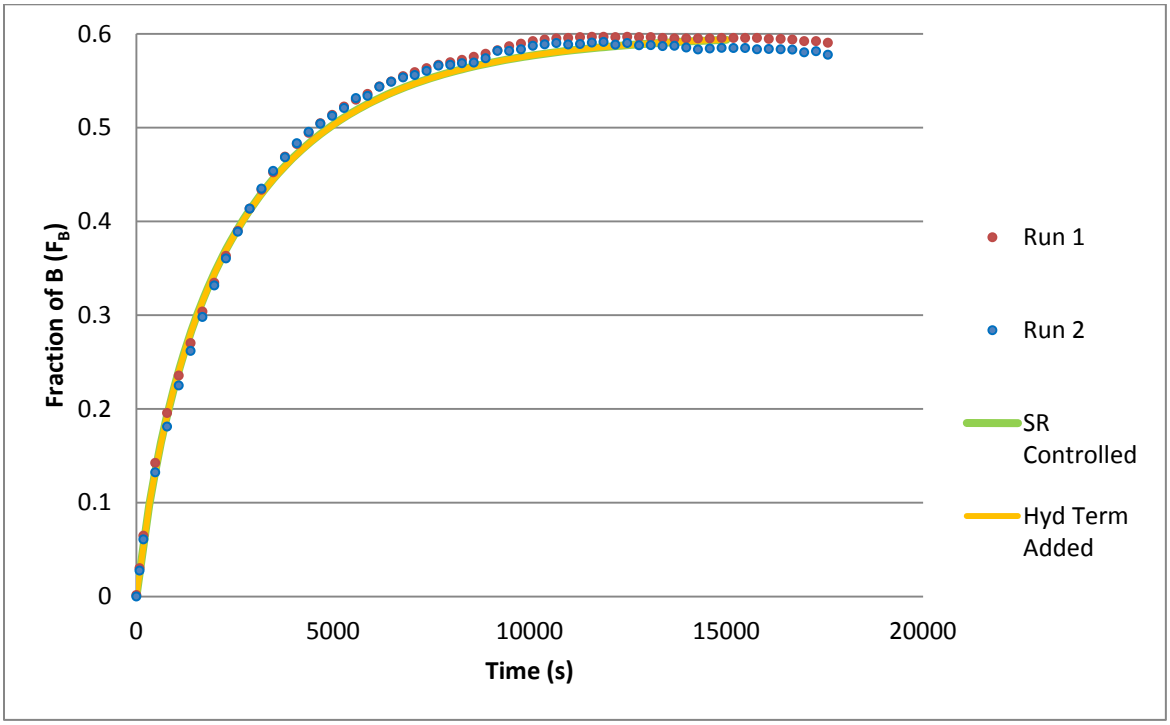

Figure 5-23 - Methyl viologen reduction data and models with and without hydrogen. Data from experiments performed at -800 mV. Data has been thinned to allow the model to be shown. Models overlap almost completely.

6 CONCLUSIONS AND FUTURE WORK

The research recorded in this thesis has provided insights into the foundational principles that will govern the use of BERs. There is, however, much that still needs to be done in order to fully understand these systems and much that needs to be done in order to apply them industrially. This chapter summarizes the conclusions made in this work relating to the original objectives described in Section 1.6 and also makes some suggestions and recommendations for future work that should be performed in order to further understand these complicated and potentially important systems.

6.1 Conclusions

6.1.1 Reactor Design

The reactor that was designed and used in these experiments met the requirements outlined when describing this scope of work. It had temperature control, was sterilizable, was able to become fully anaerobic, could switch feed gases, had the ability to incorporate variable stir-rates, and was able to be attached to a flow-through system for kinetic experiments. While some improvements can be made to the overall reactor design, the reactors used were sufficient for the work that was performed.

6.1.2 Kinetic Modeling of Electron Mediators

The data was found to conform to a proposed three-step mechanism with the surface reaction as the rate limiting step. Each different set of data from three different overpotentials (-800 mV, -900 mV, and -1000 mV) was fit to the model and fit accordingly. The fitted rate constants can be found in Chapter 5. Since the reactions are surface reaction limited, reactor design becomes an important aspect to optimize the performance of BER technology.

It was also observed that the initial rate, which was also the maximum rate, did not vary significantly with overpotential. While the rates were unaffected, the thermodynamic equilibrium was vastly affected with different induced voltage potentials. This shift in equilibrium caused different final conversions and allowed for additional constraints on the fitted rate constants. Possible effects of hydrogen adsorption on the electrode was also discussed and it was found that the presence of hydrogen would indicate that the limiting rate constants could be faster than those presented with a model devoid of hydrogen adsorption.

6.2 Future Work

6.2.1 Future Studies in Indirect Reduction of NAD^+

This thesis has established the basics of electrode reduction of redox carriers that could lead to eventual reduction of $NAD(P)^+$ to NAD(P)H, but two different mechanisms exist by which this reduction could take place. The first is uncatalysed indirect reduction of $NAD(P)^+$ by a reduced electron carrier species. This chemical link has been established in whole cell systems [Park], but aqueous feasibility and kinetics have not been established. The other method by which NAD^+ can be reduced is via biocatalysis that facilitates the transfer of electrons from the electron mediators to $NAD(P)^+$. Once instance of this recorded in literature is the utilization of

methyl viologen by ferredoxin-NAD(P)$^+$ reductases [Kim 1988]. In fact, it has been established that methyl viologen can replace ferredoxin in all enzymatic reactions [Peguin 1994].

More research possibilities probably exist through the second biocatalytic route. Initial future work describing the interaction of various electron mediators with NAD(P)$^+$ reductases in vitro would allow for greater understanding of required concentrations of both electron mediator and enzyme required for realistic industrial application. Other possible future work could include introduction of immobilized electron mediators and reductases to the electrode surface, allowing for extremely fast kinetics at the electrode surface due to the proximity of the substrate to its enzyme. This could also confine all reactions to the surface of the electrode, which would decrease backend product separation costs.

6.2.2 **Future Work with P11**

Although an initial proof-of-concept experiment utilizing neutral red did not result in growth or product formation, the theoretical feasibility of BER utilization in conjunction with the P11 enzymatic pathway remains intact. There is no convincing evidence that a solution cannot be found that would result in cell growth, product formation, or both. Here we will discuss possible solutions that would lead to positive results.

The first and most obvious iteration that could be performed is to attempt the same experiment with a different electron mediator species. Neutral red was chosen because of its lack of toxicity and due to prior evidence in similar experiments. Viologens, quinones, and other mediator species, however, may interact with distinct enzymes unique to P11 with which neutral red was incompatible. It has been suggested that P11 utilizes ferredoxin in its electron transport chain, and as stated above, methyl viologen is able to replace ferredoxin in enzymatic reactions.

It is completely feasible, therefore, that methyl viologen could succeed where neutral red failed. This would prove to be the simplest solution.

The most likely reason for the lack of growth and metabolite utilization is a lack of the ability to utilize neutral red to drive an electron transport chain that results in ATP production. Bacteria, in general, are very robust and maintain different mechanisms by which they are able to form ATP and sustain growth and viability. Once P11 has been fully sequenced, careful analysis of its genome can reveal the possible mechanisms this particular species has developed in order to circumvent a lack of CO or H_2 in order to facilitate growth. If a pathway is identified that would allow for ATP production and subsequent bacterial growth, product formation should be able to occur.

If neither of these solutions resolves the problem, the final step that could be taken would be to augment the P11 genome with proteins that are able to utilize known electron mediators. *A. succinogenes* was able to utilize neutral red and CO_2 as the only substrates in both growth and methane formation [Park 1999]. The possibility exists for these reactions to take place, but it seems that P11 lacks at least once critical enzyme that would allow for neutral red metabolism similar to *A. succinogenes*. A careful study of the genomes of the two bacteria and their metabolic pathways could reveal the deficiencies of P11. Genetic manipulation could allow for the incorporation and expression of the critical DNA necessary to produce the enzymes that P11 lacks for neutral red utilization.

6.3 **Summary**

This work established the feasibility of utilizing CO_2 and electron mediators as the only reactants for cellular growth and product formation. While no successful experimental work was

performed in this work, the foundational principles upon which this work would be based have been established. This is also not the only possible application of BER technology, so an in-depth look at the kinetics of the reducing reactions was performed with two electron mediators, anthraquinone-2,6-disulfonate (AQDS) and methyl viologen (MV).

This in-depth look resulted in the development of a kinetic model that was able to explain the observed kinetic rates. It was established that the rate of reaction was controlled by the surface reaction, which has large implications in the future work to be performed. Kinetic rate constants for the reactions were detailed and analysis performed on parameters key to understanding the workings of the BER electron mediator reduction kinetics. This work will provide the framework for future studies and established a direction and basic understanding of bioelectrical reactor systems.

REFERENCES

1. Liljeblad, A., A. Kallinen, and L.T. Kanerva, *Biocatalysis in the Preparation of the Statin Side Chain.* Current Organic Synthesis, 2009. **6**(4): p. 362-379.

2. Wingard Jr, L.B., C.H. Shaw, and J.F. Castner, *Bioelectrochemical Fuel Cells.* Enzyme and Microbial Technology, 1982. **4**(3): p. 137-142.

3. Laane, C., K. Dekker, and C. Veeger. *Production of (Bio)Chemicals in a Bioelectrochemical Cell*. 1984. Munich, W Ger: Verlag Chemie.

4. Kohlmann, C., W. Maerkle, and S. Luetz, *Electroenzymatic synthesis.* Journal of Molecular Catalysis B Enzymatic, 2008. **51**(3-4): p. 57-72.

5. Damian, A., *Direct electrochemical regeneration of NADH on Au, Cu and Pt-Au electrodes.* Chemical and Biochemical Engineering Quarterly, 2007. **21**(1): p. 21-32.

6. Peguin, S., et al., *Enhanced alcohol yields in batch cultures of Clostridium acetobutylicum using a three-electrode potentiometric system with methyl viologen as electron carrier.* Biotechnology Letters, 1994. **16**(3): p. 269-274.

7. Skidmore, B., *Syngas Fermentation: Quantification of Assay Techniques, Reaction Kinetics, and Pressure Dependencies of the Clostridial P11 Hydrogenase.* 2010.

8. Asako, H., M. Shimizu, and N. Itoh, *Biocatalytic production of (S)-4-bromo-3-hydroxybutyrate and structurally related chemicals and their applications.* Applied Microbiology and Biotechnology, 2009. **84**(3): p. 397-405.

9. Chin, J.W., et al., *Analysis of NADPH supply during xylitol production by engineered Escherichia coli.* Biotechnology and Bioengineering, 2009. **102**(1): p. 209-220.

10. Park, D.H., et al., *Microbial Utilization of Electrically Reduced Neutral Red as the Sole Electron Donor for Growth and Metabolite Production.* Appl. Environ. Microbiol., 1999. **65**(7): p. 2912-2917.

11. Thrash, J.C., et al., *Electrochemical stimulation of microbial perchlorate reduction.* Environmental Science & Technology, 2007. **41**(5): p. 1740-1746.

12. Sakai, S. and T. Yagishita, *Microbial production of hydrogen and ethanol from glycerol-containing wastes discharged from a biodiesel fuel production plant in a bioelectrochemical reactor with thionine.* Biotechnology and Bioengineering, 2007. **98**(2): p. 340-348.

13. Rozendal, R.A., et al., *Towards practical implementation of bioelectrochemical wastewater treatment*, in *Trends in Biotechnology*2008. p. 450-459.

14. Sakai, H., et al., *A high-power glucose/oxygen biofuel cell operating under quiescent conditions.* Energy & Environmental Science, 2009. **2**(1): p. 133-138.

15. Surareungchai, W., A.P.F. Turner, and S. Saini. *Kinetics of electron transfer of a bioelectrochemical reaction in binary organic solvent-water media*. 1995. Stockholm, Sweden: IEEE.

16. Feleke, Z., et al., *Selective reduction of nitrate to nitrogen gas in a biofilm-electrode reactor.* Water Research, 1998. **32**(9): p. 2728-2734.

17. Peguin, S. and P. Soucaille, *Modulation of metabolism of Clostridium acetobutylicum grown in chemostat culture in a three-electrode potentiostatic system with methyl viologen as electron carrier.* Biotechnology and Bioengineering, 1996. **51**(3): p. 342-348.

18. Hongo, M. and M. Iwahara, *Electrochemical Studies on Fermentation.1. Application of Electro-Energizing Method to L-Glutamic Acid Fermentation.* Agricultural and Biological Chemistry, 1979. **43**(10): p. 2075-2081.

19. Cast, K.L. and J.R.V. Flora, *An evaluation of two cathode materials and the impact of copper on bioelectrochemical denitrification.* Water Research, 1998. **32**(1): p. 63-70.

20. Harvey, P.I. and F.K. Crundwell, *The effect of As(III) on the growth of Thiobacillus ferrooxidans in an electrolytic cell under controlled redox potentials.* Minerals Engineering, 1996. **9**(10): p. 1059-1068.

21. Sadoff, H.L., H.O. Halvorson, and R.K. Finn, *Electrolysis as a Means of Aerating Submerged Cultures of Microorganisms.* Appl. Environ. Microbiol., 1956. **4**(4): p. 164-170.

22. Emde, R. and B. Schink, *Enhanced Propionate Formation by Propionibacterium-freudenreichii Subsp Freudenreichii in a 3-Electrode Amperometric Culture System.* Applied and Environmental Microbiology, 1990. **56**(9): p. 2771-2776.

23. Taya, M., et al., *Enhanced Cell-Density Culture of Thiobacillus-Ferrooxidans in a Membrane-type Bioreactor with Electrolytic Reduction Unit for Ferric Ion.* Journal of Chemical Engineering of Japan, 1991. **24**(3): p. 291-296.

24. Szekeres, S., et al., *Hydrogen-dependent denitrification in a two-reactor bio-electrochemical system.* Water Research, 2001. **35**(3): p. 715-719.

25. Hayes, A.M., J.R.V. Flora, and J. Khan, *Electrolytic stimulation of denitrification in sand columns.* Water Research, 1998. **32**(9): p. 2830-2834.

26. Skadberg, B., et al., *Influence of pH, current and copper on the biological dechlorination of 2,6-dichlorophenol in an electrochemical cell.* Water Research, 1999. **33**(9): p. 1997-2010.

27. Tanaka, T. and N. Kuroda, *Improvement of submerged biofilter process by bioelectrochemical method.* Journal of Environmental Engineering-Asce, 2000. **126**(6): p. 541-548.

28. Aulenta, F., et al., *Electron transfer from a solid-state electrode assisted by methyl viologen sustains efficient microbial reductive dechlorination of TCE.* Environmental Science & Technology, 2007. **41**(7): p. 2554-2559.

29. Gregory, K.B., D.R. Bond, and D.R. Lovley, *Graphite electrodes as electron donors for anaerobic respiration.* Environmental Microbiology, 2004. **6**(6): p. 596-604.

30. Blake, R.C., G.T. Howard, and S. McGinness, *Enhanced Yields of Iron-Oxidizing Bacteria by in-situ Electrochemical Reduction of Soluble Iron in the Growth-Medium.* Applied and Environmental Microbiology, 1994. **60**(8): p. 2704-2710.

31. Fan, Y.Z., H.Q. Hu, and H. Liu, *Enhanced Coulombic efficiency and power density of air-cathode microbial fuel cells with an improved cell configuration.* Journal of Power Sources, 2007. **171**(2): p. 348-354.

32. Jang, J.K., et al., *Construction and operation of a novel mediator- and membrane-less microbial fuel cell.* Process Biochemistry, 2004. **39**(8): p. 1007-1012.

33. Marshall, C.W. and H.D. May, *Electrochemical evidence of direct electrode reduction by a thermophilic Gram-positive bacterium, Thermincola ferriacetica.* Energy & Environmental Science, 2009. **2**(6): p. 699-705.

34. Kim, T.S. and B.H. Kim, *Electron flow shift in<u>Clostridium</u><u>acetobutylicum</u> fermentation by electrochemically introduced reducing equivalent.* Biotechnology Letters, 1988. **10**(2): p. 123-128.

35. Girbal, L., *How Neutral Red Modified Carbon and Electron Flow in Clostridium-Acetobutylicum Grown in Chemostat Culture at Neutral pH.* FEMS Microbiology Reviews, 1995. **16**(2-3): p. 151-162.

36. Park, D.H. and J.G. Zeikus, *Utilization of Electrically Reduced Neutral Red by Actinobacillus succinogenes: Physiological Function of Neutral Red in Membrane-Driven Fumarate Reduction and Energy Conservation.* J. Bacteriol., 1999. **181**(8): p. 2403-2410.

37. Park, D.H., C. Vieille, and J.G. Zeikus, *Bioelectrocatalysts: Engineered oxidoreductase system for utilization of fumarate reductase in chemical synthesis, detection, and fuel cells.* Applied Biochemistry and Biotechnology, 2003. **111**(1): p. 41-53.

38. Cervantes, F.J., et al., *Competition between methanogenesis and quinone respiration for ecologically important substrates in anaerobic consortia.* FEMS Microbiology Ecology, 2000. **34**(2): p. 161-171.

39. Cervantes, F.J., et al., *Contribution of quinone-reducing microorganisms to the anaerobic biodegradation of organic compounds under different redox conditions.* Biodegradation, 2008. **19**(2): p. 235-246.

40. Parachin, N.S., M. Carlquist, and M.F. Gorwa-Grauslund, *Comparison of engineered Saccharomyces cerevisiae and engineered Escherichia coli for the production of an optically pure keto alcohol.* Applied Microbiology and Biotechnology, 2009. **84**(3): p. 487-497.

41. Patel, R.N., *Biocatalysis: Synthesis of chiral intermediates for drugs.* Current Opinion in Drug Discovery & Development, 2006. **9**(6): p. 741-764.

42. Hilterhaus, L. and A. Liese, *Building blocks*, in *White Biotechnology*, R. Ulber and D. Sell, Editors. 2007, Springer-Verlag Berlin: Berlin. p. 133-173.

43. Alanvert, E., et al., *Highly stereoselective biocatalytic reduction of alpha-halo ketones.* Tetrahedron-Asymmetry, 2009. **20**(21): p. 2462-2466.

44. Gamenara, D. and P.D. de Maria, *Candida spp. redox machineries: An ample biocatalytic platform for practical applications and academic insights.* Biotechnology Advances, 2009. **27**(3): p. 278-285.

45. Rozendal, R.A., et al., *Towards practical implementation of bioelectrochemical wastewater treatment.* Trends in Biotechnology, 2008. **26**(8): p. 450-459.

46. Laane, C., et al., *Use of a Bioelectrochemical Cell for the Synthesis of (Bio)Chemicals.* Enzyme and Microbial Technology, 1984. **6**(4): p. 165-168.

47. Khera, J. and A. Chandra, *Microbial Fuel Cells: Recent Trends.* Proceedings of the National Academy of Sciences India Section a-Physical Sciences, 2012. **82**(1): p. 31-41.

48. Thrash, J.C. and J.D. Coates, *Review: Direct and Indirect Electrical Stimulation of Microbial Metabolism.* Environmental Science & Technology, 2008. **42**(11): p. 3921-3931.

49. Madigan, M.T. and J.M. Martinko, *Brock: Biology of Microorganisms*. 11 ed2006: Benjamin Cummings.

50. White, D., *Inorganic Metabolism* in *Physiology and Biochemistry of Prokaryotes*2000. p. 314 - 335.

51. Purec, L., A.I. Krasna, and D. Rittenberg, *The Inhibition of Hydrogenase by Carbon Monoxide and the Reversal of this Inhibition by Light*.* Biochemistry, 1962. **1**(2): p. 270-275.

52. Froment, G.F., *Chemical reactor analysis and design / Gilbert F. Froment, Kenneth B. Bischoff*, ed. K.B.j.a. Bischoff1979, New York :: Wiley.

53. Carey, F.A., *Organic Chemistry*. 6th ed2006, New York: McGraw-Hill.

54. Wolszczak, M. and C. Stradowski, *Methylviologen cation radical, its dimer and complex in various media.* International Journal of Radiation Applications and Instrumentation Part C Radiation Physics and Chemistry, 1989. **33**(4): p. 355-359.

55. Quintela, P., A. Diaz, and A. Kaifer, *Dimerization of methylviologen cation radical in anionic micellar and polyelectrolyte solutions.* Langmuir, 1988. **4**(3): p. 663-667.

56. Baker, C.J., et al., *Interference by Mes [2-(4-morpholino)ethanesulfonic acid] and related buffers with phenolic oxidation by peroxidase.* Free Radical Biology and Medicine, 2007. **43**(9): p. 1322-1327.

57. Thorneley, R.N.F., *A convenient electrochemical preparation of reduced methyl viologen and a kinetic study of the reaction with oxygen using an anaerobic stopped-flow apparatus.* Biochimica et Biophysica Acta (BBA) - Bioenergetics, 1974. **333**(3): p. 487-496.

58. Chen, C., *Thermodynamic, kinetic and efficiency analysis of methyl viologen.* 2012.

APPENDIX I - CHAPTER 3 THERMODYNAMIC CALCULATIONS

Definitions and Constants

$kJ := 1000J$ $\underset{\sim}{ORIGIN} := 1$ $R_g := 8.314\frac{J}{mol\cdot K}$ $T_{ref} := (25 + 273.15)K$ $mM := 1\cdot 10^{-3}\cdot\frac{mol}{L}$

$F_F := 96485.3415\cdot\frac{C}{mol}$ $MW_{wat} := 18.02\cdot\frac{gm}{mol}$ $\rho_{wat} := 1\cdot\frac{kg}{L}$ $C_{wat} := \frac{\rho_{wat}}{MW_{wat}}$

Gibb's Free Energy of Formations

$$G_f := -\begin{pmatrix} 394.359 \\ 137.15 \\ 39.87 \\ 237.178 \\ 181.75 \\ 369.41 \\ 50.75 \\ 362.4 \\ 517.81 \end{pmatrix}\cdot\frac{kJ}{mol}\begin{pmatrix} CO2 \\ CO \\ Proton \\ Water \\ Ethanol \\ AceticAcid \\ Methane \\ FormicAcid \\ LacticAcid \end{pmatrix}$$

Gibbs energy of formations taken from Thauer et. al. 1977, H+ is at pH of 7

Kinetic Coefficients for Overall Product Forming Reactions

columns are for for following reactions:

1 - Ethanol from CO2, 2 - Acetic Acid from CO2, 3 - Methane from CO2, 4 - Formic Acid from CO2, 5 - H2 H+ couple, 6 - Lactic Acid from CO2, 7 - Ethanol from Acetic Acid, 8 - CO from CO2

$$\nu := \begin{pmatrix} -2 & -2 & -1 & -1 & 0 & -3 & 0 & -1 \\ 0 & 0 & 0 & 0 & 0 & 0 & 0 & 1 \\ -12 & -8 & -8 & -2 & -2 & -12 & -4 & -2 \\ 3 & 2 & 2 & 0 & 0 & 3 & 1 & 1 \\ 1 & 0 & 0 & 0 & 0 & 0 & 1 & 0 \\ 0 & 1 & 0 & 0 & 0 & 0 & -1 & 0 \\ 0 & 0 & 1 & 0 & 0 & 0 & 0 & 0 \\ 0 & 0 & 0 & 1 & 0 & 0 & 0 & 0 \\ 0 & 0 & 0 & 0 & 0 & 1 & 0 & 0 \end{pmatrix} \qquad n_e := \begin{pmatrix} -12 \\ -8 \\ -8 \\ -2 \\ -2 \\ -12 \\ -4 \\ -2 \end{pmatrix}$$

Calculating total Change in Gibb's Free Energy and Standard Potentials $\iota := 1..8$

$$\Delta G_{0_\iota} := \sum_{i=1}^{9}\left(\nu_{i,\iota}\cdot G_{f_i}\right) \qquad E_{0_\iota} := \frac{\Delta G_{0_\iota}}{n_{e_\iota}\cdot F_F} \qquad K_{rxn} := \exp\left(\frac{-\Delta G_0}{R_g\cdot T_{ref}}\right)$$

$$\Delta G_{ij} = \begin{pmatrix} -373.874 \\ 263.912 \\ 188.218 \\ 111.699 \\ 70.74 \\ 432.173 \\ 108.962 \\ 99.771 \end{pmatrix} \frac{kJ}{mol} \qquad E_{ij} = \begin{pmatrix} 323 \\ -342 \\ -244 \\ 579 \\ -413 \\ -373 \\ -265 \\ -317 \end{pmatrix} mV$$

$$\Delta G_N := -320mV \cdot 2 \cdot F = 6.175 \times 10^4 \frac{J}{mol} \qquad \Delta G_{NAD} := \Delta G_N + \Delta G_{fo} = -75.399 \frac{kJ}{mol}$$

This is from NAD+ to NADH

Possible Electron Donors and Their Standard Potentials:
methyl viologen: -448 mV
benzyl viologen: -360 mV
AQDS is at -184 mV
NAD+ at -320

Calculating Cell Thermodynamic Equilibrium Constants with each electron donor

$$E_{eq_i} := \begin{pmatrix} -448 \\ -360 \\ -184 \\ -320 \end{pmatrix} mV \qquad \Delta E_{cell} := E_{eq_i} - E_{eq_j} \qquad \begin{pmatrix} 0.125 \\ 0.037 \\ 0.136 \\ -2.911 \times 10^{-3} \end{pmatrix} V$$

$$K_{cell_i} := \exp\left(\frac{-12 \cdot F \cdot \Delta E_{cell}}{R \cdot T_{rel}}\right) = \begin{pmatrix} 2.570 \times 10^{21} \\ 3.339 \times 10^{7} \\ 0.000 \times 10^{0} \\ 2.368 \times 10^{-1} \end{pmatrix} \qquad K_{cell_3}{}^{15} = 6.629 \times 10^{-13}$$

Solving for donor molecule concentration requirements at standard state conditions for ethanol reaction products and reactants (1 atm CO2, pH 7, 1 mol/L of ethanol)

$$K = \frac{\left(\frac{C_{EtOH}}{1\frac{mol}{L}}\right)^{a} \cdot \left(\frac{C_{CO_2}}{1\frac{mol}{L}}\right)^{a}}{\left(10^{-pH}\right)^{b} \cdot \left(\frac{C_{red}}{1\frac{mol}{L}}\right)^{b}}$$

Where a = 12/number of electrons donated per donor molecule.
and b = 12-number of protons donated per donor molecule
for methyl viologen, a=12 and b=12
for benzyl viologen, a=12 and b=12
for AQDS, a=3 and b=6
for NADH, a=6 and b=6

$$a = \begin{pmatrix} 12 \\ 12 \\ 3 \\ 6 \end{pmatrix} \qquad b = \begin{pmatrix} 12 \\ 12 \\ 6 \\ 6 \end{pmatrix}$$

At standard conditions, the concentration of ethanol is 1 mol/L and pH is 7, so both of these values are unity. Therefore:

$\frac{C_{red}}{C_{ox}} = K^{\frac{1}{n}}$ This is the ratio that will now be solved $i = 1 .. 4$

$Ratio_i := (K_{cell_i})^{\left(1-\frac{1}{n}\right)}$ $Ratio = \begin{pmatrix} 7.451 \times 10^{13} \\ 6.236 \\ 2.471 \times 10^{9} \\ 1.254 \end{pmatrix}$ This is the number of reduced molecules required for every oxidized molecule in order to achieve equilibrium of 1 mol/L of ethanol

Calculating the nonstandard half reaction potentials

$C_{app} := \begin{pmatrix} 10^{-3} \\ 0.2 \\ 0.5 \\ 1 \\ 2 \end{pmatrix} \frac{mol}{L}$ $P_{app} := \begin{pmatrix} 10^{-3} \\ 0.1 \\ 5 \cdot atm \\ 1 \\ 2.2 \end{pmatrix}$ $P_{appH} := \begin{pmatrix} 10^{-4} \\ 1 \\ 5 \\ 10^{1} \end{pmatrix}$ $pH := 7$ $T_{cell} := 37 + 273.15K$

$n := 1..5$ $j := 1..5$ $k := 1..7$

Calculating actual Potential (E) for different half reactions

Ethanol from CO2

$E_{cell}(C_{alc}, pH, P_{CO2}, n)_j := E0_1 - \frac{R_g \cdot T_{cell}}{n \cdot 12 \cdot F} \cdot \ln\left[\frac{\frac{C_{alc}}{1\frac{mol}{L}}}{\left(\frac{P_{CO2}}{1 \cdot atm}\right)^2 \cdot \left(\frac{10^{-pH}}{10^{-7}}\right)^{12}}\right]$

MV and MV2+ half reaction

$E_{MV}(C_{MVred}, C_{MVox}, n)_k := E0_2 - \frac{R_g \cdot T_{cell}}{n \cdot F} \cdot \ln\left[\frac{\frac{C_{MVred}}{1\frac{mol}{L}}}{\frac{C_{MVox}}{1\frac{mol}{L}}}\right]$

Formate from CO2

$$E_{For}(C_{for},pH,P_{CO2},n) := E_{0_1} - \frac{R_g \cdot T_{cell}}{n \cdot 2 \cdot F} \cdot \ln\left[\frac{\frac{C_{for}}{1\cdot\frac{mol}{L}}}{\left(\frac{10^{-pH}\cdot\frac{mol}{L}}{10^{-7}\cdot\frac{mol}{L}}\right)\cdot\left(\frac{P_{CO2}}{1\cdot atm}\right)}\right]^n$$

H2 and H+ half reaction

$$E_{H2}(P_{H2},pH,n) := E_{0_3} - \frac{R_g \cdot T_{cell}}{n \cdot 2 \cdot F} \cdot \ln\left[\left[\frac{\frac{P_{H2}}{1\cdot atm}}{\left(\frac{10^{-pH}\cdot\frac{mol}{L}}{10^{-7}\cdot\frac{mol}{L}}\right)^2}\right]^n\right]$$

NAD+ and NADH half reaction

$$E_{NAD}(C_{NAD},C_{NADH},pH,n) := E_{0_4} - \frac{R_g \cdot T_{cell}}{n \cdot 2 \cdot F} \cdot \ln\left[\left[\frac{\frac{C_{NADH}}{1\cdot\frac{mol}{L}}}{\frac{C_{NAD}}{1\cdot\frac{mol}{L}}\cdot\frac{10^{-pH}}{10^{-7}}}\right]^n\right]$$

CO and CO2 half reaction

$$E_{COpH}(P_{CO},P_{CO2},pH,n) := E_{0_5} - \frac{R_g \cdot T_{cell}}{n \cdot 2 \cdot F} \cdot \ln\left[\frac{P_{CO}\cdot\frac{C_{wat}}{1\cdot\frac{mol}{L}}}{P_{CO2}\cdot\left(\frac{10^{-pH}}{10^{-7}}\right)^2}\right]$$

Calculating equilibrium formate maximum at regassing pressures $MW_{for} := 46.03\cdot\frac{gm}{mol}$

Coupled with Hydrogen

Given $C_{For} = 3\cdot10^{-6}\cdot\frac{mol}{L}$ $E_{For}(C_{For},6.3,pH_{ss},1) = E_{H2}(1.3,pH_{ss},6.1)$

$C_{For12} := Find(C_{For}) = 1.996\cdot10^{-6}\cdot\frac{mol}{L}$ $C_{ss} := C_{For12}\cdot MW_{For} = 9.188\cdot10^{-5}\cdot\frac{gm}{L}$

Coupled with CO

Given $C_{Forg} := 1 \cdot 10^{-6} \cdot \frac{mol}{L}$ $E_{For}(C_{Forg}, 6, .3 \cdot 34psi, 1) = E_{CODH}(.4 \cdot 34psi, .3 \cdot 34psi, 6, 1)$

$C_{ForCODH} := Find(C_{Forg}) = 50.307 \cdot \frac{mol}{L}$ $C_F := C_{ForCODH} \cdot MW_{For} = 2.316 \times 10^{3} \cdot \frac{gm}{L}$

Calculating equilibrium CO maximum at regassing pressures

Coupled with Hydrogen

Given $P_{CO} := 1 \cdot 10^{-6} \cdot atm$ $E_{H2}(.3 \cdot 34psi, 6, 1) = E_{CODH}(P_{CO}, .3 \cdot 34psi, 6, 1)$

$P_{COH2} := Find(P_{CO}) = 3.672 \times 10^{-8} \cdot atm$

Calculating equilibrium formate maximum at partial pressures measured just before regassing

Coupled with Hydrogen

Given $C_{Forg} := 1 \cdot 10^{-6} \cdot \frac{mol}{L}$ $E_{For}(C_{Forg}, 6, 14.0psi, 1) = E_{H2}(2.09psi, 6, 1)$

$C_{ForH2} := Find(C_{Forg}) = 5.614 \times 10^{-7} \cdot \frac{mol}{L}$ $C_F := C_{ForH2} \cdot MW_{For} = 2.584 \times 10^{-5} \cdot \frac{gm}{L}$

Coupled with CO

Given $C_{Forg} := 1 \cdot 10^{-6} \cdot \frac{mol}{L}$ $E_{For}(C_{Forg}, 6, 14psi, 1) = E_{CODH}(3.55psi, 14psi, 6, 1)$

$C_{ForCODH} := Find(C_{Forg}) = 13.132 \cdot \frac{mol}{L}$ $C_F := C_{ForCODH} \cdot MW_{For} = 604.453 \cdot \frac{gm}{L}$

Calculating equilibrium CO maximum at highest gas utilization seen

Coupled with Hydrogen

Given $P_{CO} := 1 \cdot 10^{-6} \cdot atm$ $E_{H2}(2.09psi, 6, 1) = E_{CODH}(P_{CO}, 14.0psi, 6, 1)$

$P_{COH2} := Find(P_{CO}) = 1.033 \times 10^{-8} \cdot atm$